2009

Mechanism of Signal Transduction By The Staphylococcus Aureus Quorum Sensing Receptor AGRC

Elizabeth A. George Cisar

MECHANISM OF SIGNAL TRANSDUCTION BY THE *STAPHYLOCOCCUS AUREUS* QUORUM SENSING RECEPTOR AGRC

A Thesis Presented to the Faculty of

The Rockefeller University

in Partial Fulfillment of the Requirements for

the degree of Doctor of Philosophy

by

Elizabeth A. George Cisar

June 2009

MECHANISM OF SIGNAL TRANSDUCTION BY THE *STAPHYLOCOCCUS AUREUS* QUORUM SENSING RECEPTOR AGRC

Elizabeth A. George Cisar, Ph.D.

The Rockefeller University 2009

Bacteria use receptor histidine kinases to sense extracellular cues and convert them into intracellular signaling events that allow them to respond to their environment. In *Staphylococcus aureus*, each individual cell must sense the size of its overall population in order to synchronize virulence factor expression with the entire population. This task is carried out by the *accessory gene regulator* (*agr*) quorum sensing system. The *agr* autoinducing peptide (AIP) pheromone activates the AgrC receptor histidine kinase, resulting in downstream modulation of virulence factor expression. As *S. aureus* is a dangerous pathogen, understanding virulence regulation is of great interest, and the *agr* system has been extensively studied. However, little was known about the mechanism of ligand-induced signal transduction by AgrC at the outset of this work. Moreover, AgrC is member of a unique class of histidine kinases, for which the activation mechanisms are equally speculative, although several of these receptors function in important quorum sensing processes. The aim of this work was to elucidate molecular mechanisms of AIP–AgrC signaling, focusing on inhibitor structure–activity relationships and understanding how ligand binding results in AgrC kinase activation. A new Fmoc-based synthetic route to AIPs and α-thioester peptides was developed and used to construct a series of inhibitor AIPs to define the minimal inhibitory pharmacophore. The minimized scaffold should provide a foundation for future medicinal chemistry efforts. The AgrC activation mechanism was probed via direct biochemical analysis of the receptor, which

was previously unattainable, and mutagenesis. The results indicate that AgrC is a dimer and *trans*-autophosphorylates and that signal transduction occurs symmetrically within the dimer due to intermolecular conformational changes. This mechanism may be a general means by which dimeric quorum sensing receptors rapidly elicit a response upon signal detection.

Acknowledgments

A great deal of gratitude is owed to my mentors, Tom Muir and Richard Novick, who patiently provided great support and guidance throughout the course of my thesis work. Tom provided just the right amount of direction to ensure that net forward progress was made overall while leaving room for me to learn by making important connections myself and developing my own ideas. Thanks to Tom for teaching me to be a scientist.

I am very grateful to the many labmates and collaborators who generously provided essential assistance in this work: Eddie Geisinger of the Novick Lab was a wonderful teammate on this project, and he constructed most of the new strains used in this work; Jesse Wright introduced me to the *agr* project and taught me how to perform the reporter assay;

Labmates Matt Pratt and Kyle Chiang provided key advice for small molecule syntheses and development of protocols for western blot and immunoprecipitation, and they were always available to help; Matthew Sekadat taught me how to perform solid phase peptide synthesis; Peter Moyle helped in the optimization of western blotting; and Miquel Vila-Perello, Michael Hahn, J. P. Pellois, Mette Jensen, Maya Bar-Dagan, Steve Lockless, Amy Tyszkiewicz, and all other Muir Lab members provided great suggestions, support, and additional assistance and made the lab a fun place to work;

Mike Goger of the New York Structural Biology Center provided vital assistance in the acquisition of TOCSY and ROESY NMR spectra, and took time to teach me how to optimize parameters and make chemical shift assignments;

Alison North of the Rockefeller University Bioimaging Center taught me how to use the fluorescence microscope and gave key advice for sample preparation.

I thank my committee members, Tarun Kapoor and Seth Darst of Rockefeller University and Tadhg Begley of Cornell University for valuable perspective and advice throughout the development of this project. I am also very grateful to external member Frederick Hughson of Princeton University for joining my thesis defense committee and offering additional perspective on this work.

I am grateful to have been part of the excellent Tri-institutional Training Program in Chemical Biology, which provided the opportunity to pursue a Ph.D.

Enormous thanks goes to my family, my parents Robert and Gayle George, my sister Debbie George-Reichley, and my brother Richie George for support and encouragement throughout this sometimes arduous process and for doing their best to take an interest in and understand my subject of study.

A most heartfelt thanks goes to my wonderful husband, Justin Cisar, who not only provided endless emotional support, but without whose help I may not have passed my first class in graduate school. His unwavering kindness and generosity can never be repaid.

Table of Contents

Acknowledgments iii
Table of Contents iv
List of Figures v
List of Tables vii
List of Abbreviations viii

Chapter 1: Introduction 1
1.1 The Regulation of Virulence in a Superbug 1
1.2 Molecular Mechanisms of the *agr* System 9
1.2.1 AIP Biosynthesis 9
1.2.2 AIP Structure–Activity Relationships 14
1.2.3 AIP Recognition by the Receptor Histidine Kinase, AgrC 19
1.2.4 The AgrA Response Regulator 31
1.2.5 Output of the *agr* Response 33
1.3 Goals of this Work 35

Chapter 2: Inhibitors of AgrC Prepared by Fmoc-Based Peptide Synthesis 37
2.1 Introduction 37
2.2 A New Synthetic Method for Thioester Peptides and AIPs via Fmoc-SPPS 38
2.3 Minimal Determinants for AIP Inhibition of AgrC 43
2.3.1 Design and Synthesis of trAIP-II Analogues 45
2.3.2 Structure–Activity Relationships of trAIP-II 48
2.3.3 2D NMR Analysis of trAIP-II Analogues 53

Chapter 3: Mechanism of Signal Transduction by AgrC 60
3.1 Introduction 60
3.2 AgrC is a Pre-formed Dimer that *trans*-autophosphorylates 61
3.2.1 Design, Characterization, and Testing of Complementary AgrC Mutants 62
3.2.2 AgrC Homodimerizes in the Absence and Presence of AIP 71
3.3 The AIP Signal is Transduced Symmetrically within AgrC Dimers 73
3.3.1 One Intact Sensor Domain is Sufficient for Activation 74
3.3.2 Both AIP-dependent and Constitutive AgrC Signaling is Symmetric 77
3.4 Model of AgrC Signaling 82

Chapter 4: Discussion 84
4.1 Summary and Implications of this Work 84
4.2 Future Directions 99
4.2.1 AIP–AgrC Cross-linking 99
4.2.2 Inhibition of AgrB 103
4.2.3 Quantitative AIP–AgrC Binding Assay 106
4.2.4 AgrC Structure and Further Mechanistic Insights 107
4.2.5 The *in vivo* Role of *agr* in Virulence 112
4.3 Conclusion 114

Chapter 5: Materials and Methods 115

Appendix 138

References 141

List of Figures

Figure 1	Coordination of Virulence Factor Expression with *S. aureus* Population Growth	3
Figure 2	Network of Genetic Loci that Control Virulence in *S. aureus*	5
Figure 3	The *agr* Locus and Variation of the Four Specificity Groups	8
Figure 4	AgrD Sequence Alignment and Proposed Mechanism of AIP Biosynthesis	11
Figure 5	AIP Synthesis via Boc-Based Solid Phase Peptide Synthesis	16
Figure 6	Sequence Alignment of Staphylococcal AIPs	18
Figure 7	HPK_{10} Family Alignment and AgrC Domain Structure	20
Figure 8	AgrC Topology	23
Figure 9	Dose-response Curves for AIP-II and Derivatives Against AgrC-IV::III.	28
Figure 10	AgrA Domain Structure and LytTR Domain Crystal Structure	32
Figure 11	RNAIII Structure	34
Figure 12	Synthetic Routes for Fmoc-Based Thioester Peptides	39
Figure 13	HPLC–MS Analysis of trAIP-II Macrocyclization Reaction	42
Figure 14	Testing the Proposed Mechanism of Macrocyclization	44
Figure 15	Structures of trAIP-II and Derivatives Synthesized for Study of the Minimal Inhibitory AIP Pharmacophore	46
Figure 16	Inhibition Curves for trAIP-II Derivatives Against AgrC-I & II	50
Figure 17	log IC_{50} Values of trAIP-II Derivatives Against AgrC-I vs. AgrC-II	52
Figure 18	ROESY Spectrum of trAIP-II Derivative *N*-MeS3	54
Figure 19	Chemical Shift Index Values versus Inhibitory Potencies	56

Figure 20	The Minimal Inhibitory AIP Pharmacophore	59
Figure 21	Probing Conserved Catalytic Motifs in the AgrC HK Domain	63
Figure 22	Functional Characterization of AgrC-GFP	65
Figure 23	Characterization of AgrC-GFP Constructs by Fluorescence Microscopy	66
Figure 24	Characterization of AgrC-GFP Constructs by Western Blot	67
Figure 25	Co-expression of AgrC-I Complementary Mutants	70
Figure 26	Co-immunoprecipitation of AgrC-I-GFP and AgrC-I-HA	72
Figure 27	Activities of N-terminally Truncated Variants of AgrC	75
Figure 28	Analysis of AgrC Mutant Heterodimers Containing Sensor Domains with Different Ligand Recognition Properties	76
Figure 29	Analysis of Mutant Heterodimers Containing AgrC Receptors of Two Different *agr* Groups	79
Figure 30	Ligand-independent Signaling by AgrC Mutant Heterodimers Containing One Constitutive R238H Mutant	81
Figure 31	Inhibition of Mutant Heterodimers by AIP-III	94
Figure 32	Model of AgrC Signal Transduction	97
Figure 33	Structures of AIP Derivatives Containing Cross-linkers	100
Figure 34	Synthesis of Cysteine Protease Inhibitor Designed for AgrB	105
Figure 35	Experimental Scheme for *trans* Expression of AgrC Domains	111

List of Tables

Table 1	Activities of AIP Derivatives Made Prior to this Work	15
Table 2	Activities of AIPs and AIP Derivatives Against AgrC Sensor Domain Chimeras	24
Table 3	Activities of AgrC-I/IV Mutants	30
Table 4	Mass Spectrometry and Activity Characterization of trAIP-II and Ten trAIP-II Analogues	49
Table 5	Activities of AgrC Mutants and Mutant Heterodimers	68
Table 6	Activities of AIP Derivatives Containing Cross-linkers	102
Table 7	Strains and Plasmids Used in this Study	132
Table 8	Oligonucleotide Primers Used in this Study	135

List of Abbreviations

agr	accessory gene regulator
AIP	autoinducing peptide
Boc	*tert*-butoxycarbonyl
CA	catalytically active kinase subdomain of the HK domain
CI	confidence interval
DHp	dimerization/phosporylation site subdomain of the HK domain
DIEA	diisopropylethylamine
DMAP	dimethylaminopyridine
DMF	*N*, *N*-dimethylformamide
DMSO	dimethyl sulfoxide
EC_{50}	half maximal effective concentration
Fmoc	9-fluorenylmethoxycarbonyl
GFP	green fluorescent protein
HA	hemagglutinin peptide from influenza virus
HATU	2-(1H-7-Azabenzotriazol-1-yl)-1,1,3,3-tetramethyluronium hexafluorophosphate
HBTU	2-(1H-Benzotriazole-1-yl)-1,1,3,3-tetramethyluronium hexafluorophosphate
HF	hydrogen fluoride
HK	histidine kinase domain
HPK	histidine protein kinase
HPLC	high pressure liquid chromatography
IC_{50}	half maximal inhibitory concentration
MS	mass spectrometry
NMR	nuclear resonance spectroscopy
PyBop	Benzotriazole-1-yl-oxy-tris-(dimethylamino)-phosphonium hexafluorophosphate
SDS-PAGE	sodium dodecyl –protein acrylamide gel electrophoresis
SEM	standard error measurement
TBS	*tert*-butyl dimethyl silyl
TCS	two-component system
TFA	trifluoroacetic acid

Chapter 1: Introduction

1.1 The Regulation of Virulence in a Superbug

Staphylococcus aureus is an opportunistic pathogen and a major health threat worldwide. *S. aureus* is part of the commensal microbial flora of approximately 30% of the adult population and only becomes pathogenic if the bacteria are given the opportunity to invade mucous membranes or soft tissue (1). Most infections are cleared by the immune system or treatable with antibiotics; however, a weakened immune system, surgery, and implanted medical devices are risk factors for potentially fatal infections (2). Thus, *S. aureus* thrives in hospitals, where vulnerable patients being treated for an unrelated problem may become infected with their commensal strain or with a strain spread in the hospital; and infections that advance too quickly for successful antimicrobial treatment and/or are resistant to multiple antibiotics often prove fatal. Methicillin resistant *S. aureus* (MRSA) are multidrug resistant bacteria that were first isolated in 1961 and are now estimated to be responsible for over 18,000 deaths in the United States per year (3). Furthermore, while nosocomial MRSA are the leading cause of fatal infections, the incidence of community-acquired MRSA is also increasing at an alarming rate (4). The only antibiotic against which *S. aureus* has not gained widespread resistance is vancomycin; but in 1999, the first incidences of *S. aureus* infection with intermediate vancomycin resistance (VISA) were reported in the U. S. (5, 6). Therefore, much attention is focused on preventive measures, responsible use of antibiotics to slow the development of resistance, and development of new treatments to combat this growing problem (7-9). Key to these important efforts is to further our understanding of *S. aureus* virulence and pathogenesis.

S. aureus is an especially dangerous pathogen due to the relatively fast host-to-host transmission rate of virulent strains compared to avirulent strains (10), its ability to acquire antibiotic resistance, and its large, diverse arsenal of virulence factors that make it both uniquely adept at evading the host immune system and very toxic. Although disease is the very unfortunate outcome for the host, the sole function of virulence factors is to enable the bacteria to survive in the hostile conditions of the host environment (11). There are two main classes of virulence factors, each associated with different phases of population growth (Figure 1) (1). During the lag and exponential phases, *S. aureus* cells produce cell wall-associated factors that facilitate tissue attachment and evasion of the host immune system, allowing the bacteria to accumulate and possibly form a biofilm. For example, microbial surface components recognizing adhesive matrix molecules (MSCRAMMS) adhere to the extracellular matrix to give the bacteria an attachment point in the host. Protein A binds IgG antibodies that form a protective coat and hide them from the immune system. Once the population size is sufficient, the cell wall-associated factors are down-regulated in late exponential phase and stationary phase, allowing the bacteria to detach from their original colonization site and establish an invasive infection. At the same time, the bacteria secrete enzymes and toxins, termed exoproteins, to degrade host tissue and to promote spread of the infection. The degradative enzymes include proteases and hemolysins, which lyse red blood cells by creating pores in the cell membranes or by hydrolyzing membrane lipids. Enterotoxins are the causative agents of *S. aureus* food poisoning and contribute to toxic shock syndrome and other diseases by stimulating T-cells to produce proinflammatory cytokines in excessive amounts (1, 11).

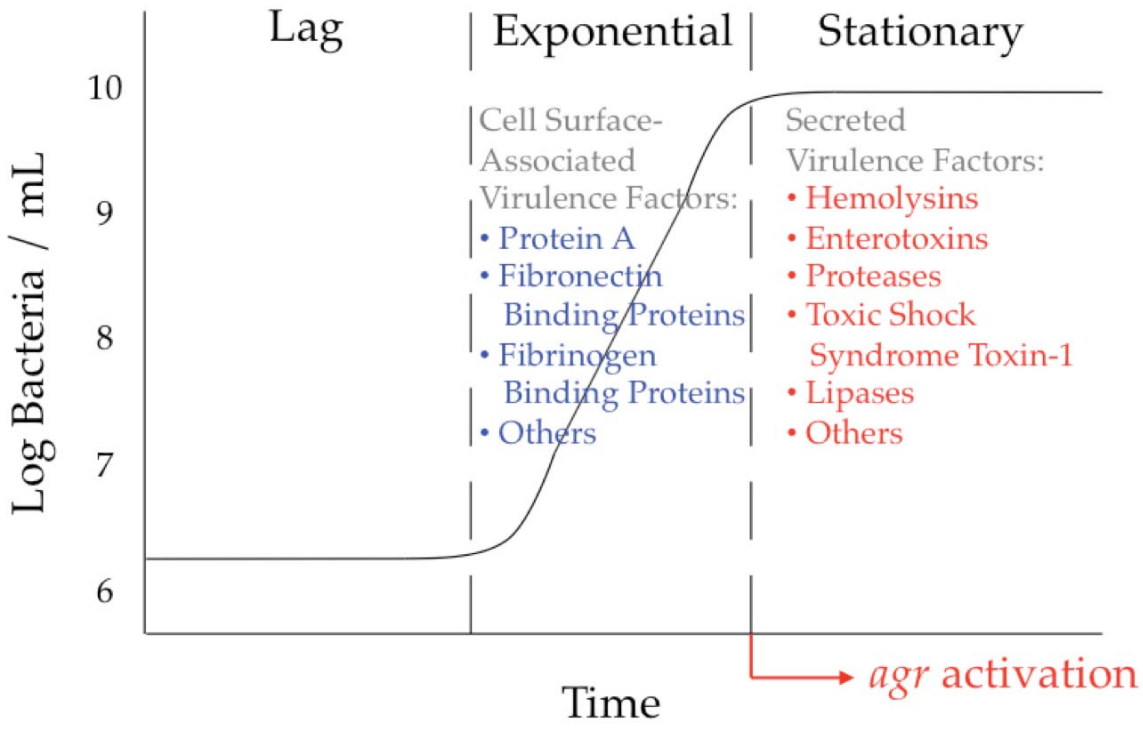

Figure 1. Coordination of Virulence Factor Expression with *S. aureus* Population Growth. Adapted from (11). During exponential growth, cell surface-associated virulence factors are highly expressed in order to promote attachment to the host extracellular matrix and evasion of the host immune system. In stationary phase, the cell surface-associated virulence factors are down-regulated and expression of secreted exoproteins is induced to promote invasion of the host and impart toxicity. The bacteria sense the increase in population density via the *agr* system, which is activated at the transition between exponential and stationary phases and regulates expression of these two classes of virulence factors.

The *accessory gene regulator* (*agr*) system of *S. aureus* coordinates production of the two main classes of virulence factors with different phases of growth, in many cases by directly modulating their expression levels (12, 13). While *agr* is thus considered to be a global regulator of virulence, it is one of several genetic loci connected in a complex signaling network that precisely regulates the staphylococcal virulon (Figure 2) (14-17). The *staphylococcal accessory regulator* (*sar*) is an important regulator of virulence that mediates many of its effects by influencing *agr* expression: SarA, SarU, and SarR up-regulate *agr* transcription; contrarily SarR and SarT indirectly down-regulate *agr* by repressing expression of SarA and SarU, respectively; and some Sar proteins regulate virulence factors independently of *agr*. In a variety of infection models, loss of function mutations in either *agr* or *sar* exhibit reduced virulence, and the virulence of double agr^- sar^- mutants is, in some models, further reduced (18-21). However, the precise role of *agr* in the establishment of infection is unknown. Other important loci include *S. aureus exoprotein expression* (*sae*) (22), which may act downstream of *agr* to maintain hemolysin and coagulase expression (23), *staphylococcal respiratory response* (*srr*), which is required for optimal growth in anaerobic conditions and inhibits *agr* output (24), and *repressor of toxins* (*rot*), which counteracts many effects of *agr* but also induces expression of some exoproteins (25-27).

The *agr* response synchronizes virulence factor expression among all members of the staphylococcal population via a bacterial communication mechanism called quorum sensing. The ability to communicate is essential for bacteria to carry out many fundamental group functions, including virulence, competence, bioluminescence, and biofilm formation (28). Quorum sensing

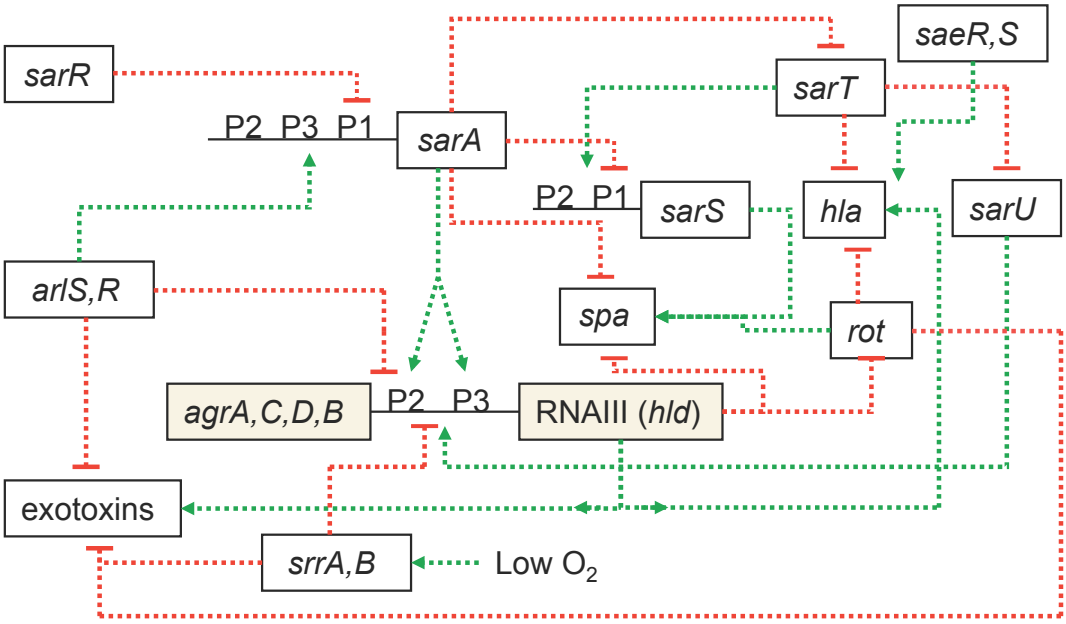

Figure 2. Network of Genetic Loci that Control Virulence in *S. aureus*. The expression of virulence genes such as α-hemolysin (*hla*), δ-hemolysin (*hld*), other exotoxins, and Protein A (*spa*) is modulated by a complex, interactive network of many regulatory loci, including *agr*.

systems facilitate these processes by allowing each individual bacterium to sense the density of the entire population of which it is a member. Bacteria constitutively secrete signaling molecules known as autoinducers that accumulate to concentrations proportional to the bacterial population density in a closed system. An autoinducer activates its target only after reaching a certain threshold concentration, at which point it triggers a specific, coordinated response through target gene transcription. Consequently, activation of energetically demanding processes is limited to instances in which there are enough bacteria present to elicit the desired effect. In Gram-positive bacteria such as staphylococci, the autoinducers are short peptides, often bearing post-translational modifications, called autoinducing peptides (AIPs) (28). At concentrations indicating a quorum, each AIP binds its corresponding receptor, resulting in either activation or inhibition of target gene transcription. In staphylococci, quorum sensing for coordinated virulence factor production is mediated by the *agr* AIP and signaling system (29, 30).

The *agr* signaling system is a canonical two-component system (TCS). TCSs are ubiquitous in bacteria, allowing them to sense and react to a variety of stimuli, including osmolarity, pH, oxygen, chemoattractants, and autoinducers (31). Each TCS is typically composed of a receptor histidine protein kinase (HPK) that senses the signal and a response regulator (RR) transcription factor that modulates gene expression. The HPK receptors are typically dimeric and consist of a sensory domain and an histidine kinase (HK) domain, which is further divided into two subdomains: an α-helical coiled-coil region containing the dimerization interface and histidine phosphorylation site (DHp), and the catalytic kinase domain (CA) (32). Stimulus perception by the sensory domain

triggers activation of the HK domain, resulting in *trans*-autophosphorylation of the contralateral histidine and phosphotransfer to a conserved aspartate in the associated RR.

The *agr* locus contains two divergent promoters, P2 and P3, which modulate transcription of RNAII and RNAIII, respectively (Figure 3A) (30). RNAII encodes the *agr* TCS and two genes required for AIP biosynthesis. AgrB is an integral membrane protein required to process the AgrD propeptide, resulting in secretion of a mature AIP that contains a thiolactone macrocycle formed between a conserved cysteine sulfhydryl group and the α-carboxylate (19, 29). AgrC is a polytopic HPK that autophosphorylates and activates the AgrA RR upon binding to the AIP. AgrA then binds and activates transcription at the P2 and P3 promoters (30, 33), resulting in a positive feedback loop and RNAIII transcription. RNAIII is the δ-hemolysin mRNA and a regulatory RNA that modulates expression of many virulence factors (13, 34). In addition to RNAII & III of the *agr* locus, AgrA was recently found to directly activate transcription of proinflammatory, leukolytic peptides that enhance virulence called phenol-soluble modulins (PSMs), demonstrating that RNAIII is not the sole effector of the *agr* response (35, 36).

The *agr* locus, conserved among the staphylococci and with homologs in many other species, has undergone an interesting evolutionary divergence, giving rise to variant specificity groups, of which there are four in *S. aureus* and two or more in several other staphylococcal species (37-39). The sequence variability of each *agr* specificity group is contained within *agrB*, *agrD*, and the transmembrane sensor domain of *agrC* (Figure 3B), while *agrA* and the HK

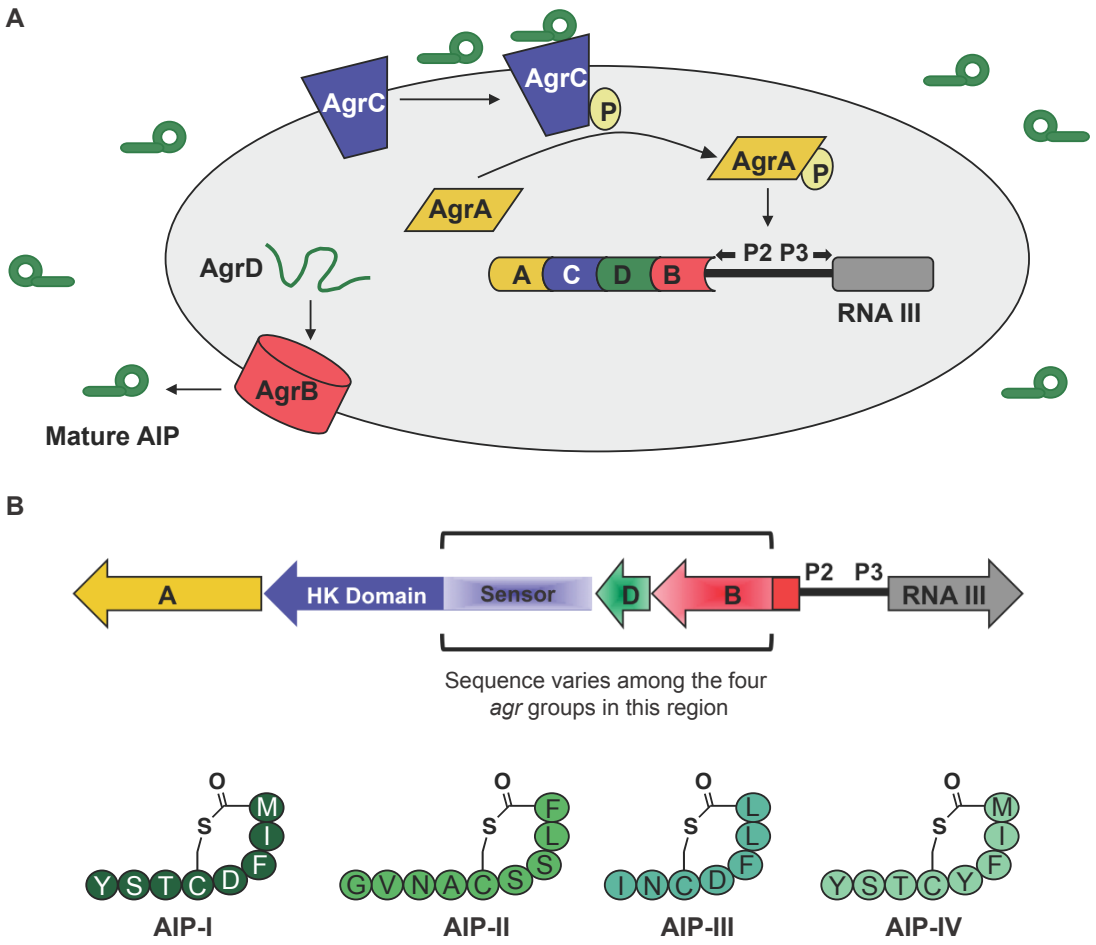

Figure 3. The *agr* Locus and Variation of the Four Specificity Groups. (A) The AgrD propeptide is processed and secreted, in part, by AgrB to form the mature AIP. At the appropriate AIP concentration, the AIP binds the sensor domain of the receptor histidine kinase, AgrC, resulting in autophosphorylation and phosphotransfer to AgrA. Phosphorylated AgrA activates transcription at the *agr* P2 and P3 promoters, resulting in a positive feedback loop of the *agr* system and RNAIII transcription, which mediates many downstream effects. **(B)** The sequence variation among the four *agr* groups is contained within *agrB*, *agrD*, and the sensor domain of *agrC*. The sequences and structures of the four AIPs are shown.

domain of *agrC* are identical across all four *S. aureus agr* groups. Each *S. aureus agr* group synthesizes a distinct AIP of seven to nine amino acids, which activates the cognate AgrC receptor, and the group identity of the AgrC sensor domain alone dictates the specificity of AIP recognition for any given population (40). Remarkably, cross-group AIP–AgrC interactions are inhibitory (37), with heterologous AIPs acting as competitive antagonists (41) and/or inverse agonists (42). The only exception to this intergroup interference is the cross-activation observed between groups I & IV, the AIP sequences of which differ by just a single amino acid. Intraspecies quorum sensing interference may be unique to *S. aureus*, as cross-group inhibition has not been observed among the three known *agr* groups of *S. epidermidis* (39). The *in vivo* relevance and therapeutic implications of this intriguing phenomenon are poorly understood and the subject of ongoing study in several laboratories; nevertheless, cross-group antagonism is a valuable tool for studying AIP structure-activity relationships and makes *agr* an especially attractive model system for the study of quorum sensing in Gram-positive bacteria.

1.2 Molecular Mechanisms of the *agr* System

The *agr* system is one of the most extensively studied quorum sensing systems, and the work of several labs has provided a relatively detailed picture of the molecular mechanisms of this pathway. The understanding of this system is nonetheless a work in progress, and the following section details what is known as well as gaps in knowledge that are yet to be filled.

1.2.1 AIP Biosynthesis

Significant progress has been made toward elucidating the mechanism of AIP biosynthesis since the initial 1997 report that AgrB is involved (29). Given

that the AIP sequences are nested within the AgrD precursors of all four *agr* groups (Figure 4A), processing of each AgrD propeptide to form a cyclic AIP requires three chemical transformations: two proteolytic cleavage steps and thiolactone formation. The order of the two cleavage events and at least some of the proteases involved are now known, but the mechanism of thiolactonization remains purely hypothetical.

The first proteolytic step removes the C-terminal tail of AgrD and is mediated by AgrB, as determined by western blot analysis of crude lysates containing epitope-tagged versions of AgrD (43). The intermediate corresponding to the N-terminal portion of AgrD plus the AIP sequence was observed only when AgrB was present, and the C-terminal AIP–AgrD fragment was not detected. If AgrB indeed functions as a protease, then one would expect to find conserved catalytic residues in the protein. There are in fact several conserved histidine, serine, and cysteine residues that potentially fit the bill. Mutagenesis experiments found that two of these residues, His77 and Cys84, are required for production of an active AIP (43). According to a topological model of AgrB (44), His77 and Cys84 are located on or near the cytoplasmic face of the protein, making them potentially accessible to AgrD (Figure 4B). Thus, AgrB may be a cysteine protease, although definitive proof of this hypothesis awaits further biochemical characterization of the purified protein.

After years of speculation that other proteins in addition to AgrB may be involved in AIP production (43-45), a recent study finally revealed that SpsB, a type I signal peptidase, carries out the second cleavage event of AgrD-I, removing the N-terminal region (46). A synthetic group I peptide substrate, NIAAYST tagged with fluorescein, was added to various lysate fractions, and the

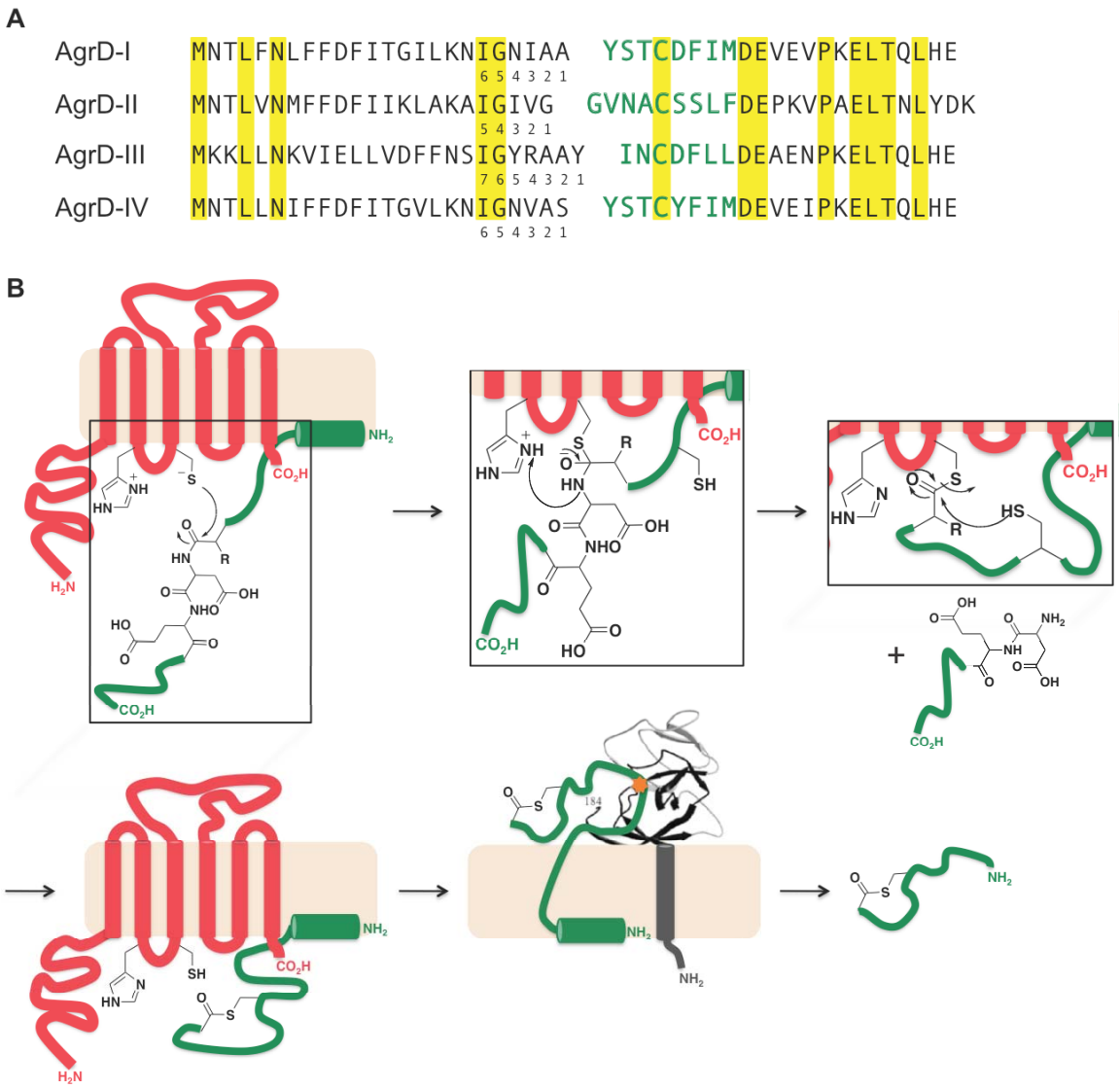

Figure 4. AgrD Sequence Alignment and Proposed Mechanism of AIP Biosynthesis. (A) AgrD sequences with the AIP portions in green and conserved residues shaded yellow. The N-terminal P sites are numbered. **(B)** Proposed mechanism of AIP biosynthesis. The AgrB (38) topology is based on Zhang et al. (44). C-terminal cleavage of AgrD (green) is mediated by His77 and Cys84 of AgrB to yield an acyl-enzyme intermediate, which is released via intramolecular transthioesterification. Translocation by an unknown mechanism allows N-terminal cleavage by the serine signal peptidase SpsB (44), via a serine/lysine catalytic diad (star). The structure is a homologous peptidase from *B. subtilis* (47).

cleavage products were identified by comparing their agarose gel retention times to synthetic standards. Through a series of fractionation and inhibition experiments, the proteolytic activity was attributed to the type I signal peptidase SpsB. The role of SpsB or other peptidases in the processing of the group II, III, and IV AIPs is yet to be determined. SpsB is identical in all *agr* groups, but the residues N-terminal to the AIP sequence within AgrD are not (Figure 4A).

There is a conserved Asp-Glu motif immediately following each embedded AIP sequence, and this acidic motif presumably acts as the recognition site for cleavage by AgrB. However, the molecular determinants underlying N-terminal processing are less obvious from sequence analysis. The N-terminal region of each AgrD peptide contains a putative amphipathic helix that anchors AgrD to the membrane, and specific processing of AgrD by AgrB is maintained even when all residues N-terminal to P10 of AgrD are replaced with an unrelated amphipathic helical sequence (48). There is a conserved Ile-Gly motif just N-terminal to each AIP sequence, but since the lengths of the AIPs vary, it is separated from the site of cleavage by a different number of amino acids in AIPs-I/IV, II, and III (Figure 4A). Moreover, the substrate used in the study that revealed the involvement of SpsB in N-terminal processing of AIP-I did not include the Ile-Gly motif (46). Important sequence requirements for cleavage by SpsB are a basic or hydrophobic residue at P2, a proline at P5 that induces a helical turn (49), and possibly an alanine at P1 (50). All four N-terminal AgrD sequences contain a hydrophobic residue at P2 and a glycine (of the Ile-Gly motif) at or adjacent to P5 that might induce a turn (Figure 4A). However, the P1 and P3 residues are also hydrophobic in most cases, and the position of the glycine is not consistent in each AgrD sequence as noted above. Furthermore,

only AgrD-I has an alanine at P1. Thus, either AgrD contains additional recognition elements that are not evident in its primary structure or proteins other than SpsB cleave the N-terminus of AgrD in groups II, III, and IV.

The group specificity of AgrD processing by AgrB is not as rigid as that of AIP–AgrC interactions. While AgrB can only process the cognate AgrD in most cases, group III AgrB (AgrB-III) can process AgrD-I to form an activator of AgrC-I, and AgrB-I can process AgrD-III to form an inhibitor of AgrC-I (37). AgrB-I & -IV may also be capable of processing both AgrD-I & -IV, as the sequences of these two groups are very similar, but this hypothesis has yet to be tested. In an effort to understand the basis for AgrB–AgrD specificity, Zhang et al. constructed a panel of AgrB-I/II chimeras by swapping homologous segments of the two proteins, then determined their ability to synthesize active AIPs from AgrD-I & II in a reporter assay (51). The authors narrowed down the determinants of specificity in AgrB-I to amino acids 43 to 67 and to residues 126 and 141 in AgrB-II. While the lack of expression and localization data for the mutant proteins is a caveat of this study, it is nonetheless interesting that the specificity determinants for AgrB-I and AgrB-II appear to be in different regions of the primary sequence. Further study will be needed to reveal the how these patches impart specificity and which features of the AgrD propeptides they recognize.

Based on all of the studies reviewed above, the working model of AIP formation is shown in Figure 4B. First, AgrD anchors to the membrane and is recognized by AgrB, which generates an acyl-enzyme thioester intermediate upon nucleophilic attack by the catalytic cysteine. Transthioesterification by the conserved AgrD cysteine mediates release from AgrB. The resulting N-terminal AgrD–AIP thiolactone intermediate is transported through the membrane by

AgrB or an unknown protein and cleaved by the SpsB signal peptidase, releasing the mature AIP into the extracellular milieu. While the proposed concomitant amidolysis, transthioesterification mechanism is appealing, the final word on this fascinating maturation process awaits the development of a reconstituted AgrB/AgrD system.

1.2.2 AIP Structure-Activity Relationships

A large effort has been made toward determining the structure–activity relationships of the four AIPs by employing synthetic methods and a rapid, quantitative *agr*P3::*blaZ* reporter assay (19, 29, 40, 41, 52-54). Efficient chemical synthesis of AIPs combine solid-phase peptide synthesis (SPPS) and solution phase chemistry (19, 52, 53). In the most efficient protocol using Boc chemistry, the linear peptide is first synthesized by SPPS on an α-thioester-generating resin, then cleaved from the solid support, and the final AIP product is obtained by spontaneous transthioesterification of the unprotected peptide α-thioester in neutral aqueous solution (52) (Figure 5). Synthetic AIPs are extremely potent agonists and antagonists of cognate and non-cognate AgrC receptors, respectively, with EC_{50} and IC_{50} values in the low nanomolar range (19). The recognition determinants for agonism are much more stringent than those for antagonism, consistent with the requirement for group-specific AIP–AgrC interactions for activation but not inhibition (19, 40, 53). For example, the exocyclic "tail" residues are dispensable for inhibition but not activation (19, 40). Indeed, some truncated AIPs consisting of only the pentapeptide macrocycles inhibit all four *S. aureus* AgrC receptors, including the cognate AgrC (Table 1). Furthermore, replacement of the AIP thiolactone linkage with a lactam or lactone

Table 1. Structure-Activity Relationships of AIPs Made Prior to this Work.

AIP Derivative	AIP Sequence	AgrC Activation				AgrC Inhibition			
		I	II	III	IV	I	II	III	IV
AIP-I	YSTCDFIM	+++	–	–	+	–	+++	+++	–
AIP-II	GVNACSSLF	–	+++	–	–	+++	–	+++	+++
AIP-III	INCDFLL	–	–	+++	–	+++	+++	–	++
AIP-IV	YSTCYFIM	++	–	–	+++	–	+++	+++	–
AIP-I–II	YSTCSSLF	–	–	–	–	+++	++	+++	+++
AIP-II–I	GVNACDFIM	–	–	–	–	++	+++	++	+
AIP-II Lactone	GVNASSSLF	–	–	nt	nt	+++	–	nt	nt
AIP-II Lactam	GVNA(Dapa) SSLF	–	+	nt	nt	+++	–	nt	nt
trAIP-II	CSSLF	–	–	–	–	++	++	+++	++
trAIP-I	CDFIM	+	–	–	–	+	+++	++	–
trAIP-IV	CYFIM	–	–	–	–	++	+++	+++	+
trAIP-I/IV 2A	CAFIM	–	–	–	–	+++	+++	+++	+++
AIP-II G1A	AVNACSSLF	–	+++	nt	nt	+++	–	nt	nt
AIP-II V2A	GANACSSLF	–	++	nt	nt	+++	–	nt	nt
AIP-II N3A	GVAACSSLF	–	–	–	–	+++	++	+++	+++
AIP-II S6A	GVNACASLF	–	+++	nt	nt	+++	–	nt	nt
AIP-II S7A	GVNACSALF	–	+++	nt	nt	+++	–	nt	nt
AIP-II L8A	GVNACSSAF	–	–	nt	nt	–	–	nt	nt
AIP-II F9A	GVNACSSLA	–	–	nt	nt	–	–	nt	nt
AIP-I Y1A	ASTCDFIM	++	nt	nt	nt	–	nt	nt	nt
AIP-I S2A	YATCDFIM	+++	nt	nt	nt	–	nt	nt	nt
AIP-I T3A	YSACDFIM	++	nt	nt	nt	–	nt	nt	nt
AIP-I/IV 5A	YSTCAFIM	–	–	–	–	+++	+++	+++	+++
AIP-I/IV 5N	YSTCNFIM	+++	–	++	–	–	+++	–	+++
AIP-I/IV 5F	YSTCFFIM	+++	–	–	+++	–	+++	+++	–
AIP-I F6A	YSTCDAIM	+	nt	nt	nt	–	nt	nt	nt
AIP-I I7A	YSTCDFAM	+	nt	nt	nt	–	nt	nt	nt
AIP-I M8A	YSTCDFIA	+	nt	nt	nt	–	nt	nt	nt
AIP-I M8I	YSTCDFII	+++	–	–	++	–	+++	+++	–
AIP-III 8 AA	YINCDFLL	nt	nt	–	nt	++	nt	++	nt
AIP-III 9 AA	AYINCDFLL	nt	nt	–	nt	nt	nt	++	nt

+, ++, +++ = weak to strong activity. – = no activity detected. nt = not tested. Dapa = diaminopropanoic acid. trAIP = truncated AIP. AA = amino acids.

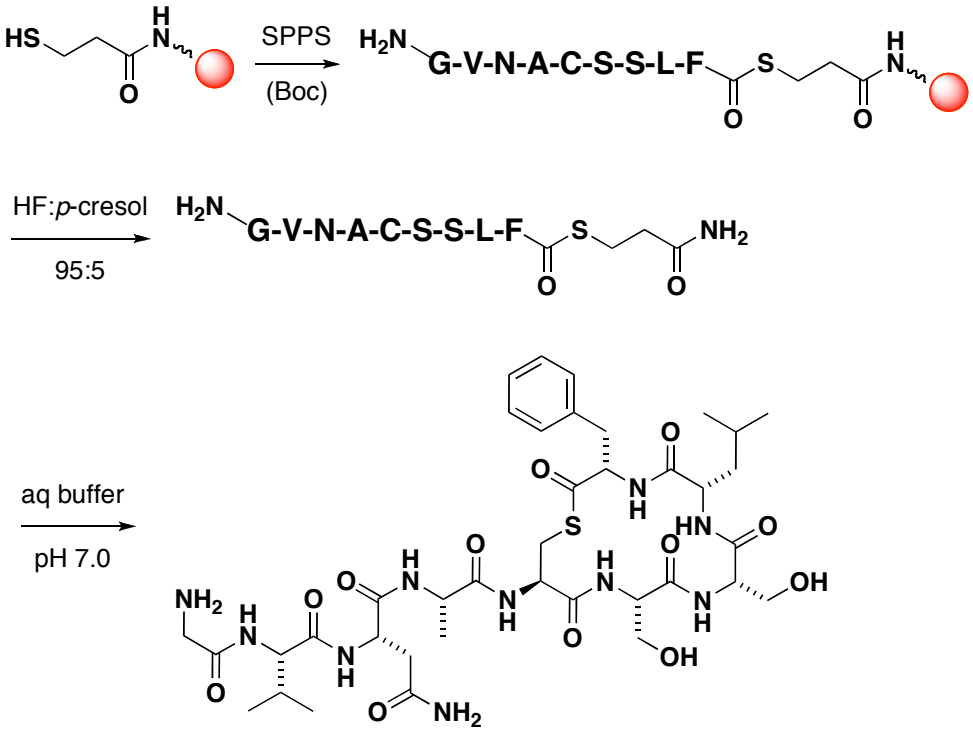

Figure 5. AIP Synthetic Route via Boc-Based Solid Phase Peptide Synthesis. A mercapto-propionic linker is synthesized on resin, and coupling of the C-terminal amino acid results in thioester formation. Chain elongation is achieved with standard Boc-based solid phase peptide synthesis (SPPS) conditions, The peptide is cleaved from the resin with anhydrous HF and cyclized via intramolecular transthioesterification upon addition of aqueous buffer at neutral pH. The synthesis of AIP-II is shown as an example.

causes a dramatic reduction in agonistic potency but has virtually no effect on antagonism (19, 53). However, linear versions of the AIPs are completely inactive, demonstrating that a macrocyclic structure is one requirement for inhibition as well as for activation (19). The presence of two bulky hydrophobic residues at the C-terminus, a strongly conserved feature of the staphylococcal AIPs (Figure 6), also seems to be critical for binding and activity since alanine substitutions at either of these positions in AIP-II result in a dramatic reduction in agonist and antagonist potency (19). Thus, the macrocycle and hydrophobic motif are important for bioactivity, and the thioester and tail residues are additionally required for receptor activation but not for binding or inhibition.

While all four *S. aureus* AIPs follow the general paradigm described above, determinants of specific AIP–AgrC interactions vary considerably among the different groups. Alanine scanning mutagenesis revealed that the key residues for receptor activation lie in different positions in the sequences of different AIPs (19, 53). For example, Asp5 of AIP-I, which lies in the macrocycle, and Asn3 of AIP-II, which is in the tail, are critical determinants for specific activation of the corresponding AgrC-I & -II receptors. Loss of these side chain functionalities in the AIP-I D5A and AIP-II N3A mutants results in loss of specificity but not activity, as the mutant peptides maintain antagonism of non-cognate AgrC receptors and are converted to antagonists of their cognate receptors (Table 1). Conversely, substitution of an amide for the acid in AIP-I D5N unexpectedly converts the peptide to an AgrC-III agonist (52). Finally, non-native appendages, such as biotin, can be conjugated to the N-terminus of AIP-I without significantly affecting activity, but the addition of one amino acid to the N-terminus of AIP-III leads to a loss of agonism (52).

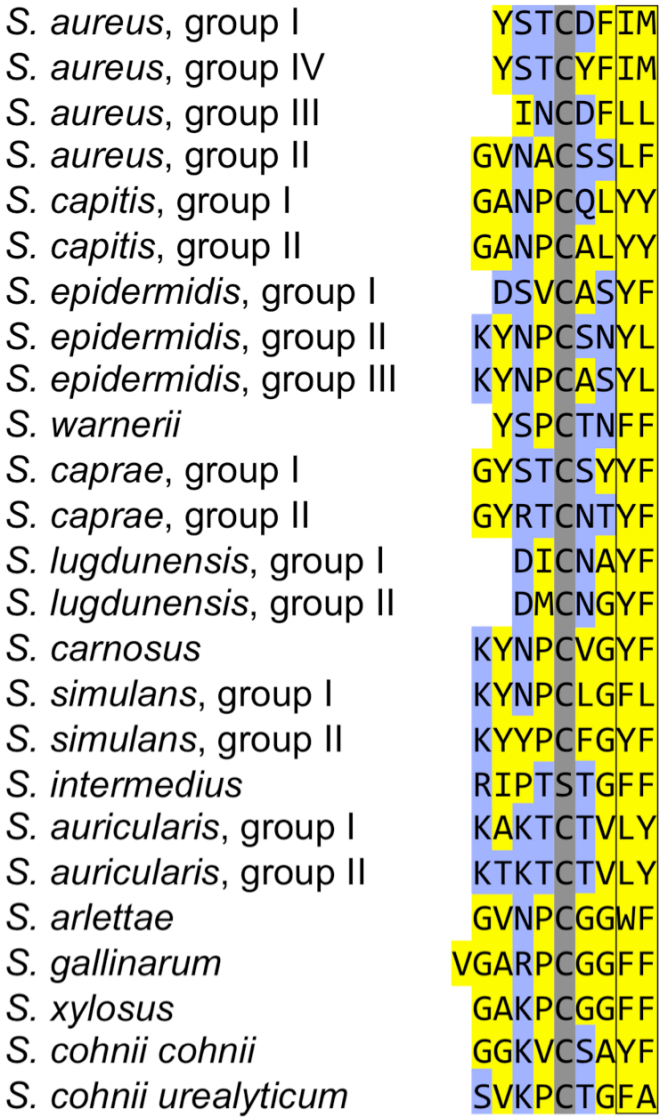

Figure 6. Sequence Alignment and Hydrophobicity Profiles of Known and Predicted Staphylococcal AIPs. Polar residues are shaded blue and non-polar residues are shaded yellow, highlighting the conserved C-terminal hydrophobic motif outlined in black. The conserved cysteine is shaded in gray, and note that the *S. intermedius* AIP contains a serine instead of a cysteine that forms a lactone instead of a thiolactone. This figure is adapted from Wright et al. (55).

The mechanism of intergroup *agr* interference is thought to be competitive antagonism of the AgrC receptor (41). The relaxed AIP sequence requirements for antagonism suggest that an AIP binding event is sufficient for blocking activation of AgrC by a cognate AIP and that AgrC activation requires an additional, specific agonistic interaction. Wash-out and order of addition experiments indicated that both agonists and antagonists bind AgrC in a reversible manner (41), consistent with competitive antagonism and contradictory to an earlier model involving receptor acylation by the thioester-containing AIP (19). To further test this idea, AgrC was treated with various concentrations of antagonistic AIPs to construct a series of AgrC activation curves (41). As expected for simple competitive antagonism, the curves shifted in dextral fashion in the presence of increasing antagonist. However, the derived Schild slopes were significantly less than unity, the value expected for simple antagonism. Moreover, inverse agonism was recently observed in constitutively active AgrC mutants (42), raising the possibility that some non-cognate AIPs induce and/or stabilize an inactive receptor conformation. Ultimately, a direct AgrC-AIP binding assay will be needed to fully understand the molecular pharmacology of agonism and antagonism of the receptor.

1.2.3 AIP Recognition by the Receptor Histidine Kinase, AgrC

AgrC is a member of the small, unique HPK_{10} family of quorum sensing receptors in Gram-positive bacteria (Figure 7A) (56). These receptors have polytopic transmembrane sensor domains and distinctive sequences surrounding the phosphorylation site histidine and catalytically important N-box and G-box residues. They also lack a D-box motif, typically involved in

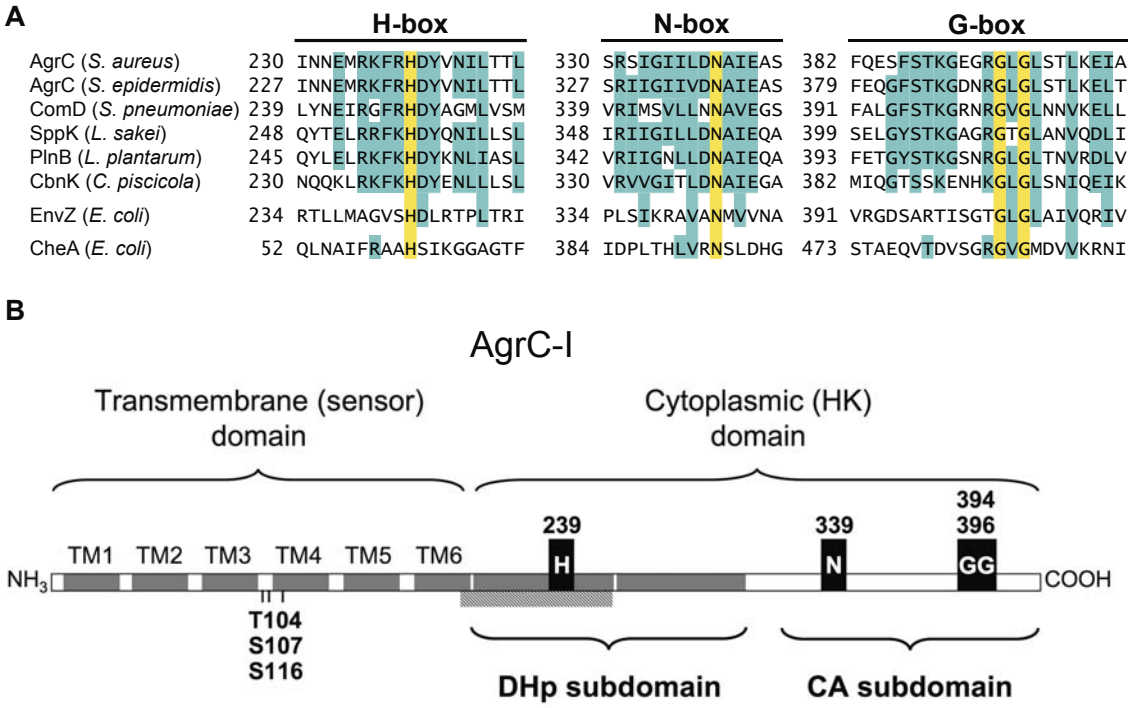

Figure 7. Histidine Protein Kinase Family 10 Alignment and AgrC Domain Structure. (A) Alignment of three conserved motifs among six HPK_{10} family members and two distantly related HPKs of Gram negative bacteria (56). Residues that are identical among all HPKs shown are shaded yellow and other conserved motifs are shaded turquoise. The H-box histidine is the site of phosphorylation, and the N-box and G-box asparagine and glycines are important for ATP binding. **(B)** The domain structure of AgrC, including the locations of the residues shaded yellow in (A). The hash marks indicate a predicted coiled-coil. The transmembrane topology of AgrC-I is shown (57), along with three residues important for recognition of AIP-I (58).

nucleotide binding, and a coiled-coil HAMP (*h*istidine kinase, *a*denylyl cyclase, *M*CP, and *p*hosphotase) domain, which links the sensor and HK domains and often plays roles in dimerization and signal transduction in other HPKs (59-61). AgrC contains a putative coiled-coil in the DHp subdomain (Figure 7B), which may mediate homodimerization; but at the outset of this study, there was no definitive proof that AgrC is a homodimer either before or after AIP binding. It is generally believed that AIP binding results in *trans*-autophosphorylation of an AgrC dimer and subsequent phosphorylation of AgrA on a conserved aspartate residue (33, 57). However, experimental evidence for this model was missing prior to this work, and the question of how AgrC transduces the extracellular AIP signal to trigger intracellular kinase activation was open.

While both activation and inhibition determinants of the AIPs have been extensively studied as described in Section 1.2.2, work to understand the corresponding specificity determinants in the AgrC receptors has just recently begun. In the first study to probe this question, AgrC sensor domain chimeras were constructed (55). Segments of the proximal and distal halves of the sensor domains were switched among different receptor specificity types, corresponding to different S. aureus agr groups. These intradomain chimeras were then tested for activation and inhibition specificity against synthetic AIPs and AIP analogues. This approach facilitated localization of the region of receptor–ligand specificity and uncovered a key hydrophobic AgrC–AIP recognition, which may explain the mechanism of staphylococcal cross-group interference.

The AgrC sensor domain comprises the first ~205 amino acids out of 430 and contains six predicted transmembrane domains (Figure 7, 8) (57). Although the sensor domains of the four AgrC receptors are divergent, the transmembrane topology appears to be highly conserved, as judged by the spacing of the putative hydrophobic α-helices (55). Residues 86-93 within the third transmembrane domain are identical in AgrC-I, III, & IV and were chosen as the junction site for the AgrC chimeras (Figure 8). The resulting constructs were transduced into a β-lactamase reporter strain (52) in order to analyze their activities. In general, the functionality of each chimera was proportional to the degree of sequence conservation between the two contributing receptors. AgrC-I & IV sensor domains share 87% sequence identity, and both AgrC-I::IV (N-terminal portion of AgrC-I fused to C-terminal portion of AgrC-IV sensor domain) and AgrC-IV::I were functional. Chimeras involving AgrC-III (~54% sequence identity with AgrC-I & IV) were functional but had unpredictable activities. Finally, chimeras involving AgrC-II, the receptor of the most divergent *agr* group, were not functional. Attempts to detect AgrC and the chimeras by western blot were unsuccessful in this study; thus, it was unclear whether the lack of function was due to poor expression or the inability to respond to the AIP agonist. The activities of the six functional chimeras, AgrC-I::IV, IV::I, I::III, III::I, III::IV, and IV::III, were tested (55).

The chimeras of the group I & IV receptors were activated by both AIP-I & IV and inhibited by AIP-II and truncated AIP-II (trAIP-II), in line with the trends observed with the two native receptors (Table 2). However, AgrC IV::I was activated much more strongly by AIP-I than AIP-IV; whereas, the opposite was

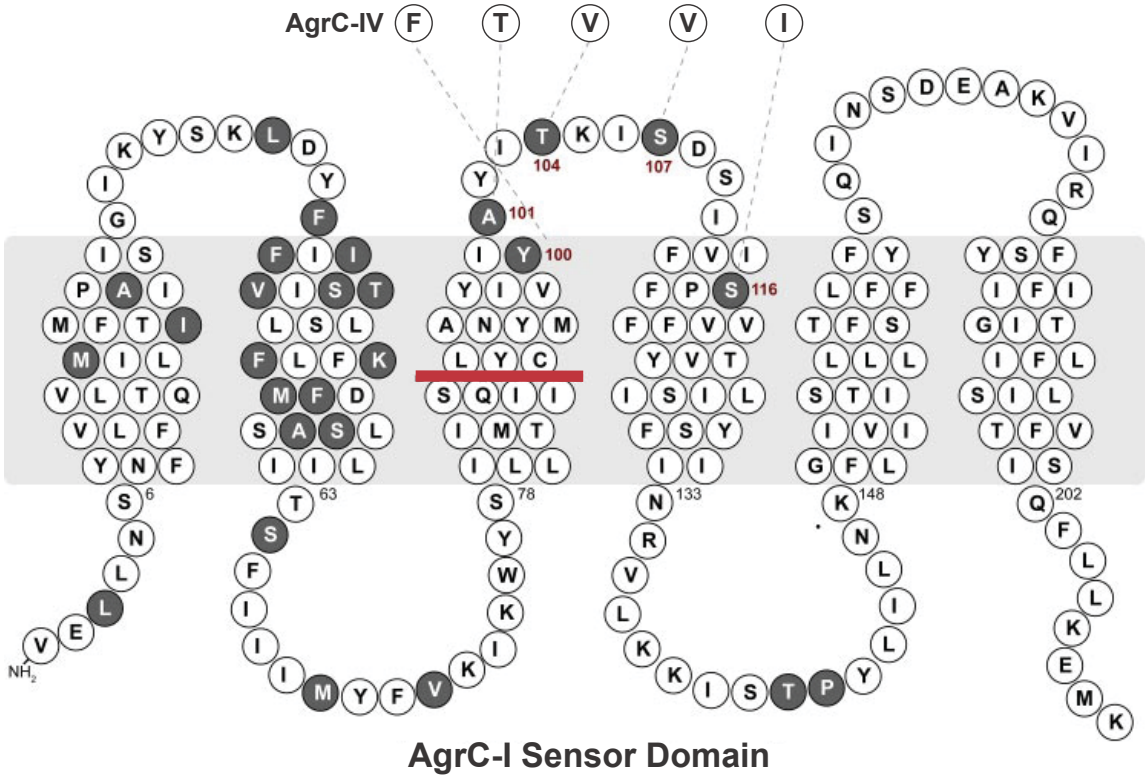

Figure 8. AgrC Topology. The red line in the third transmembrane region represents the chimeric junction used in the study by Wright et al. (55). The sequence shown is of AgrC-I, and the shaded residues indicate the amino acids that differ in AgrC-IV. Five key residues for group I/IV specificity are highlighted (58), and the corresponding amino acids of AgrC-IV are shown. This figure is adapted from Geisinger et al. (58), and the topology shown is based on Lina et al. (57).

Table 2. Activities of AIPs and AIP Derivatives against AgrC Sensor Domain Chimeras.

AIP Derivative	AgrC-I::IV	AgrC-IV::I	AgrC-III::I	AgrC-III::IV	AgrC-I::III	AgrC-IV::III
	Activation EC_{50} (nM), (95% CI)					
AIP-I	+ 1220, (1050-1410)	++ 30, (15-45)	+ 1700, (1500-1900)	-	+	++
AIP-II	-	-	-	-	+ 3100	+ 640
AIP-III	-	-	-	-	++ 48	++ 4
AIP-IV	++ 6, (5-7)	++ 120, (110-125)	-	+ 340, (290-410)	++	++
AIP-I/IV 5N	-	+ 440, (350-530)	-	-	++	++
AIP-I/IV 5A	-	-	-	-	++	++
trAIP-II	-	-	-	-	++ 160	++ 50
AIP-II N3A	nt	nt	nt	nt	++	++
AIP-II L8A	nt	nt	nt	nt	-	-
AIP-II F9A	nt	nt	nt	nt	-	-
AIP-II F9Nal	nt	nt	nt	nt	-	-
Linear AIP-I	nt	nt	nt	nt	+ 3100	+ 6700
Linear AIP-II	-	nt	nt	nt	-	+
	Inhibition IC_{50} (nM), (95% CI)					
AIP-I	nt	nt	nt	+	nt	nt
AIP-II	+	+	+	+	nt	nt
AIP-III	-	+	+	+	nt	nt
AIP-IV	nt	nt	+	nt	nt	nt
AIP-I/IV 5N	+	nt	+	+	nt	nt
trAIP-II	+	+	+	+	nt	nt
AIP-II L8A	nt	nt	nt	nt	nt	-
AIP-II F9A	nt	nt	nt	nt	nt	-
Linear AIP-II	-	nt	nt	nt	-	nt

Chimeras are notated as AgrC-X::Y, referring to the *agr* group identities of the N-terminal (X) and C-terminal (Y) portions of the sensor domain. Precise EC_{50} and IC_{50} values and 95% confidence intervals are given if known. Number of plus (+) symbols indicates the approximate activity. + = EC_{50} or IC_{50} value <200 nM. ++ = EC_{50} or IC_{50} value >200 nM. - = no detectable activity. nt = not tested.

true for AgrC-I::IV (Table 2). As previously suggested by Lina et al. (57), this result indicates that the major determinant of AIP recognition is in the distal, C-terminal region of the sensor, at least within *agr* groups I & IV. The corresponding moiety within the AIP that makes the defining group-specific contact with the AgrC distal region is the residue at position five within the thiolactone ring, as it is the only difference between AIP-I & IV (Figure 3). Furthermore, an AIP derivative with asparagine at this position (AIP-I/IV 5N) that activates AgrC-I but inhibits AgrC-IV (52), has precisely the same effects with the AgrC-IV::I & I::IV chimeras, activating the former and inhibiting the latter (Table 2). Nonetheless, the N-terminal, proximal region of AgrC also contributes a significant role in receptor specificity, as AIP-I was much more potent against AgrC-I::IV than against the native AgrC-IV (Table 1 & 2).

The sensor domain chimeras in which the proximal region was derived from AgrC-III followed the trend of the AgrC-I/IV chimeras but were much less sensitive to activation by the AIPs. For example, AgrC-III::I was activated by AIP-I at concentrations two orders of magnitude higher than that required to activate AgrC-IV::I and was not cross-activated by AIP-IV (Table 2). Similarly, AgrC-III::IV was activated by AIP-IV but not AIP-I or III. In fact, AIP-IV and AIP-I/IV 5N inhibited AgrC-III::I, and AIP-I inhibited AgrC-III::IV, adding support to the idea that the proximal region of the AgrC sensor plays a role in specificity, albeit inferior to that of the distal region.

The results with the final AgrC-I::III & IV::III chimeras were quite surprising. Akin to the behavior of the chimeras described above, they were preferentially responsive to AIP-III; however, both of these chimeras were also strongly activated by many other AIP analogs (Table 2). These included several

potent inhibitors of AgrC-III, such as AIP-I, II, & IV (19, 37), and inhibitors of all four agr groups, such as AIP-I D5A and trAIP-II (40, 52). Even linear AIP-I & II, which are generally inert against AgrC (37, 53), were found to weakly activate one or both of these chimeras. Moreover, no AIP or AIP derivative tested could inhibit activation of either receptor. Whereas the requirements for activation are typically much stricter than those for inhibition, AgrC-I::III & IV::III seemed poised for activation by any ligand that can bind. These chimeras appeared to no longer be regulated by putative group-specific determinants that are presumed to be responsible for activation of native AgrC receptors.

One commonality among all the AIPs and AIP derivatives that activated AgrC-I::III & IV::III and, in fact, among all known AIPs (Figure 6) is the presence of two hydrophobic, usually bulky amino acids at the C-terminus. With the exception of the central cysteine, no other positions in the AIPs are so strongly conserved. Replacement of the corresponding residues with alanine in the AIP-II derivatives L8A & F9A abolished agonism and antagonism of AgrC by these peptides (Table 1) (19). These observations, along with the results involving AgrC-I::III & IV::III led to the hypothesis that an AIP agonist makes two types of interactions with the receptor: a general hydrophobic interaction mediated by at least one of the C-terminal nonpolar residues in the peptide; and a sequence-specific contact that results in activation via change(s) in receptor conformation. According to this premise, a distortion within the AgrC-I::III & IV::III chimeras bypasses the need for specific contacts, and all that is required for activation is the ability to bind. A major prediction of this hypothesis is that removal of one or both bulky, hydrophobic C-terminal side chains will eliminate binding and thus eliminate activation of the AgrC-I::III & IV::III chimeras.

To test this prediction, AgrC-I::III & IV::III were treated with AIP-II L8A & F9A and found to be completely insensitive to these peptides (Figure 9 and Table 2). In contrast, AIP-II N3A and AIP-I D5A, which contain alanine substitutions at sites crucial for activation of native AgrCs and inhibit all four *S. aureus agr* groups (41, 52), were strong activators of AgrC-I::III & IV::III. This finding suggests that an alanine replacement at either of the C-terminal positions in the hydrophobic patch of the AIP causes a significant defect on receptor binding. However, an AIP-II variant with naphthylalanine at position nine, designed to increase the C-terminal hydrophobicity and therefore the potency of AIP-II failed to activate the native and chimeric AgrC receptors, suggesting that a steric constraint superseded the hydrophobic interaction in this case.

Based on the finding that the determinants for specific recognition of AIP-I vs. IV are localized to the C-terminal region of the AgrC sensor domain, Geisinger et al. (58) set out to find the individual amino acids responsible for the ligand specificity. Of the 27 amino acid differences between the AgrC-I & IV sensor domains, only seven are located in the C-terminal region of interest (Figure 8). According to a topological model of AgrC (57), five of those seven residues are located in or near one extracellular loop, while the other two are facing the cytoplasm. Thus, the five residues of interest in AgrC-IV were systematically replaced with the corresponding amino acids in AgrC-I, and reciprocal mutations were made in AgrC-I. The activities of the resulting constructs showed that the main specificity determinants between AgrC-I & IV are indeed the five divergent residues in the second extracellular loop.

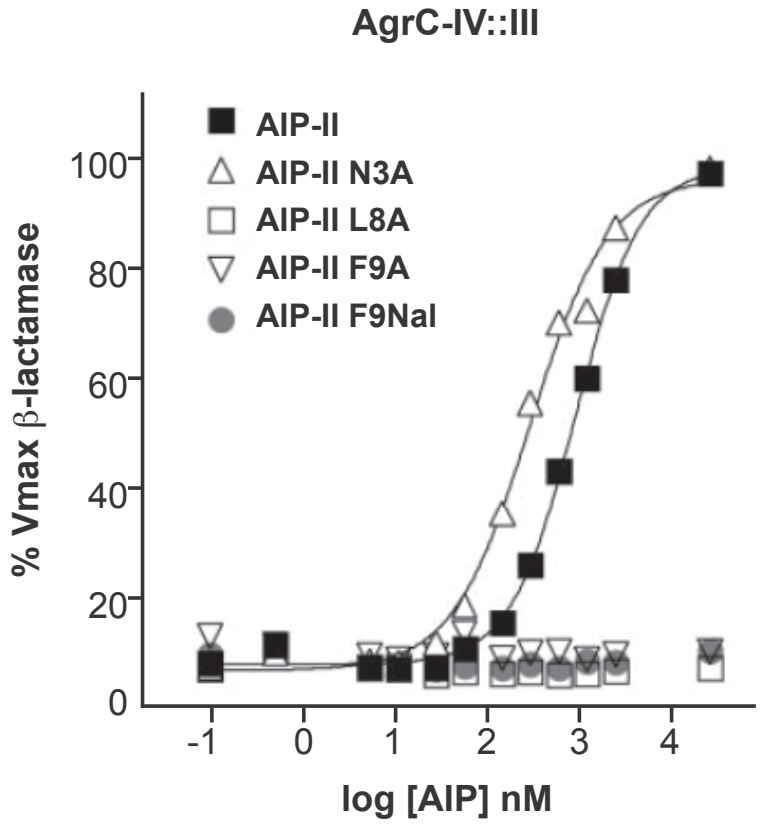

Figure 9. Dose-response Curves for AIP-II and Derivatives against AgrC-IV::III. Data are presented as percent maximal activation of the receptor by AIP-II expressed as Vmax β-lactamase activity. All data points represent two to three replicates, and error bars represent standard error measurements (SEM). Nal = naphthylalanine.

Initially, all five residues (100, 101, 104, 107, and 116) were swapped between AgrC-I & IV, and the activities of the resulting constructs, AgrC-IV (100-116 C-I) and AgrC-I (100-116 C-IV), were quantified in a β-lactamase reporter assay (52). The mutations switched the specificities of both receptors almost completely (Table 3), indicating that the determinants of AgrC specificity for groups I & IV indeed lie in the central extracellular loop (Figure 8). AgrC-IV (100-116 C-I) was more sensitive to AIP-I than AIP-IV with EC_{50} values matching those for wild type (WT) AgrC-I and vice versa, the only exception being that AgrC-I (100-116 C-IV) was more sensitive to AIP-I than WT AgrC-IV.

To assess the individual contributions of each residue, many AgrC-I & IV mutants were constructed in which one to four of the residues of interest were switched between the two receptors. This analysis facilitated further narrowing of the major specificity determinants to Thr/Val104, Ser/Val107, and Ser/Ile116, although the specificity switch exhibited by these three changes was not quite as robust as when all five residues were swapped (Table 3).

Examination of the key specificity determinants of the AIPs and AgrCs revealed an interesting trend. Position five of AIP-I (Asp) and positions 104, 107, and 116 in AgrC-I (Thr, Ser, Ser) are all polar amino acids, while the corresponding positions in AIP-IV (Tyr) and AgrC-IV (Val, Val, Ile) are all nonpolar (Figure 8). Thus, Geisinger et al. (58) hypothesized that polar versus nonpolar interactions drive specificity in this case. Position five of AIP-I/IV was replaced with different polar and nonpolar residues to test whether these AIP derivatives also followed the observed trend. Whereas the activity of AIP-I/IV 5N was consistent with the hypothesis and activated WT AgrC-I but not AgrC-IV; surprisingly, AIP-I/IV 5L also activated AgrC-I but not AgrC-IV (Table 3). In

Table 3. Activities of AgrC-I/IV Mutants.

AgrC Variant	AIP-I	AIP-IV	AIP-I/IV 5N	AIP-I/IV 5L
	Activation EC_{50} (nM), (95% CI)			
AgrC-I	11, (9-12)	100, (86-130)	85, (61-120)	20, (15-28)
AgrC-IV	1500, (1000-2100)	16, (13-20)	–	–
AgrC-IV (100-116 C-I)	25, (22-28)	140, (130-160)	180, (160-200)	290, (170-490)
AgrC-I (100-116 CI-IV)	44, (34-58)	7, (6-8)	nt	nt
AgrC-IV (104, 107, 116 C-I)	37, (31-43)	45, (38-55)	130, (110-160)	19, (17-22)
AgrC-I (104, 107, 116 C-IV)	520, (440-620)	290, (250-330)	nt	nt
AgrC-IV (107, 116 C-I)	50, (40-63)	56, (45-71)	150, (130-170)	29, (23-36)
AgrC-I (107, 116 C-IV)	450, (330-610)	100, (85-120)	nt	nt
AgrC-IV (100, 101 C-I)	1100, (1000-1300)	620, (560-670)	–	nt
AgrC-I (100, 101 C-IV)	8, (7-9)	15, (12-18)	nt	nt

95% CI = 95% confidence interval. – = no activity up to the highest concentration tested, > 10 μM. nt = not tested.

fact, AIP-I/IV 5F is the only position five substitution that has been shown to strongly activate AgrC-IV (Table 1) (52). These results suggest that the ligand specificity of AgrC-I is broader than that of AgrC-IV, and further work will be required to determine the exact nature of the interaction of position five of AIP-IV with AgrC-IV.

In a subsequent, similar study, Jensen et al. (62) swapped the five key residues in the middle extracellular loop of AgrC-I & IV plus residues in or near the first extracellular loop (Figure 8). When residues 35, 38, 39, 41, 42, 44, and 45 of AgrC-IV were mutated to the corresponding amino acids of AgrC-I, the potency of AIP-IV dropped more than two orders of magnitude, and the reciprocal substitutions in AgrC-I abolished the ability of AIP-I to activate it. However, inhibition did not appear to be affected by the mutations, as AIP-I/IV 5A was a potent inhibitor of both mutant receptors. This result suggests that the loop one residues contribute important determinants for activation, consistent with the earlier findings using AgrC sensor domain chimeras (55). An alternative possibility is that the seven replacements in AgrC result in poor expression that explains the weakened activation relative to WT receptors.

1.2.4 The AgrA Response Regulator

The AgrA RR contains 238 amino acids split into two main domains, as predicted by homology modeling (Figure 10A) (63). The putative phosphorylation site aspartate is in the N-terminal CheY-like receiver domain, which presumably modulates DNA binding by the C-terminal LytTR domain. The majority of RRs bind DNA via helix-turn-helix or winged helix motifs, but RRs of the LytTR family contain a novel fold (63, 64). Recently, a crystal structure of residues 137-238 of AgrA in complex with a 15-base pair DNA duplex showed

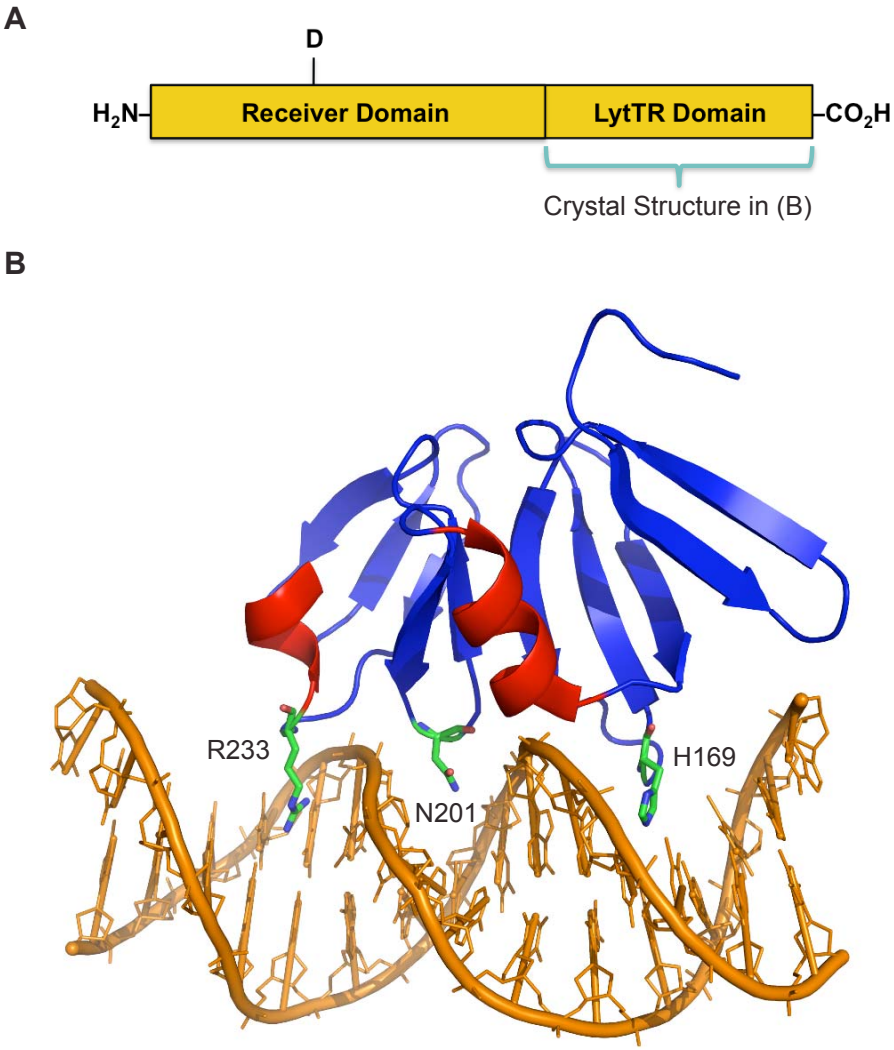

Figure 10. AgrA Domain Structure and LytTR Domain Crystal Structure. (A) AgrA domain structure. The N-terminal CheY-like receiver domain is phosphorylated by AgrC, causing an activating conformational change in the C-terminal DNA binding LytTR domain. The approximate position of the phosphorylation site aspartate based on sequence alignment is shown. **(B)** The structure of the LytTR domain in complex with DNA was recently solved (64), demonstrating that AgrA has a novel ten-stranded β fold arranged into three antiparallel β sheets. Three key residues that interact with DNA are indicated. The β strands are colored blue, and the helices are colored red.

that it contains a novel 10-stranded β fold (Figure 10B) (64). His169 and Arg233 make base-specific contacts with DNA, and subsequent mutagenesis confirmed they are essential for DNA binding. However, the structure did not provide an explanation for the previous observation that the appropriate length of the C-terminus is essential for activity (65). A frameshift mutation in *agrA* resulting in a C-terminal amino acid sequence of KKNIIR instead of KKI is the cause of a delay in RNAIII production and lack of hemolytic activity in *S. aureus* strain RN4220. Addition of acetyl phosphate promotes homodimerization of AgrA, suggesting that the phosphorylated dimer is the active species (33). Thus, the AgrA C-terminus may be important for homodimerization, stability, or other protein–protein interactions (33, 64). Additionally, the conformational changes associated with phosphorylation and how they regulate the LytTR domain as well as the recognition of and interaction with AgrC by AgrA are yet to be characterized.

1.2.4 Output of the *agr* Response

The primary effector molecule of the *agr* response, RNAIII, acts as both a messenger and antisense RNA to carry out multiple functions (13). The 514 nucleotide transcript contains fourteen hairpin stem loops (Figure 11), including three C-rich hairpins, which is unusual for an AT-rich organism such as *S. aureus* (66). Nucleotides 85-165 encode the exotoxin δ-hemolysin, and 300 nucleotides downstream, the 3′-end regulates its expression through a poorly understood mechanism (66, 67). The RNAIII 5′-region directly up-regulates *hla* (α-hemolysin) by annealing to the mRNA translation initiation region, causing a conformational change that unmasks the ribosomal binding site (68). Conversely, the RNAIII 3′-end binds and occludes the ribosomal binding site of mRNAs targeted for down-

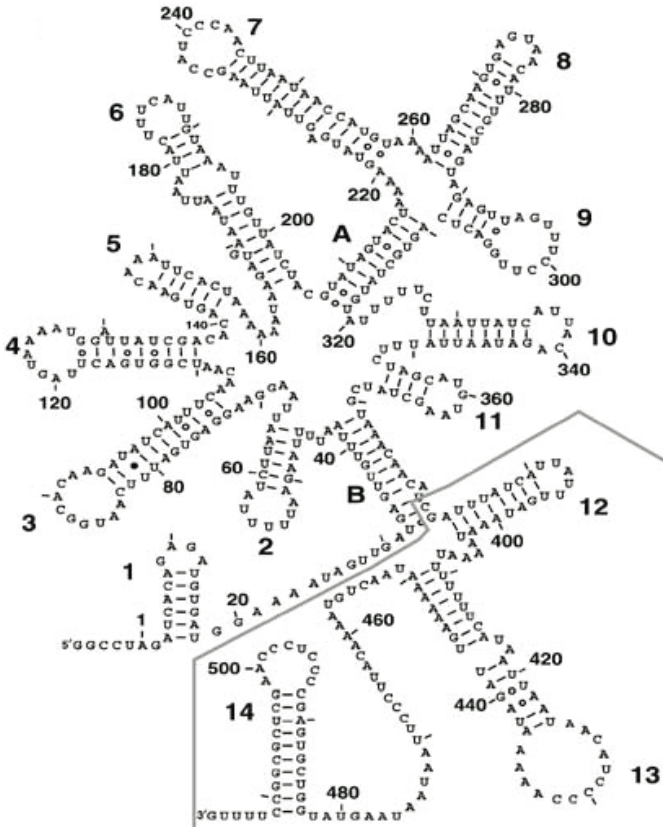

Figure 11. RNAIII Structure. The fourteen hairpin loops are numbered, as are the nucleotides. This figure is taken from Huntzinger et al., and the line drawn through the image pertains to experiments completed in that study (70).

regulation, including several cell surface-associated virulence factors and the pleiotropic transcription factor *rot* (26, 69, 70). The expression of other virulence genes modulated by *agr* may also be directly mediated by RNAIII, by regulation of transcription factors in addition to Rot, or by undiscovered targets of AgrA (35).

Until recently, the regulation of virulence via induction of transcription at the *agr* P2 and P3 promoters by AgrA was the only known output of the *agr* response. However, Queck et al. observed that genes related to carbohydrate and amino acid metabolism and staphyloxanthin pigment biosynthesis are down-regulated upon *agr* activation by a mechanism they were unable to determine (35). The effect was observed even when RNAIII was deleted, and AgrA is unlikely to be involved since the target genes lack consensus AgrA binding sequences (35). Furthermore, phenol-soluble modulins (PSMs), virulence factors prevalent in community-acquired strains of MRSA (as opposed to hospital-acquired strains) (36), were found to be up-regulated by the *agr* response independent of RNAIII expression (35). In this case, the promoter regions contain AgrA consensus binding sequences, and AgrA was shown to bind and activate transcription of PSMs.

1.3 Goals of this Work

The overall goal of this work was to elucidate molecular mechanisms of AgrC signaling in order to further develop the understanding of the polytopic peptide-sensing HPK_{10} receptor family and of virulence regulation in *S. aureus*. As described above, the requirements for inhibition of AgrC are significantly less stringent than those for activation, and while many AIP derivatives lose the

ability to activate, almost all of those tested maintain inhibition. Hence, one aim was to determine the minimal determinants within AIPs for inhibition of AgrC. This endeavor necessitated a streamlined AIP synthesis; thus, the development of a convenient method for the synthesis of Fmoc-based thioester peptides was an additional goal. While those efforts were fruitful, the major focus of this work was to elucidate the mechanism of AIP-induced activation of AgrC. The paradigm for HPK signaling is that they function as dimers and undergo *trans*-autophosphorylation (32, 71), but it was not known whether AgrC or other HPK_{10} receptors follow this model. The first step was to resolve this uncertainty, and if the hypothesis that AgrC follows this precedence is correct, a further aim was to determine whether or not AIP binding affects oligomerization. A related goal was to determine the AIP–AgrC stoichiometry. Finally, perhaps the most intriguing question regarding the mechanism of AgrC signaling is how recognition of the AIP signal is transduced through the receptor to activate the kinase domain, and the last aim of this work was to shed light on that issue.

Chapter 2: Inhibitors of AgrC Prepared by Fmoc-Based Peptide Synthesis

2.1 Introduction

Despite the fact that many AIP derivatives have been synthesized and characterized (19, 40, 41, 52-54) (Table 1), linear AIPs and those missing bulky hydrophobic side chains at the C-terminus are the only variants found thus far to lack inhibitory activity (19, 55). Even substantial modifications, which dramatically reduce the ability to activate, compromise inhibitory potency only slightly if at all. For example, removal of the four tail residues of AIP-II, nearly half of its nine amino acids, has little effect on inhibition of AgrC-I, -III, & -IV, and converts the peptide from an agonist of AgrC-II to an antagonist (40). These observations raised the question of how much further the AIP structure can be minimized before losing the ability to inhibit AgrC, and the truncated AIP-II (trAIP-II) pentapeptide provided an ideal starting point. In order to define the minimal AIP pharmacophore and discover the minimal determinants for AgrC inhibition, ten trAIP-II analogues were synthesized. The peptide backbone, side chains, thiolactone linkage, and N-terminus were modified to systematically probe each structural element of the molecule. To rapidly synthesize these peptides in parallel, an Fmoc-based method was preferred to avoid a bottleneck at the cleavage step, which requires use of anhydrous HF in Boc-based methods. The synthesis of Fmoc-based thioester peptides has been a longstanding problem due to the incompatibility of thioesters with basic Fmoc deprotection conditions. While many methods have been reported, none have gained widespread use owing to various drawbacks, including lack of generality and low yields (72, 73). Therefore, a new Fmoc-based AIP synthesis was developed for this study that is also generally useful for the preparation of linear thioester peptides.

2.2 A New Synthetic Method for Thioester Peptides and AIPs via Fmoc-SPPS

An attractive starting point from which to develop a more convenient method for the generation of thioester peptides by Fmoc-SPPS was the latent thioester-linker work of Botti et al. (74) and Warren et al. (75). In these methods, C-terminal thioesters are masked as esters during amino acid coupling steps then revealed via an intramolecular O to S acyl shift. Whereas the Warren methodology requires a solution-phase coupling step with a partially protected peptide, the simpler Botti methodology seemed more amenable to adaptation for use in an AIP synthesis. In this approach, Fmoc-cysteine (*t*-butylthio)-OH is first coupled to PEGA resin, followed by α-amino diazotization and subsequent hydrolysis under aqueous conditions to afford an α-hydroxy cysteine resin (Figure 12A). After chain elongation and cleavage from the resin, reduction of the cysteine side-chain disulfide leads to an O to S acyl shift, resulting in α-thioester formation. The authors chose thiophenol as the reducing agent (Figure 12B), as the main motivation of the work was to generate thioesters for use in native chemical ligation (76). However, TCEP was used for AIP synthesis (Figure 12D) to avoid reduction of the AIP thiolactone. AIPs were successfully generated with this slight adaptation of the Botti method, but the isolated yields were very low. This result highlights the main drawback of this method: the linker is synthesized on resin, consequently limiting the resin options to those that have good swelling properties in water that often result in low yields. To overcome this limitation, a solution-phase synthesis of 2-(*t*-butyl-dimethyl-silanyloxy)-3-*t*-butyldisulfanyl-propionic acid (**5**) (Figure 12C) was designed to make a version of the linker that can be coupled to any resin using standard approaches.

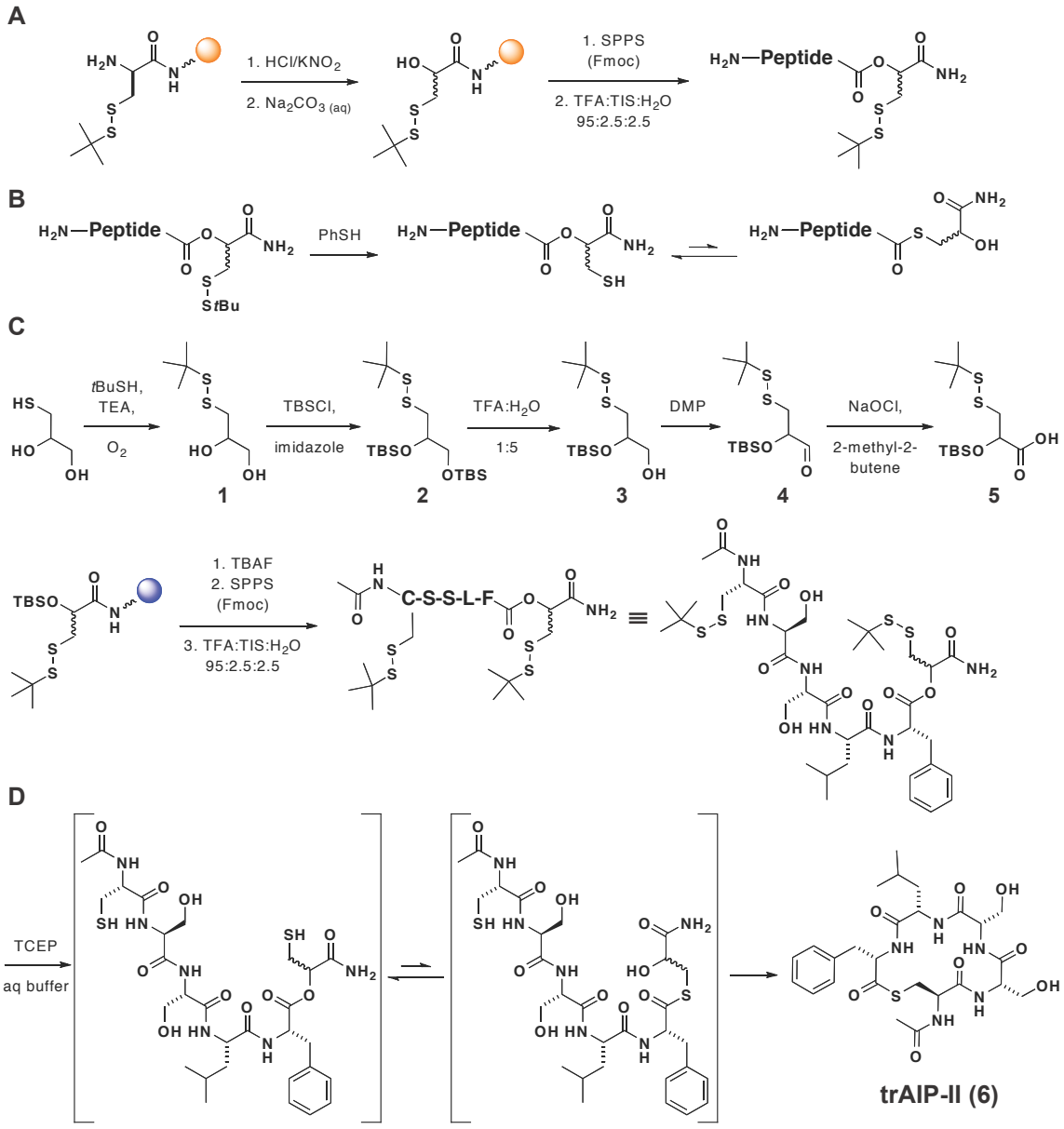

Figure 12. Synthetic Routes for Fmoc-Based Thioester Peptides. (A) Synthetic scheme of Botti et al. (74). Diazotization of the α-amine on PEGA resin (orange) in aqueous conditions yields an α-hydroxyl. **(B)** Thiophenol reduces the linker disulfide, and the resulting acyl shift reveals the thioester. **(C)** New Fmoc-based AIP synthesis. The α-hydroxy cysteine linker (**5**) is made from thioglycerol and coupled to Rink resin (blue) via standard SPPS. **(D)** Addition of TCEP results in one-pot reduction, O to S acyl shift, and transthioesterificaiton, yielding the AIP.

Initial efforts to generate α-hydroxy-cysteine-based linkers in solution from *t*-butylthiol protected L-cysteine proved to be unsatisfactory, primarily due to the poor yields associated with the diazotization/hydrolysis step. Therefore, we adopted an alternate route in which the linker was generated in five steps from commercially available thioglycerol, with an overall yield of 31%. As shown in Figure 12C, the thiol group was first protected as the *t*-butyl disulfide to give a 1,2-diol (**1**). Attempts to selectively oxidize the primary alcohol directly to the carboxylic acid using TEMPO were unsuccessful. Instead, protection of both alcohols with *t*-butyl-dimethyl silanyloxy (TBS) groups, followed by selective removal of the primary TBS group facilitated selective oxidation to the acid in two steps, using Dess-Martin periodinane and subsequent treatment with sodium chlorite.

An updated version of the synthesis was developed in collaboration with Mette Jensen, Maya Bar-Dagan, and Matt Pratt since the initial publication of this method (77). The new steps avoid the requirement of addition of a large excess of the extremely malodorous *t*-butylthiol to form the disulfide protecting group (Figure 12C and Materials and Methods). Instead, *t*-butylthiol is first activated for disulfide exchange by conjugation to 2,2′-dithiodipyridine, necessitating only 1.1 equivalents of *t*-butylthiol relative to thioglycerol as opposed to ten or more.

trAIP-II was chosen as the first AIP synthesized using the new linker, as it is a well characterized peptide (40) and would be useful for the subsequent study of minimal inhibitory AIP determinants. The α-hydroxy cysteine linker was first coupled onto Rink-amide polystyrene resin with HBTU and DIEA (Figure 12B). Following a capping procedure and on-resin removal of the TBS group with

TBAF, the C-terminal phenylalanine was double coupled to the linker using HBTU in the presence of catalytic DMAP. HPLC–MS analysis of the cleaved amino-acylated resin indicated that this loading procedure was highly efficient, as no free linker was observed in the crude mixture (data not shown). Peptide chain assembly was then performed using standard Fmoc-SPPS protocols, and the peptide was cleaved from the resin with TFA and water and TIS as scavengers. HPLC–MS analysis of the crude cleavage mixture revealed the presence of two closely eluting peaks, both with the mass expected for the desired linear peptide–linker product. The first panel in Figure 13A shows the crude cleavage mixture obtained for the linear precursor to trAIP-II. The two products were presumed to correspond to the two expected diastereomers that result from use of the racemic linker. No attempts were made to purify these putative stereoisomers since the linker would eventually be cleaved off during the cyclization reaction. Indeed, incubation of crude, linear trAIP-II in an aqueous buffer containing the reducing agent TCEP resulted in the collapse of the two peaks into a single new peak with a mass consistent with the desired thiolactone peptide (Figure 13). Homonuclear ^{1}H 2-D NMR analysis confirmed that the reaction product was trAIP-II (**6**), and the 2-D ^{1}H TOSCY spectrum was identical to an authentic sample of trAIP-II prepared by the Boc-SPPS route (Figure 5) (see Appendix for chemical shift assignments).

The macrocyclization reaction was found to be the most efficient between pH 6.6-6.8, taking approximately 1-2 h to reach completion. If the pH was below 6.6, the linear, reduced peptide intermediate predominated and proceeded very slowly to product, presumably due to a slow rate of O to S acyl shift. At higher pH values, hydrolysis of the thioester to give the α-carboxy-peptide became

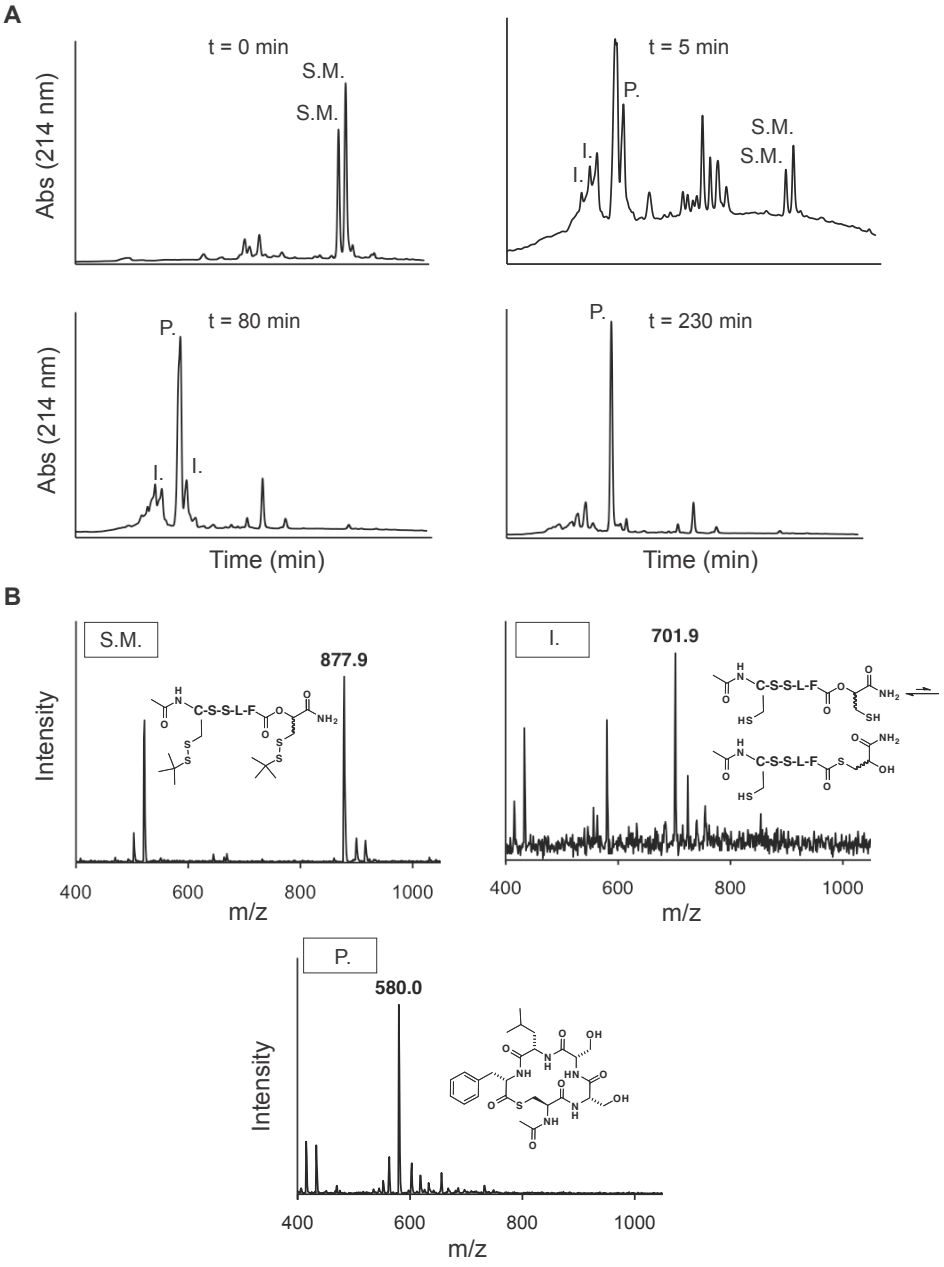

Figure 13. HPLC–MS Analysis of the Macrocyclization Reaction. (A) HPLC chromatograms of the crude reaction mixture at the time points indicated. S. M. is the protected, linear trAIP-II starting material. I. is the reduced (deprotected) intermediate(s), and P. is the product, trAIP-II. **(B)** Mass spectra of the corresponding peaks.

increasingly problematic. Within the appropriate pH range, analysis of the reaction mixture after five minutes revealed the presence of several intermediates with a mass consistent with the fully reduced version of linear trAIP-II (Figure 13). At least one of these intermediates was presumed to correspond to the linear α-thioester generated in situ following the O to S acyl shift, although it is likely a minor component due to the greater stability of oxyesters over thioesters (78). Furthermore, the linear α-thioester peptide is an obligatory intermediate in the proposed cyclization mechanism (Figure 14B), leading to the final transthioesterification step, which acts as a thermodynamic sink in the reaction. Given that acyl transfer from a hydroxyl group to a thiol group is highly unfavorable, the O to S acyl shift is predicted to occur via the entropically preferred five-membered ring as opposed to attack by a distal thiol. To directly test whether or not the N-terminal cysteine could attack the oxyester, a trAIP-II derivative with an unprotected N-terminal thiol group and protected linker thiol group was subjected to the cyclization conditions without TCEP. Consistent with the proposed mechanism, cyclization of this peptide was not observed; however, upon the addition of TCEP, the peptide cyclized efficiently (Figure 14). Thus, the N-terminal thiol attacks only the thioester that is generated by deprotection of the linker and subsequent acyl shift.

2.3 Minimal Determinants for AIP Inhibition of AgrC

The strategy used to elucidate the minimal determinants of AgrC inhibition was to systematically perturb each structural aspect of the already partially minimized trAIP-II derivative of AIP-II. Guided by previous SAR carried out with AIP-II (19, 40), ten AIP-II analogues based on the trAIP-II

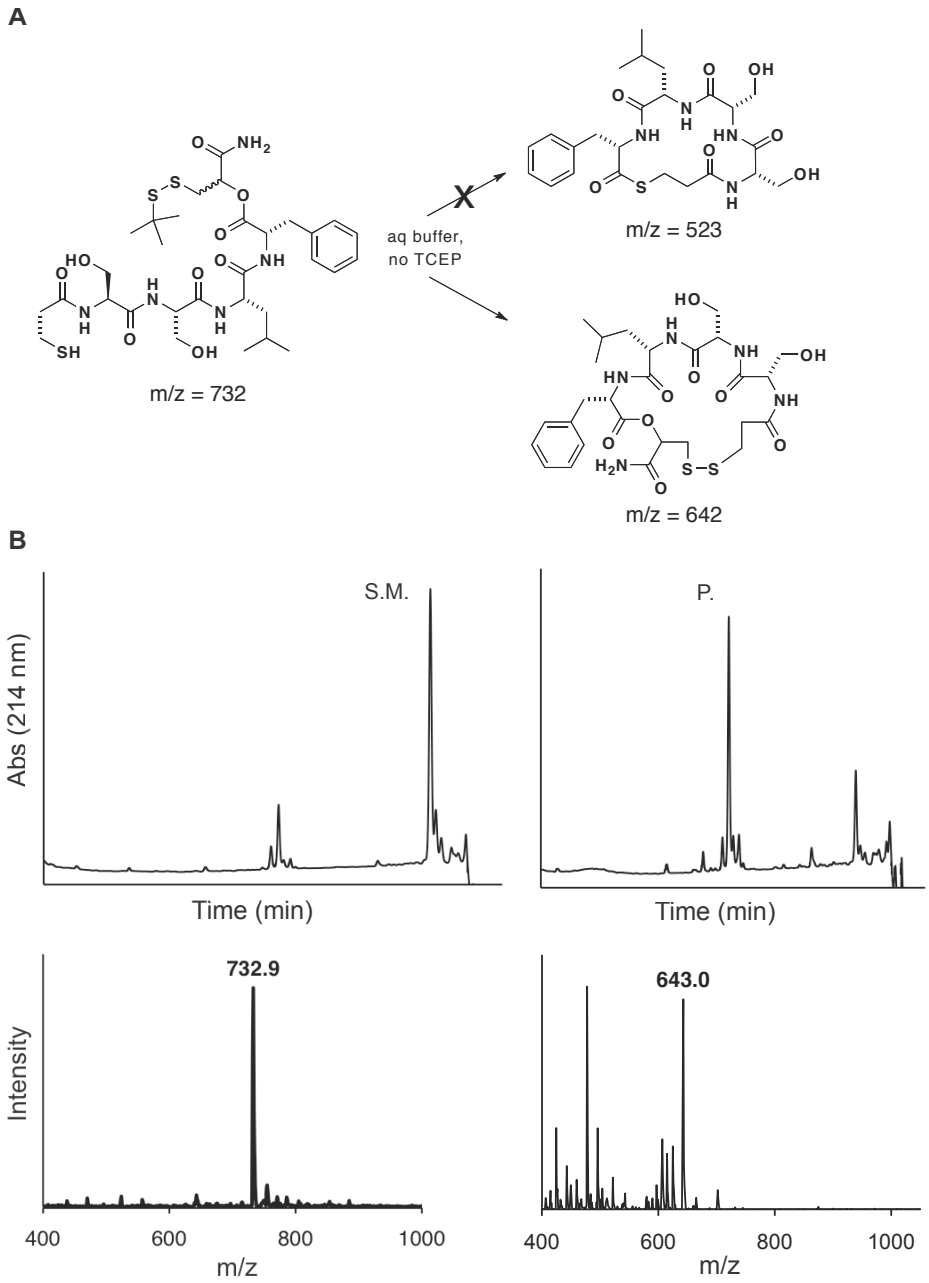

Figure 14. Testing the Proposed Mechanism of Macrocyclization. (A) Two possible products upon treatment of the partially unprotected peptide with the macrocyclization buffer minus TCEP. The thiolactone was not observed, only disulfide formation. **(B)** HPLC chromatograms and corresponding mass spectra of the reaction. The starting material (S. M.) was nearly completely consumed, and the product (P.) was the cyclic disulfide, not the thiolactone.

scaffold were synthesized (Figure 15) to test the importance of the peptide backbone, side chains, thiolactone linkage, and N-terminus for inhibition. In order to compare trends for both cognate and non-cognate inhibition, the activities of all analogues were tested against AgrC-II and AgrC-I, respectively. This SAR analysis led to the identification of a minimal pharmacophore structure with a reduced peptidic character that retains antagonism of AgrC.

2.3.1 Design and Synthesis of trAIP-II Analogues

Previously, alanine scanning of full-length AIP-II showed that the two serine hydroxyl groups of residues six and seven are not necessary for biological activity (Table 1) (19). Given this observation, the serines were replaced with glycines either individually or in combination in the first three trAIP-II analogues (Figure 15). The same alanine scanning study showed that the two C-terminal hydrophobic side chains are required for both activation and inhibition (19). Moreover, the inability of AIP-II L8A and AIP-II F9A to activate the promiscuous AgrC-I::III & IV::III sensor domain chimeras (55) confirmed that the conserved hydrophobicity of the two C-terminal residues (Figure 6) is required for biological activity. Therefore, the leucine and phenylalanine side chains were not perturbed in this study. Next, each amide in the macrocycle was *N*-methylated to probe interactions involving the AIP backbone, which had yet to be evaluated in any AIP. To test whether these side-chain and backbone modifications could be combined, the serines were completely removed and replaced with a methylene linker derived from 5-aminopentanoic acid in peptide **14** (Figure 15).

Additionally, previous SAR studies on full-length AIP-II revealed that the thiolactone linkage is a critical determinant in receptor activation, but, interestingly, not inhibition (19). For example, a lactam analogue of AIP-II is a

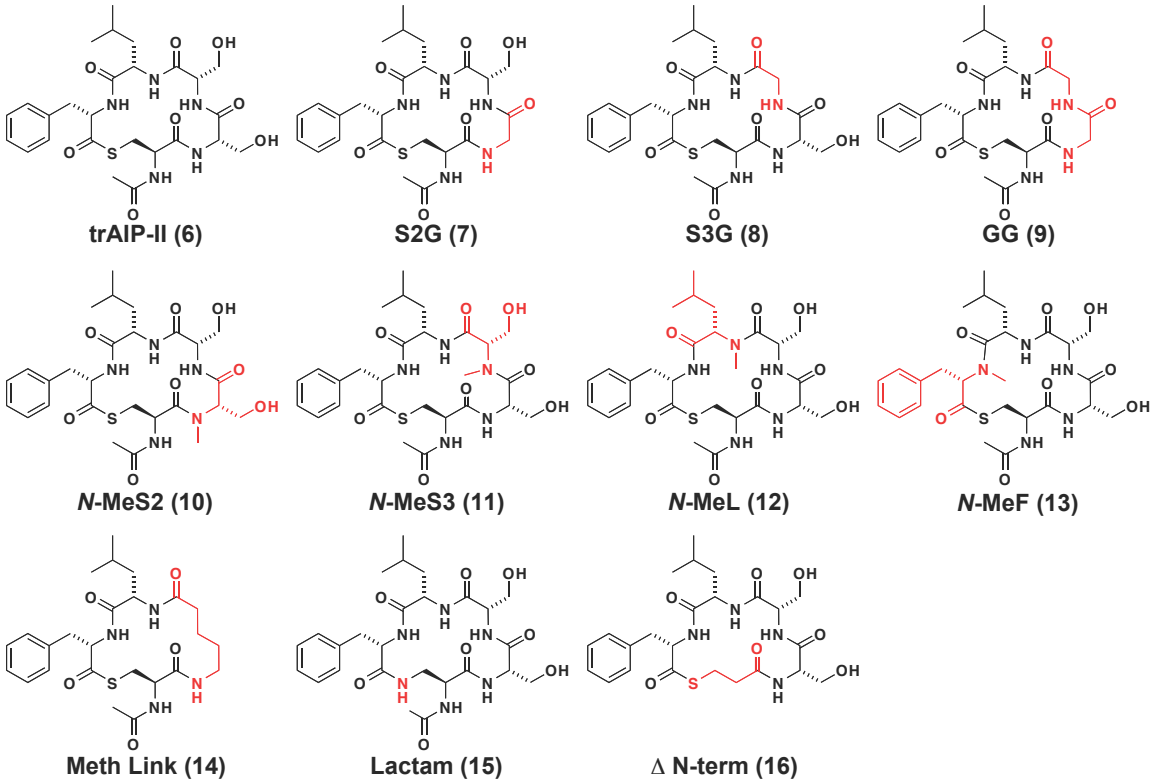

Figure 15. Structures of trAIP-II and Derivatives Synthesized for Study of the Minimal Inhibitory AIP Pharmacophore. The portions of each molecule colored red indicate the residue(s) modified relative to trAIP-II.

very poor agonist but potent antagonist of the agr response (19, 52). In contrast, the trAIP-II lactam was found to be a very poor inhibitor of AgrC-II (79). To confirm this result and to determine whether non-cognate inhibition is diminished to the same extent as cognate inhibition, the lactam (**15**) was constructed. Lastly, the acetylated α-amino group of the N-terminal cysteine was removed to make **16** (Figure 15), allowing determination of any role this vestige of the native AIP tail may play in the inhibitory activity of the peptide.

All but one of the desired thiolactone peptides was generated in good yield and purity using the general procedure shown in Figure 12B. The sole exception was *N*-MeF (**13**), which contains *N*-methylphenylalanine at the C-terminus (Figure 15). Attempts to synthesize the linear precursor to this peptide by Fmoc-SPPS on the α-hydroxy cysteine linker led to low yields, and the crude mixture contained significant amounts of deletion products lacking the last two residues, Leu and *N*-Me-Phe. These problems were attributed to diketopiperazine (DKP) formation resulting from the presence of the tertiary amide at *N*-Me-Phe, a problem that is well known for C-terminal proline containing peptides prepared by Fmoc-SPPS (80) and that has been reported as a side reaction in the synthesis of *N*-methylated peptides (81). Consequently, the α-thioester precursor to peptide *N*-MeF was generated using the Boc-SPPS strategy (Figure 5) employing *in situ* neutralization chemistry (82) during the chain assembly to suppress DKP formation. Finally, the chain elongation for the lactam analogue (**15**) was completed using standard Fmoc-SPPS, as this peptide does not contain a thioester. To form the lactam, the cysteine was replaced with diaminopropanoic acid, and the serines were deprotected with HF following

cyclization of the partially protected linear peptide in solution (Materials and Methods) (19). Characterization and analysis of the purity of all AIP analogues was completed by HPLC, MS, and NMR (Table 4 and Appendix).

2.3.2 Structure–Activity Relationships of trAIP-II

Having obtained all eleven truncated AIP-II analogues, a cell-based reporter assay was used to determine the inhibitory activities of each peptide (52). *S. aureus* cultures of strains that cannot produce AIPs but contain the AgrC–AgrA TCS cassette and β-lactamase driven by the *agr*-dependent P3 promoter were treated with the AIP analogues in the presence of the cognate AIP agonist at 125 nM, a concentration above the EC_{90} (19, 52). The extent of *agr* activation was determined by measuring β-lactamase activity via a colorimetric readout. To test both cognate and non-cognate *agr* inhibition by the trAIP-II analogues, group II & I reporter cell lines RN9372 and RN9222 (Materials and Methods) were used, respectively. The resulting dose-response curves and IC_{50} values against cognate (AgrC-II) and non-cognate (AgrC-I) receptors are shown in Figure 16 and Table 4. Importantly, the IC_{50} values for trAIP-II prepared by the new Fmoc-SPPS route were in good agreement with those previously determined for this peptide (40).

There are two interesting trends within the activity data summarized in Table 4. First, the overall rank order of the peptides, in terms of their inhibitory activities, is remarkably similar for the cognate and non-cognate *agr* groups. Second, all of the peptides that exhibited measurable inhibitory activity are more potent antagonists of the non-cognate AgrC receptor than of the cognate receptor. Furthermore, this difference in inhibitory activities against the two receptors increases significantly for the less potent analogues. This trend is more

Table 4. Mass Spectrometry and Activity Characterization of trAIP-II and Ten trAIP-II Analogues.

AIP Derivative	Mass Expected ($M+H^+$)	Mass Observed ($M+H^+$)	AgrC-I IC_{50} (nM), (95% CI)	AgrC-II IC_{50} (nM), (95% CI)
trAIP-II (Boc)	579.2	579.0	260, (95-695)	230, (190-270)
trAIP-II (Fmoc) (**6**)	579.2	580.0	90, (78-104)	293, (245-350)
S2G (**7**)	549.2	550.7	189, (151-237)	1160, (855-1560)
S3G (**8**)	549.2	550.0	40, (33-48)	194, (167-225)
GG (**9**)	519.2	520.7	77, (66-89)	238, (170-334)
N-MeS2 (**10**)	593.3	595.0	639, (534-765)	7880, (4100-15,200)
N-MeS3 (**11**)	593.3	595.0	319, (284-357)	1050, (795-1380)
N-MeL (**12**)	593.3	595.0	–	–
N-MeF (**13**)	593.3	595.0	–	–
Meth Link (**14**)	504.2	505.0	1141, (799-1630)	507,000, (*)
Lactam (**15**)	562.3	564.0	1390, (1250-1560)	167,000, (*)
Δ N-term (**16**)	522.2	524.0	1680, (1310-2170)	47,300, (33,700-66,300)

trAIP-II (Boc) is the version of the peptide made by Boc-SPPS (Figure 5) (40), and trAIP-II (Fmoc) is the version of the peptide made by the Fmoc-based synthesis described in Section 2.2 (Figure 12C, D). The IC_{50} values and the corresponding 95% confidence intervals were computed using nonlinear regression analysis (Materials and Methods). – = no inhibition observed up to the highest concentrations tested (10-100 μM). (*) = extremely large span of the 95% confidence interval (>100,000 nM).

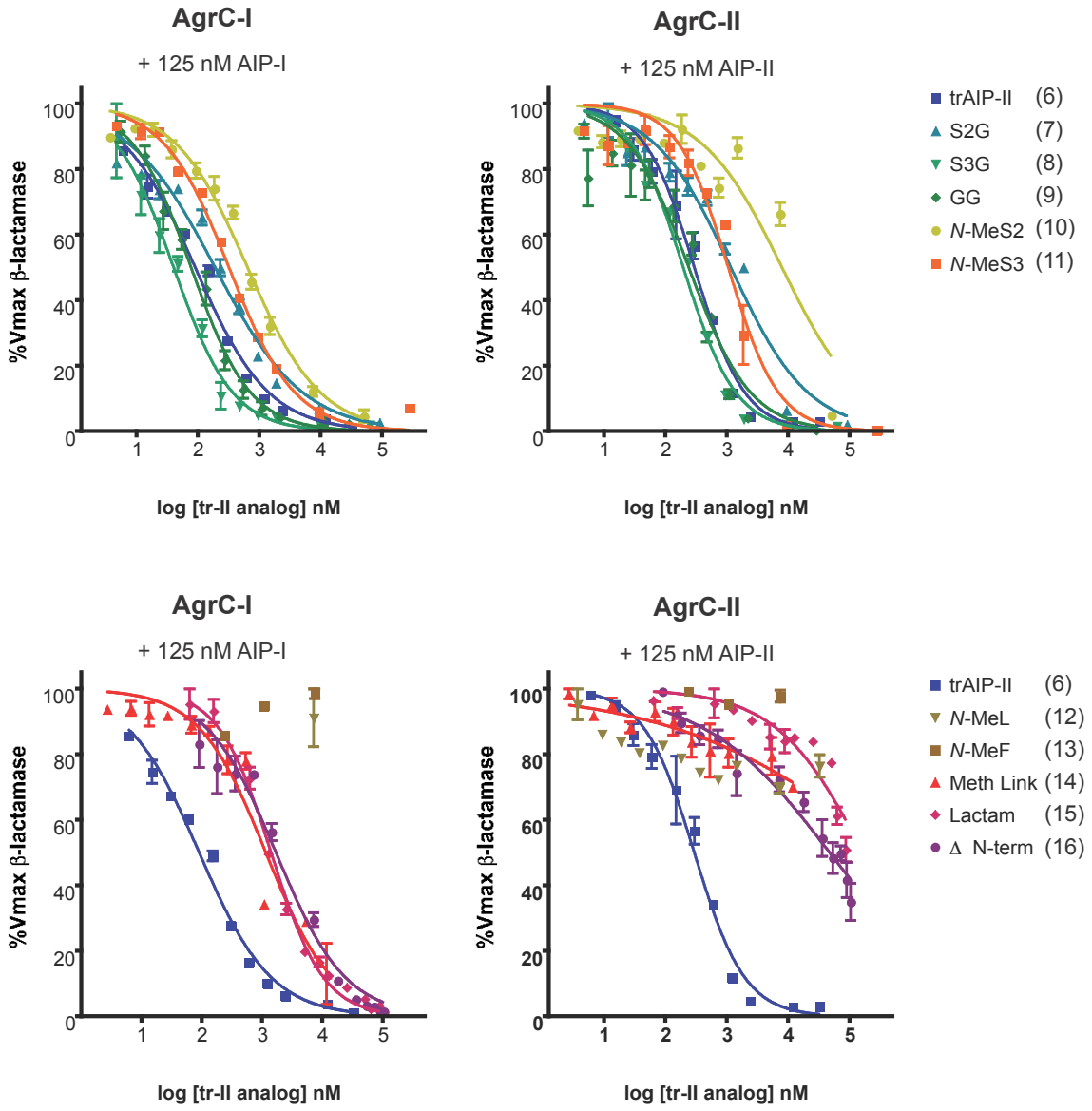

Figure 16. Inhibition Curves for trAIP-II Derivatives Against AgrC-I & II. In all cases, 125 nM agonist (AIP-I or II) plus varying concentrations of antagonist were added to reporter cells. The left panels show inhibitory activities against AgrC-I, and the right panels show activities against AgrC-II. trAIP-II is shown in all panels as a reference. Data are presented as percent maximal activation of the receptor by 125 nM agonist, expressed as Vmax β-lactamase activity. All data points represent two to three replicates, and error bars represent SEM.

clearly seen in Figure 17, which shows a log-log plot of IC_{50} values. Thus, antagonism of the non-cognate *agr* group is much more tolerant to changes in the AIP structure than is antagonism of the cognate group. For instance, replacement of the thiolactone with a lactam leads to a modest decrease in the non-cognate IC_{50} (~15-fold) relative to the effect of this change on the cognate activity (~500-fold). Similarly, replacement of the two serine residues with a methylene linker resulted in approximately 13-fold and 1700-fold reductions in non-cognate and cognate activities, respectively.

Modifications to the serine residues were generally well tolerated. Both the single and the double glycine mutants (**7**, **8**, and **9**) exhibited a minimal loss of activity (<5-fold) or actually increased potency (Table 4). *N*-methylation of the serine residues mildly affected inhibition, although cognate inhibition was somewhat sensitive to *N*-methylation of Ser2. In contrast, *N*-methylation of leucine or phenylalanine resulted in a complete loss of activity, indicating that the side chains of these amino acids are not the only functionally important portions of this region of the AIP.

The replacement of the sulfur with an NH in the lactam (**15**) resulted in a similar effect on function as replacement of both serines with a methylene linker (**14**), as both peptides have IC_{50} values of approximately 1 μM against AgrC-I and over 100μM against AgrC-II (Table 4). Thus, although the thiolactone linkage is not necessary for inhibition by full-length AIP-II (19), it is required for strong inhibition in the context of the truncated AIP. The relatively weak activity of the Meth Link peptide (**14**) cannot be explained by the loss of the serine side chains in accordance with the activity data for GG (**9**) (Table 4). It is more likely that the

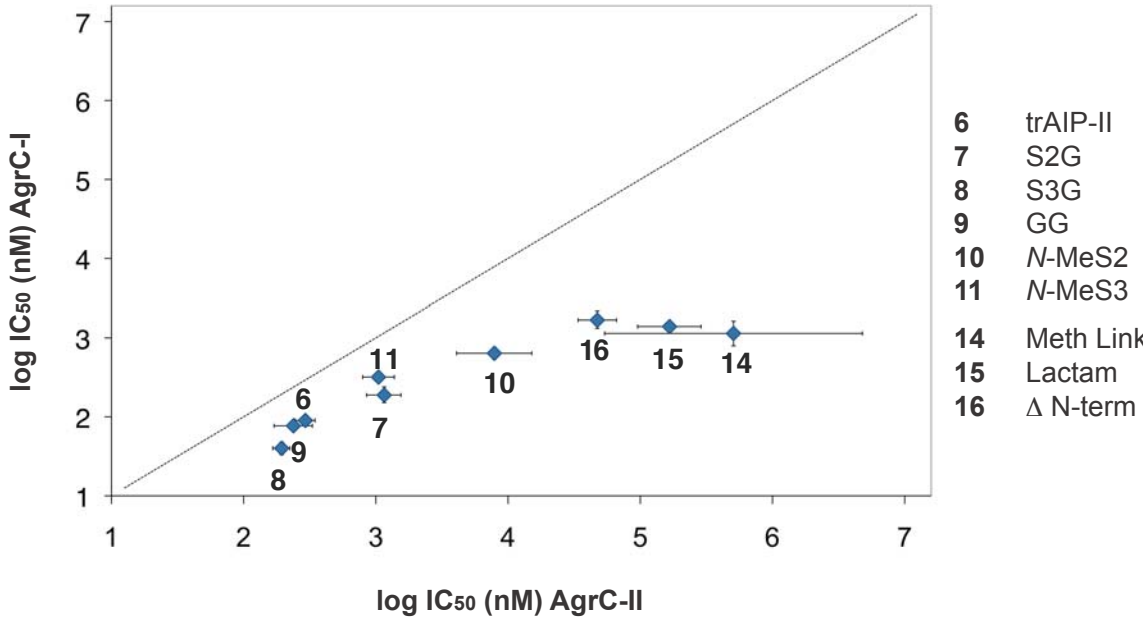

Figure 17. IC_{50} Values of trAIP-II Derivatives Against AgrC-I vs. AgrC-II. All peptides fall below the y = x (dotted) line, indicative of the fact that all are more active against AgrC-I than AgrC-II. The plot also depicts the increasing differences in inhibitory activities as the inhibitory potencies decrease. The error bars represent 95% confidence intervals.

complete loss of an amide bond or the increased flexibility introduced by the methylene linker is responsible for the reduced potency.

Lastly, the removal of the N-terminal amide group caused a dramatic loss of inhibitory activity against both cognate (~250-fold) and non-cognate (~55-fold) receptors (Table 4). This result shows that the N-terminal vestige of the exocyclic "tail" portion of the full-length AIP is in fact important for inhibition.

2.3.3 NMR Analysis of trAIP-II Analogues

To explore a possible correlation between the differential activities of the trAIP-II analogues and the solution structures of the peptides, full ^{1}H NMR chemical shifts were made (Appendix). During this effort, the ^{1}H NMR spectra of *N*-MeS3 (**11**) was found to contain twice the number of expected resonances. Indeed, standard 2-D sequential assignment methods revealed that the sample contained two species as a 1:1 mixture in DMSO-d_6 at 298 K (Figure 18A). There was no evidence for chemical heterogeneity in this peptide by HPLC–MS analysis (data not shown). Likewise, the possibility that these extra signals resulted from epimerization of the C-terminal Phe during coupling to the secondary hydroxyl of the linker was excluded since the same batch of amino-acylated resin was used for the synthesis of other peptides in the study. Further analysis of the ROESY spectrum of *N*-MeS3 revealed the presence of a strong NOE cross-peak between the two serine alpha protons in one of the species but not the other (Figure 18B). This cross-peak is consistent with the presence of a *cis* amide bond between Ser2 and *N*-Me-Ser3. Analogous to the prolyl-tertiary amide, *N*-methylation is known to increase the propensity for *trans-cis* isomerization of an amide bond (83). Two of the other three *N*-methylated

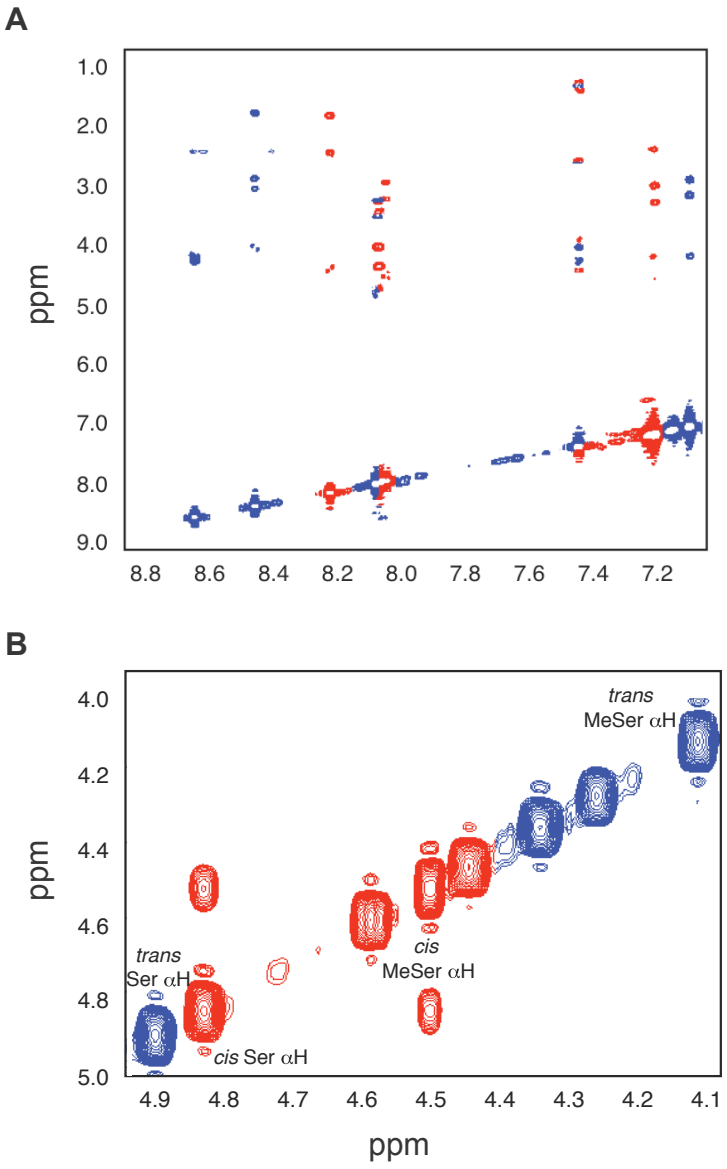

Figure 18. ROESY Spectrum of trAIP-II Derivative *N*-MeS3. (A) Amide region of the ROESY spectrum is color-coded to identify the two spin systems that correspond to the *cis* (red) and *trans* (blue) isomers. **(B)** Alpha region of the ROESY spectrum is color-coded as in (A) to show the diagnostic NOE between the two alpha protons of the *N*-MeS3 *cis* isomer.

peptides, *N*-MeL (**12**) and *N*-MeF (**13**), were also present as two conformers as indicated by NMR, with the minor conformer comprising only 10-30% of the total sample population. By analogy with *N*-MeS3, these conformers almost certainly stem from *cis-trans* isomerization of the tertiary amide bond in these peptides; however, full assignments were not made for the minor, presumably *cis*, isomers of *N*-MeL and *N*-MeF owing to their low abundance.

The chemical shift assignments of the eleven peptides were used to calculate a chemical shift index (CSI) value for each one, allowing comparison of their solution structures. The CSI is the average difference in proton ppm between the analogue of interest and trAIP-II, including protons directly bonded to the macrocyclic scaffold, other than those of the modified residue, plus the exocyclic N-terminal amide proton. The CSI values were then plotted against relative inhibitory potencies to examine any relationship between differences in activity and solution structure among the AIP derivatives compared to trAIP-II (Figure 19). According to this simple analysis, there was no observable trend between potency and overall chemical shift perturbations. For instance, *N*-MeL (**12**) and *N*-MeF (**13**), which have no measurable activity, have CSI values comparable to S3G (**8**) and GG (**9**), which are the most potent AIP analogues. Similarly, the chemical shifts around the macrocycle in the Δ N-term peptide (**16**) are largely unperturbed compared to trAIP-II, yet this analogue is one of the least potent antagonists. One interpretation of this data is that the exocyclic and two C-terminal amides of trAIP-II make specific contacts with the AgrC receptor. Alternatively, the modifications may prevent the AIP from assuming a bioactive conformation required for receptor binding.

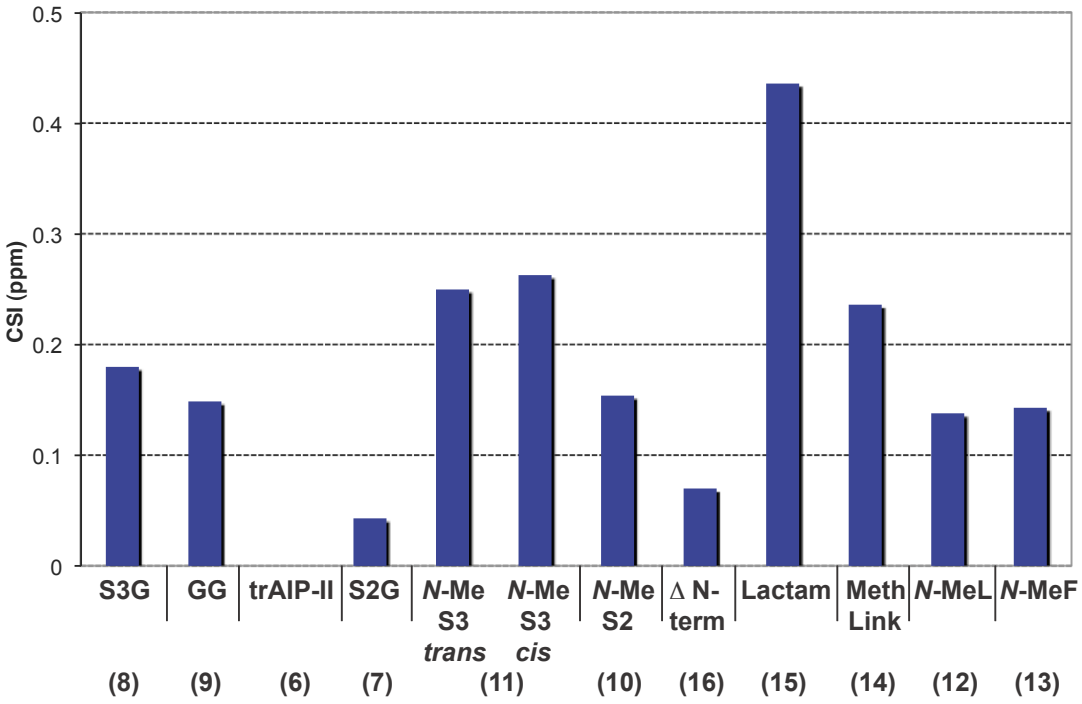

Figure 19. Chemical Shift Index Values vs. Inhibitory Potencies. The CSI values of each AIP analogues are plotted in order of decreasing potency, from left to right. The order of the *N*-MeS3 isomers is arbitrary since they were not separated; and hence, their individual potencies were not determined.

The largest CSI was observed for the lactam analogue (**15**) in which only one atom was replaced. In this case, chemical shift changes propagate around the entire macrocycle (Figure 19 and Appendix), indicating that this substitution induces far-reaching changes in the solution structure of the peptide. A similar structural effect was previously observed upon substitution of the thiolactone with a lactam in the context of full-length AIP-II (52) and trAIP-II (79). The full-length AIP-II lactam remains a potent cross-group AgrC antagonist but is an extremely weak agonist of AgrC-II (19, 52). Thus, although this major structural perturbation differentially affects inhibition of AgrC-I depending on AIP length, activity against the cognate AgrC-II is significantly reduced in both contexts.

2.3.4 Conclusions

Two prominent trends surfaced in this study regarding AIP inhibition of AgrC. First, the overall rank orders of the analogues for inhibition against cognate (AgrC-II) and non-cognate (AgrC-I) receptors were almost identical, despite the fact that the sensor domains of AgrC-II & I share only 31% sequence identity. However, non-cognate antagonism was more resistant to changes in AIP structure than cognate antagonism. Of the peptides with measurable inhibitory activity, the IC_{50} values against AgrC-I varied by no more than ~40-fold, whereas the values against AgrC-II varied by over 3 orders of magnitude (Figure 17 and Table 4). This observation is broadly in line with previous SAR studies on full-length AIPs, which revealed that cross-group antagonism is more tolerant to changes in peptide structure than intra-group agonism (52). Pharmacological studies of trAIP-II suggested that both cognate and non-cognate antagonism operates through a simple competitive binding mechanism in which trAIP-II competes with the group-specific AIP agonist for a common binding site

on the sensor domain of AgrC (41). The SAR data presented here are certainly consistent with this mechanism, but the details of the cognate and non-cognate interactions must differ since certain modifications have a more acute effect on the former interaction than the latter one.

Taken together, these results facilitated identification of the principle pharmacophore for agr antagonism by trAIP-II (Figure 20). Roughly one half of the molecule, including the cysteine and two C-terminal hydrophobic residues, is critical for activity. Conversely, the remainder of the molecule appears to be far less important and can even be replaced by an alkyl linker without a dramatic loss of non-cognate *agr* inhibition. Further study is needed to understand the basis for inhibition of multiple receptors via so few structural elements.

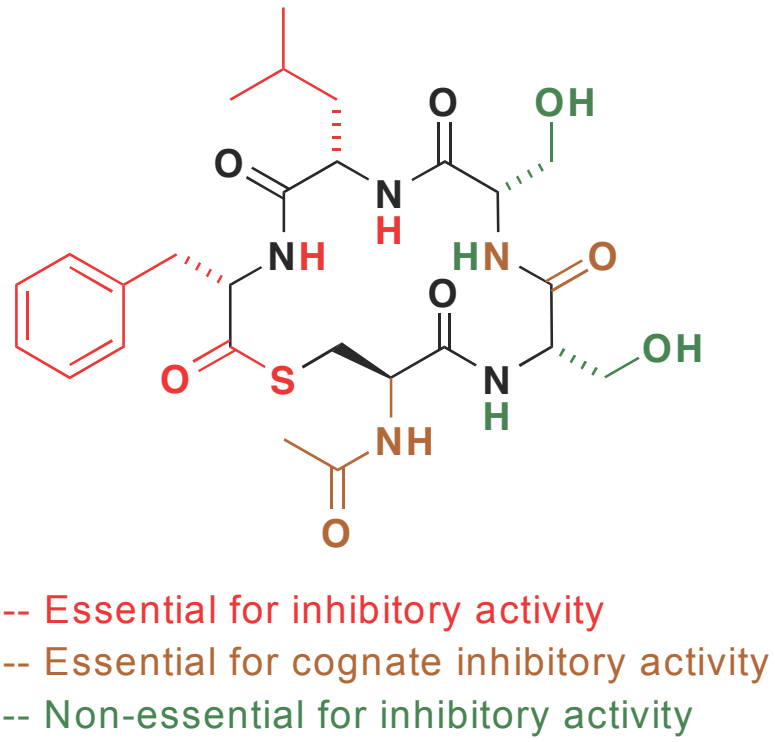

Figure 20. The Minimal Inhibitory AIP Pharmacophore. trAIP-II is color-coded to indicate which portions of the molecule are important for inhibition against cognate (AgrC-II) and non-cognate (AgrC-I) receptors.

Chapter 3: Mechanism of Signal Transduction by AgrC (This work was performed in collaboration with Edward Geisinger.)

3.1 Introduction

Knowledge of the mechanism by which AgrC transduces the AIP signal is very limited. The importance of particular motifs for ligand recognition and specificity within the AgrC sensor domain are beginning to be understood (42, 55, 58, 62). In a recent study by Geisinger et al. (42), several constitutively active AgrC mutants were isolated with single point mutations that mainly localized to the C-terminal transmembrane helix of the sensor domain and the putative coiled-coil/dimerization (DHp) subdomain (Figure 7). These intriguing findings implied that the C-terminal transmembrane helix may move toward the cytoplasm in a piston-like movement upon activation and that the DHp subdomain is important for regulation of activity. Mathiesen et al. (84) isolated constitutive mutants of the *L. sakei* receptor histidine kinase SppK, another member of the HPK_{10} peptide-sensing family. Although the sites of point mutations found to confer constitutive activity upon SppK were not conserved in AgrC, they mainly localized to the DHp subdomain. Furthermore, T233I, a constitutive mutation in ComD of *S. pneumoniae* is also in the DHp domain (85); and while this residue is conserved in AgrC (T224), the effect of an analogous mutation in AgrC is not known. Collectively, these results strongly point to the DHp subdomain as the key to the kinase activation mechanism, yet the question of how specific ligand binding triggers signal transduction and kinase activation via the DHp subdomain is open.

The goal of this study was to elucidate the AgrC signal transduction mechanism and thereby shed light on the mechanism of activation of other

members of the HPK_{10} family. Complementary mutants missing either the phosphorylation site histidine of the DHp subdomain or key catalytic residues in the CA subdomain exhibited robust activity upon co-expression, revealing that AgrC activation occurs through dimerization and *trans*-autophosphorylation. One possible function of the DHp subdomain constitutive mutations was to promote dimerization as a mechanism for activation; however, co-immunoprecipitation analysis demonstrated that dimers are pre-formed. In fact, dimerization appeared to be reduced in at least one of the DHp subdomain constitutive mutants. By combining the complementary mutants with known sensor domain mutations that alter ligand specificity (58), heterodimers were constructed in which signal input is primarily received by only one sensor. Not only was input from one sensor domain sufficient for activation, but additionally, either kinase domain was activated irrespective of whether the functional sensor domain was part of the same protomer molecule. Moreover, analogous symmetric kinase activation was observed in the absence of ligand in mutant heterodimers containing one protomer with a DHp subdomain constitutive mutation. Thus, AgrC activation is inherently symmetric via bidirectional cross-talk at the dimer interface.

3.2 AgrC is a Pre-formed Dimer that *trans*-autophosphorylates

The prototypical histidine kinase functions as a dimer and undergoes *trans*-autophosphorylation (32, 71). In order to test whether AgrC follows this paradigm, an intermolecular complementation approach was adopted, similar to that used to demonstrate functional dimerization and *trans*-autophosphorylation for HPKs in *E. coli* (86-88). The aim was to create and analyze two complementary mutants, one lacking an appropriate phosphorylation site and

one with a dysfunctional kinase, neither of which has detectable kinase activity when expressed alone. When co-expressed, mutant heterodimers would form in which each protomer would complement the other's defect only if AgrC undergoes dimerization and *trans*-autophosphorylation.

3.2.1 Design, Characterization, and Testing of Complementary AgrC Mutants

Through sequence alignment of the AgrC cytoplasmic domain with that of other HPKs, conserved residues representing the putative phosphorylation site (His239) and catalytic motifs were identified (Figure 7). The N-box asparagine (Asn339) and G-box glycine residues (Gly394 and Gly396) are essential for ATP binding in other HPKs (89, 90). Accordingly, these residues were mutated in AgrC-I, and the resulting activities were tested in *S. aureus* β-lactamase reporter cells (52). As expected, the phosphorylation site mutant H239Q was completely inactive (Figure 21). Surprisingly, mutation of the N-box (N339D) resulted in only partially reduced receptor activation unlike the effect of the corresponding mutation in EnvZ (90). Each individual G-box glycine mutant (G394A and G396A) exhibited weaker receptor activation than that observed for AgrC-I N339D, while the double mutant (G394A, G396A) was completely inactive up to the highest concentration of AIP-I tested (10 μM). Thus, AgrC-I_{H239Q} and AgrC-$I_{G394A,\ G396A}$ were selected for subsequent complementation analysis and are hereafter referred to as AgrC-I_{His} and AgrC-I_{Kin}, respectively, to indicate the particular defect of each mutant. In order to determine the cellular localization and expression levels of AgrC-I_{His} and AgrC-I_{Kin} C-terminal GFP-fusions of the two mutants and WT AgrC-I were constructed. Ligand-dependent kinase function was preserved in the AgrC-I-GFP fusion protein, as receptor activation

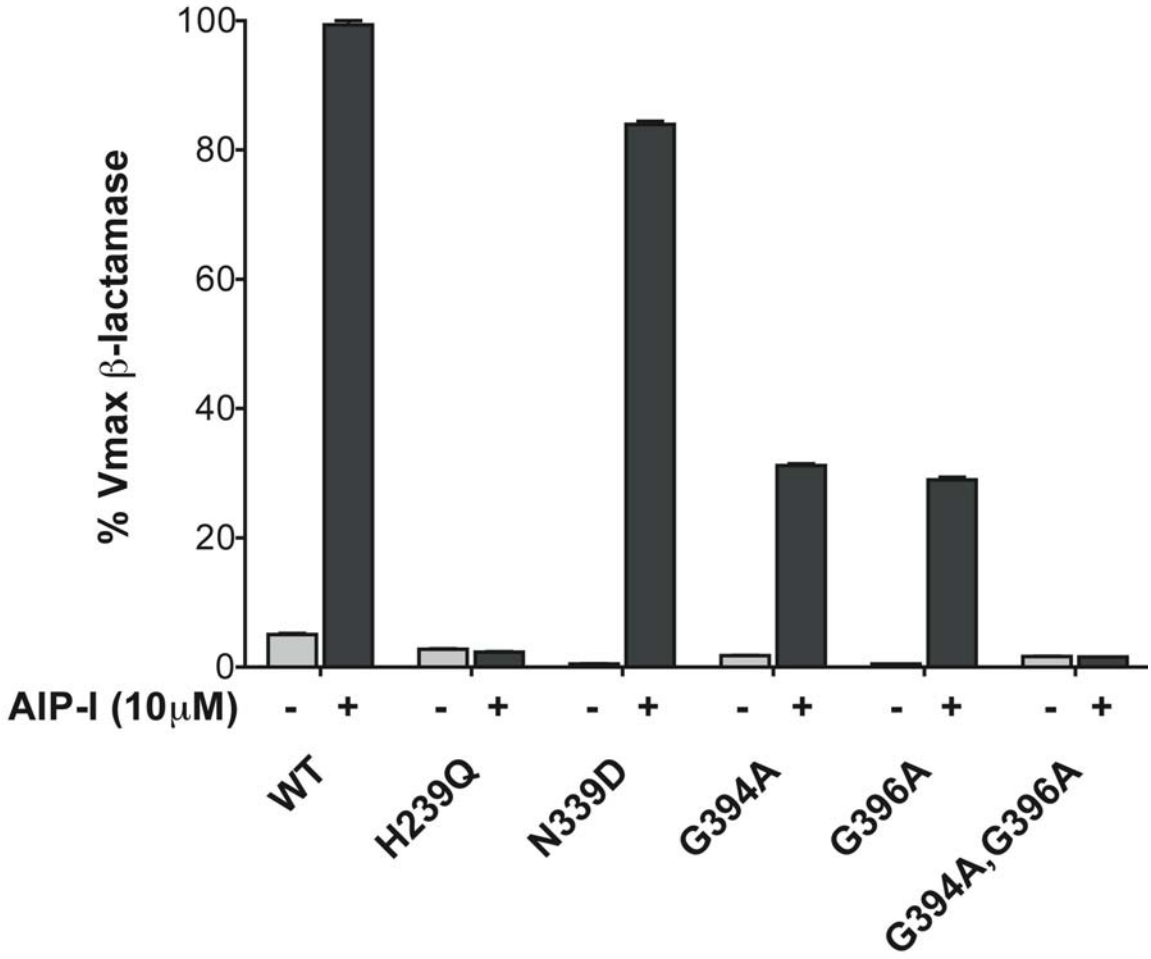

Figure 21. Probing Conserved Catalytic Motifs in the AgrC HK Domain. β-lactamase activity of reporter cells expressing the indicated AgrC-I construct following incubation with or without 10 μM AIP-I, as indicated. Data are presented as percent maximal activation of WT AgrC-I ± SEM.

by AIP-I was nearly as effective as that of WT AgrC (Figure 22 and Table 5). Fluorescence microscopy showed that AgrC-I-GFP localized to the cell membrane (Figure 23B-D). Images of AgrC-I-GFP expressing cells that produce AIP allowed direct observation of the autocatalytic induction of *agr* expression (30) and showed that AgrC is uniformly localized throughout the cell perimeter (Figure 23D). Attenuated expression of AgrC-I-GFP in an AIP producing strain that lacks *agrA* confirmed that the observed induction of AgrC expression is dependent on the AgrC-A TCS (Figure 23B). The images of cells expressing AgrC-I-GFP$_{His}$ and AgrC-I-GFP$_{Kin}$ fusions (Figure 23E, F) resembled those of uninduced cells (Figure 23B, C) expressing WT AgrC-I-GFP, suggesting that the phosphorylation site and catalytic domain mutations do not adversely affect localization.

Previous attempts to characterize several epitope-tagged versions of AgrC by western blot failed, highlighting the difficulties of working with a polytopic membrane protein presumed to express at low abundance (55). In this study, a protocol for preparation of *S. aureus* membrane fractions was adapted from *MRSA Protocols* (91), in which the cells were lysed with osmotic shock following cell wall removal by treatment with lysostaphin. Four different conditions were used for resuspension of membrane pellets, and if the samples were boiled prior to gel loading, no definitive bands appeared for either AgrC-GFP or AgrC-HA constructs (data not shown). However, when samples were loaded without being subjected to denaturing conditions, such as boiling, clear bands attributable to AgrC were detected for all resuspension conditions (Figure 24A). Multiple bands were detected for AgrC-GFP constructs, including a high molecular weight band that may represent an AgrC dimer, but none of the bands matched the expected

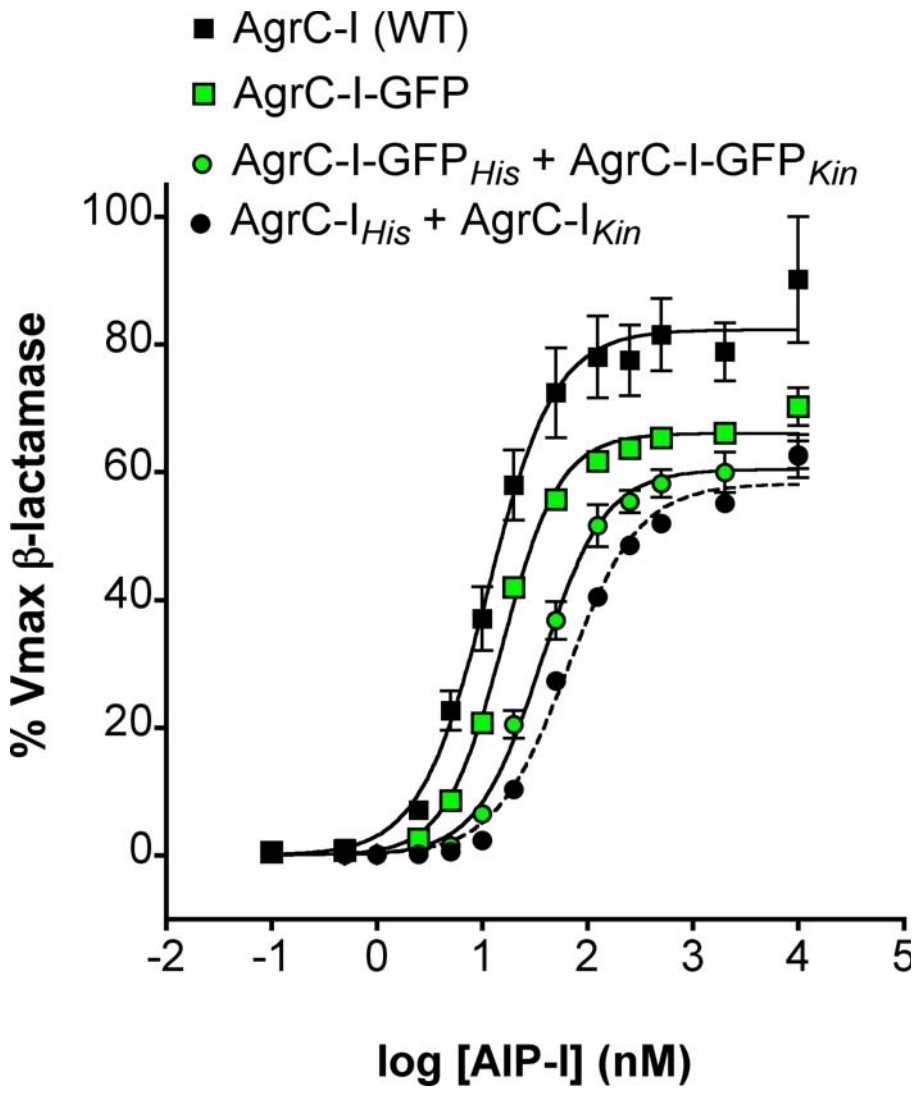

Figure 22. Functional Characterization of AgrC-GFP. β-lactamase activities of reporter cells expressing the indicated AgrC-I construct(s) following incubation with increasing concentrations of AIP-I. Data are presented as percent maximal activation of WT AgrC-I ± SEM.

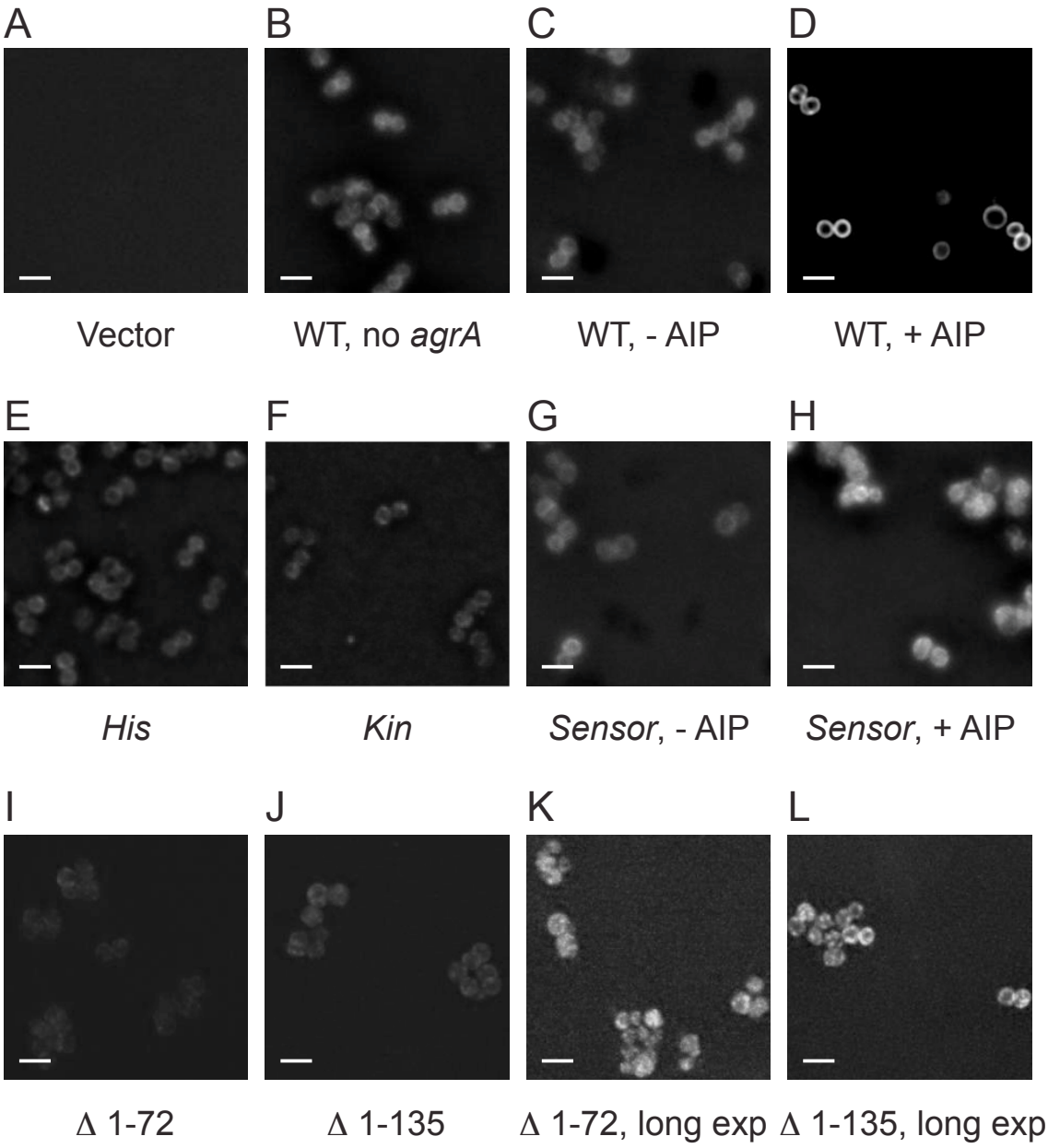

Figure 23. Characterization of AgrC-GFP Constructs by Fluorescence Microscopy. (A-L) Fluorescence images of AgrC-GFP constructs used in this study. Scale bars equal 2 μm. **(K, L)** Images with longer exposure than (A-J) for an enhanced view of the AgrC truncations, which show lower expression than the other constructs.

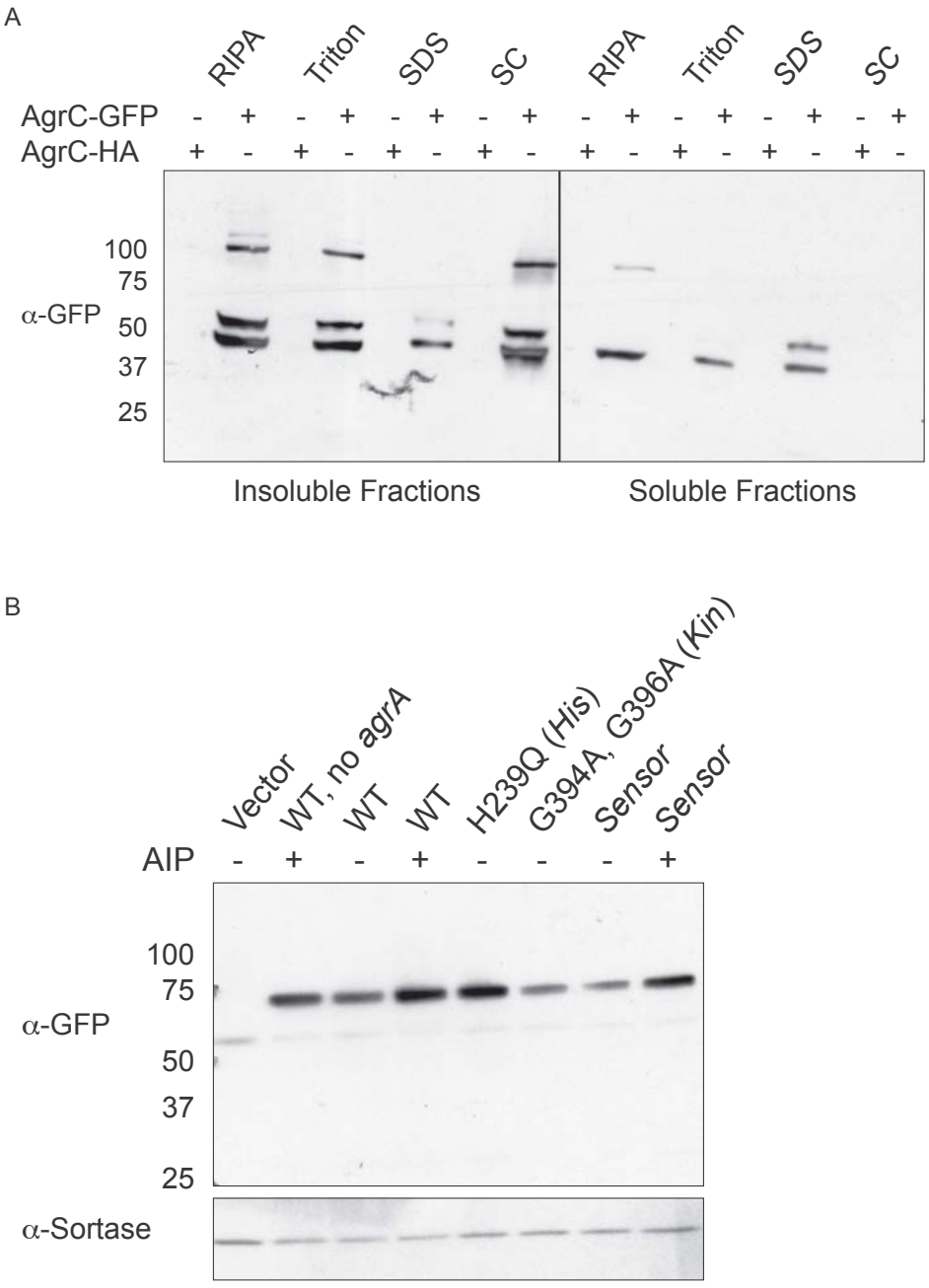

Figure 24. Characterization of AgrC-GFP Constructs by Western Blot. (A) Anti-GFP western blot of membrane fractions from cells expressing WT AgrC-GFP or AgrC-HA solubilized in RIPA (1.0% NP-40, 0.25% DOC), Triton (1.0%), SDS (0.1%), or SC (0.1 M sodium carbonate). **(B)** Anti-GFP western blot of constructs shown in Figure 23A-H. Sortase is the loading control.

Table 5. Activities of AgrC Mutants and Mutant Heterodimers.

AgrC Receptor Variants			EC_{50} (nM), (95% CI)		IC_{50} (nM), (95% CI)
WT	*His* (H239Q)	*Kin* (G394A, G396A)	AIP-I	AIP-II	AIP-III (+AIP-I)
AgrC-I			10, (8.7-13)	–	nt
	AgrC-I		–	–	n/a
		AgrC-I	–	–	n/a
	AgrC-I	AgrC-I	40, (35-45)	–	18, (13-25) *
AgrC-I-GFP			16, (14-17)	–	nt
	AgrC-I-GFP		–	–	n/a
		AgrC-I-GFP	–	–	n/a
	AgrC-I-GFP	AgrC-I-GFP	36, (31-42)	–	nt
	$AgrC\text{-}I_{Sensor}$		–	–	n/a
		$AgrC\text{-}I_{Sensor}$	–	–	n/a
	$AgrC\text{-}I_{Sensor}$	$AgrC\text{-}I_{Sensor}$	6100, (4200-9000)	–	nt
	AgrC-I	$AgrC\text{-}I_{Sensor}$	200, (170-240)	–	140, (88-230) #
	$AgrC\text{-}I_{Sensor}$	AgrC-I	310, (260-380)	–	320, (150-650) #
AgrC-II			–	2.9, (2.3-3.6)	nt
	AgrC-II		–	–	n/a
		AgrC-II	–	–	n/a
	AgrC-I	AgrC-II	21, (18-25)	17, (13-22)	15, 9.8-21) *
	AgrC-II	AgrC-I	17, (16-19)	4.5, (3.6-5.6)	17, (13-22) *

EC_{50} and IC_{50} values and 95% confidence intervals are shown for mutants individually and in combination. – = no activity observed up to the highest AIP concentration tested (>10 μM). * = 150 nM AIP-I added. # = 1 μM AIP-I added. n/a = not applicable, the variant is not active. nt = not tested in this study.

molecular weight of 77 kDa. However, treatment with dilute acid resulted in appearance of a single band at the appropriate molecular weight (Figure 24B), suggesting that the acid denatures the protein to some extent without promoting aggregation. In subsequent experiments, lysis was carried out by incubation of protoplasts in buffer containing 1.0% nonyl phenoxylpolyethoxylethanol (NP-40) and 0.25% deoxycholate (DOC), and the resulting total cell lysates were treated with dilute acid prior to gel loading. Having established conditions for reproducible western blot analysis of AgrC, the various WT and mutant AgrC-GFP constructs were analyzed. Importantly, expression of AgrC-I_{His} is comparable to WT AgrC-I, and expression of AgrC-I_{Kin} is somewhat reduced but sufficient for use in the complementation experiment (Figure 24B).

Having established that the individual AgrC-I_{His} and AgrC-I_{Kin} mutants have no measureable kinase activity and demonstrate adequate expression and appropriate localization, they were co-expressed by introducing the compatible plasmids, pEG58 and pEG59, into the reporter strain background (52). In cells co-expressing AgrC-I_{His} and AgrC-I_{Kin}, robust dose-dependent activation by AIP-I was observed with a slightly increased EC_{50} value of 40 nM compared to 10 nM for WT AgrC-I (Figure 25B and Table 5). Similar activation was observed with the GFP-fused variants (Figure 22). The maximal activity of the mutant heterodimers was moderately reduced compared to WT AgrC, consistent with the statistical expectation of the formation of inactive mutant homodimers. In order to rule out plasmid recombination as a source of active AgrC in this hybrid strain, plasmid size was confirmed by agarose gel electrophoresis of whole cell minilysates, and each plasmid was backcrossed to a naïve reporter background to reconfirm the inactivity of each individual mutant (data not shown).

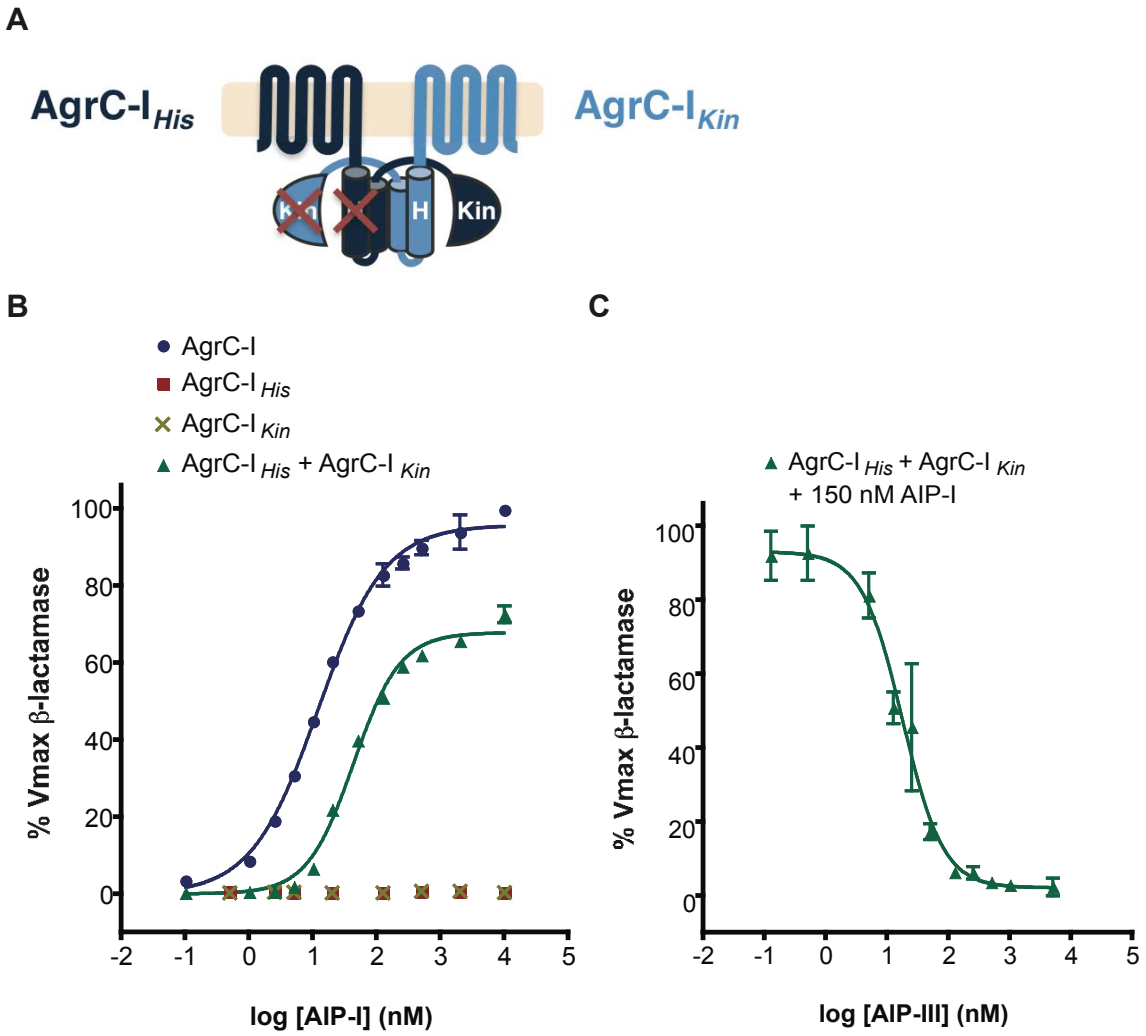

Figure 25. Co-expression of AgrC-I Complementary Mutants. (A) Schematic of a heterodimer formed between AgrC-I_{His} and AgrC-I_{Kin}. **(B)** Activation curves for the indicated constructs following treatment with AIP-I. Percent activity is relative to maximal activation of WT AgrC-I ± SEM. **(C)** Inhibition of the complementary pair by AIP-III in the presence of a constant concentration (150 nM) of AIP-I. Percent activity is relative to maximal activation by 150 nM AIP-I ± SEM.

To ensure that the complementary mutations do not alter ligand recognition, the ability of a non-cognate AIP to block AIP-I-induced activation of the mutant heterodimer was assessed. Treatment of reporter cells co-expressing both mutants with a fixed concentration of AIP-I and increasing concentrations of AIP-II or AIP-III resulted in a dose-dependent decrease in activity (Figure 25C and Table 5). Thus, AgrC-I_{His} and AgrC-I_{Kin} form functional heterodimers that maintain WT ligand specificity. Collectively, these results demonstrate that intermolecular complementation occurs between an AgrC-I phosphorylation site mutant and a catalytic domain mutant. The possibility that AgrC autophosphorylation may occur in *cis* was not ruled out, but this study definitively showed that *agr* activation can occur via *trans*-autophosphorylation of AgrC dimers or higher order oligomers.

3.2.2 AgrC Homodimerizes in the Absence and Presence of AIP

Histidine kinases typically function as dimers (32, 71); however, the influence of ligands on the oligomeric state has not been investigated for most HPKs. Two exceptions are VirA of *A. tumefaciens* (92) and the HPK-associated aspartate receptor, Tar (93) for which the fundamental dimeric units were shown to be independent of ligand binding. In order to determine whether AgrC exists as a pre-formed or ligand-induced dimer, co-immunoprecipitation of differentially tagged versions of AgrC in the absence and presence of AIP was performed. First, cells co-expressing GFP and HA-tagged complementary mutants, AgrC-I-GFP_{His} and AgrC-I-HA_{Kin}, were analyzed to ensure that heterodimers formed by AgrC-I-GFP and AgrC-I-HA are functional. This pair exhibited robust dose-dependent activation by AIP-I, with an EC_{50} of 31 nM (Figure 26A). Next, immobilized GFP antibodies were used to

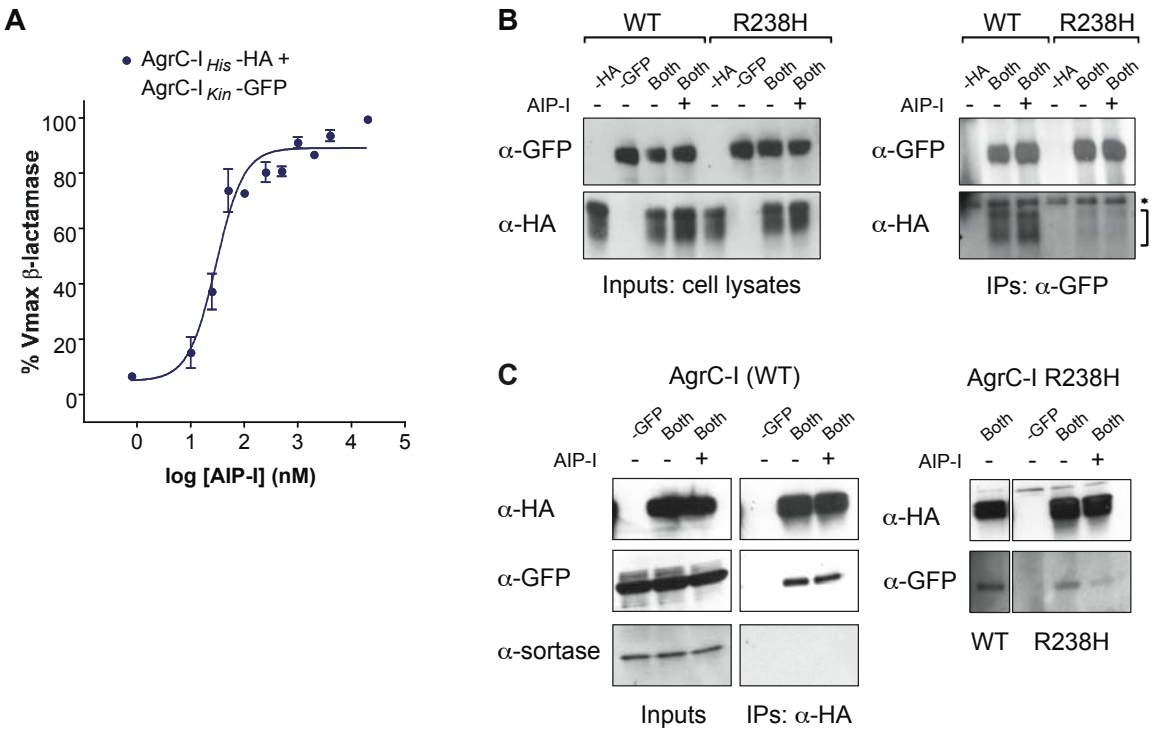

Figure 26. Co-immunoprecipitation of AgrC-I-GFP and AgrC-I-HA. (A) Activity of reporter cells co-expressing AgrC-I-GFP$_{His}$ and AgrC-I-HA$_{Kin}$ following treatment with increasing concentrations of AIP-I. Data are presented as percent maximal activity of this AgrC-I pair ± SEM. **(B)** Immunoprecipitation of lysates from cells co-expressing WT AgrC-I-GFP and AgrC-I-HA or AgrC-I$_{R238H}$-GFP and AgrC-I$_{R238H}$-HA using an α-GFP affinity matrix. Asterisk indicates IgG bands, and bracket indicates AgrC-HA bands. **(C)** Immunoprecipitation, including Sortase control, as in (B) except an α-HA affinity matrix was used.

immunoprecipitate AgrC from total lysates of cells co-expressing WT AgrC-I-HA and AgrC-I-GFP. Western blot analysis showed that AgrC-HA is immunoprecipitated only when AgrC-GFP is present and that AgrC-HA interacts with AgrC-GFP in the absence and presence of AIP (Figure 26B). Similar results were obtained when HA antibodies were used to immunoprecipitate the complex (Figure 26C).

In order to rule out the possibility that these results were due to non-specific interactions with membrane proteins, the immunoprecipitate elutions were probed for the presence of Sortase, an unrelated membrane protein involved in anchoring proteins to the cell wall. While Sortase appeared in the total lysate inputs, it was not present in the samples eluted from the beads (Figure 26C). Furthermore, formation of AgrC-GFP/AgrC-HA dimers was not observed when a mixture of lysates from cells expressing only AgrC-GFP or AgrC-HA was analyzed by immunoprecipitation (data not shown), indicating that dimerization occurs only in the cell and not following lysis. These results confirm the dimeric nature of AgrC and demonstrate that the dimers form independent of ligand binding.

3.3 The AIP Signal is Transduced Symmetrically within AgrC Dimers

As the complementary mutants allow isolated detection of the activity of AgrC heterodimers vs. homodimers, they could facilitate activity measurements of heterodimers containing two different sensor domains. Thus, various aspects of AgrC signaling were analyzed by combining the complementary mutants with sensor domain mutants. This experimental system proved to be very powerful and revealed the surprising result that the AIP signal is propagated both linearly within one AgrC molecule and laterally across the dimer interface.

3.3.1 One Intact Sensor Domain is Sufficient for Activation

First, the AIP:AgrC stoichiometry was evaluated by testing whether one complete sensor domain is sufficient for ligand-induced activity in a heterodimer containing one truncated sensor domain. N-terminal truncations of both WT AgrC-I and AgrC- I_{Kin} were constructed by deleting progressive segments of the transmembrane sensor domain. When expressed individually, none of the resulting homodimers displayed significant activity in response to AIP-I (Figure 27A). However, co-expression of full-length AgrC-I_{His} with a truncated mutant lacking most of the sensor domain (AgrC-$I_{\Delta 1\text{-}135,\ Kin}$) resulted in significant, dose-dependent activity (Figure 27A, B). The maximal activation was significantly reduced compared to the full-length complementary mutants, which may be due to poor expression and/or membrane localization of the truncations (Figure 23I-L). Nonetheless, one intact sensor domain is sufficient for activation, consistent with a model of 1:1 AIP:AgrC stoichiometry.

In order to overcome the limitation of poor localization, an analogous experiment was carried out using a full-length AgrC-I mutant that exhibits expression and membrane localization similar to WT but greatly reduced sensitivity to AIP-I (Figure 23G, H and 24B) (58). AgrC-I T104V, S107V, S116I is approximately 50-fold less sensitive to AIP-I than WT AgrC (58), and for simplicity, is hereafter referred to as AgrC-I_{Sensor}. The phosphorylation site and catalytic mutations were next introduced into AgrC-I_{Sensor}; and accordingly, co-expression of AgrC-$I_{Sensor,\ His}$ and AgrC-$I_{Sensor,\ Kin}$ resulted in very weak activity with an EC_{50} value of 6.1 μM (Figure 28C and Table 5). However, when AgrC-I_{His} was combined with AgrC-$I_{Sensor,\ Kin}$, activation by AIP-I was restored close to that

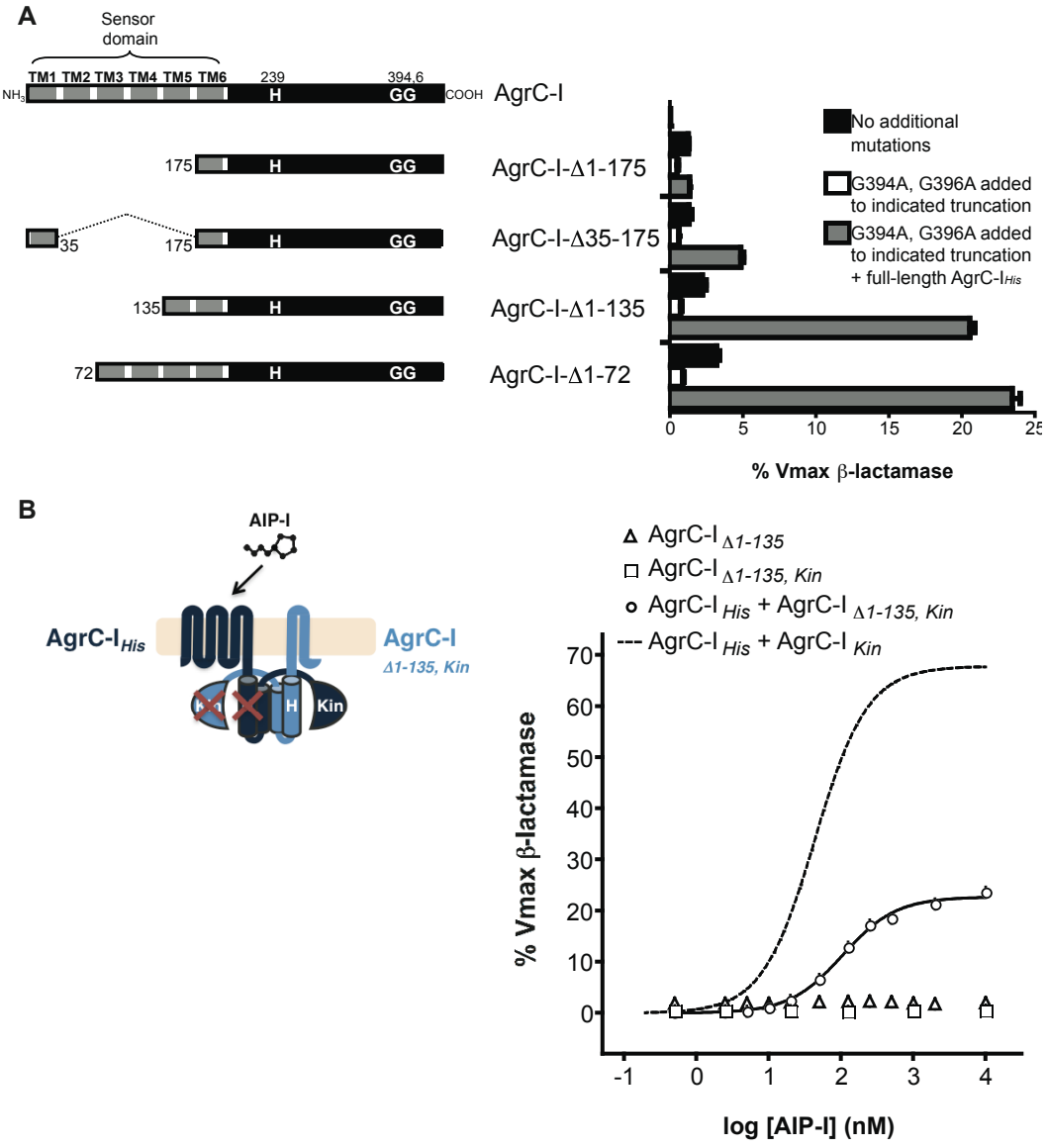

Figure 27. Activities of N-terminally Truncated Variants of AgrC. (A) Activities of the indicated AgrC-I truncation mutants following treatment with a saturating concentration (10 mM) of AIP-I. The gray bars represent the activities upon co-expression with full-length AgrC-I_{His}. **(B)** Schematic of AgrC-I_{His} + AgrC-$I_{\Delta 1\text{-}135,\ Kin}$ and the activity of that pair following treatment with AIP-I. Individual mutants and the full-length AgrC-I_{His}/AgrC-I_{Kin} pair are shown for reference. Data are presented as percent maximal activation of WT AgrC-I ± SEM.

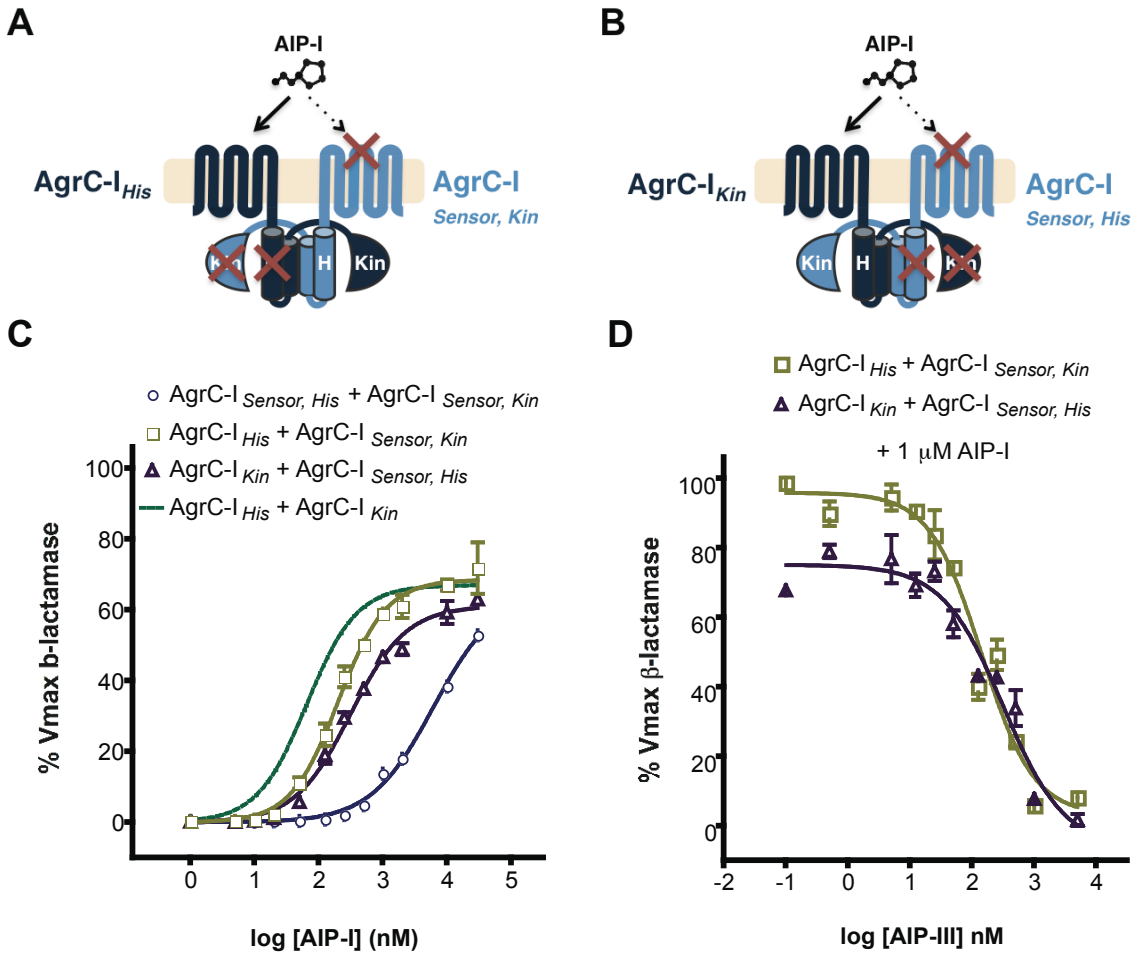

Figure 28. Analysis of AgrC Mutant Heterodimers Containing Sensor Domains with Different Ligand Recognition Properties. (A) Schematic of AgrC-I_{His}/AgrC-$I_{Sensor,\ Kin}$ heterodimer with a WT sensor domain linked to a functional kinase domain. **(B)** Schematic of AgrC-I_{Kin}/AgrC-$I_{Sensor,\ His}$ heterodimer with a WT sensor domain linked to a dysfunctional kinase domain. **(C)** Activities of reporter cells co-expressing the constructs indicated following treatment with AIP-I. Percent activity is relative to maximal activation of WT AgrC-I ± SEM. **(D)** Activities of reporter cells indicated following treatment with increasing concentrations of AIP-III in the presence of 1 μM AIP-I. Percent activity is relative to maximal activation of AgrC-I_{His}/AgrC-I_{Kin} by 1 μM AIP-I ± SEM.

observed for the AgrC-I_{His} /AgrC-I_{Kin} pairing with WT sensor domains (Figure 28A, C and Table 5), consistent with the above observation that only one WT sensor is required for activation of an AgrC dimer. Additionally, the maximal activities of heterodimers involving AgrC-I_{Sensor} were similar to that observed with the AgrC-I_{His} /AgrC-I_{Kin} pair, unlike the result with the truncated receptors.

3.3.2 Both AIP-dependent and Constitutive AgrC Signaling is Symmetric

Having established that only one functional sensor domain is required for activation, the AgrC-I_{Sensor} heterodimers were used to test the simple hypothesis that each receptor protomer transduces the activating signal directly to its own kinase. In this proposed mechanism of asymmetric activation, only the kinase domain linked to the functional sensor domain is predicted to be activated. For example, in the AgrC-I_{His}/AgrC-$I_{Sensor,\ Kin}$ heterodimer, AgrC-I_{His} contains WT sensor and kinase domains and phosphorylates AgrC-$I_{Sensor,\ Kin}$ (Figure 28A, C). In contrast, the reciprocal pair of AgrC-$I_{Sensor,\ His}$ and AgrC-I_{Kin} is predicted to be inactive since the functional sensor and kinase domains are located in different protomers of the dimer and therefore separated (Figure 28B). Surprisingly, AgrC-I_{Kin}/AgrC-$I_{Sensor,\ His}$ exhibited robust dose-dependent activation that was nearly indistinguishable from that observed for AgrC-I_{His}/AgrC-$I_{Sensor,\ Kin}$, as reflected in the EC_{50} values of 310 and 200 nM, respectively (Figure 28C and Table 5). The AIP-I-induced activation of both heterodimeric pairs was inhibited by AIP-III in a dose-dependent fashion (Figure 28D and Table 5), demonstrating that antagonism by non-cognate AIPs is maintained and the heterodimers are not artificially poised for activation. Thus, instead of following the predicted linear signaling mechanism, AgrC activation appears to be symmetric. Ligand binding to one functional sensor domain stabilizes or induces conformational changes

that may be propagated across the dimer interface to activate either kinase domain. Alternatively, a composite AIP binding pocket formed by both sensor domains could account for the result, as a 1:2 AIP:AgrC stoichiometry has not been formally excluded, but this possibility is not supported by the results obtained with the truncated AgrC variants.

To further test the idea of symmetric signaling by AgrC, heterodimers were constructed in which the two receptors belong to two of the most divergent *agr* specificity groups, I & II. The sensor domains of AgrC-I & II share only 31% sequence identity, and AIP-I & II are potent cross-group inhibitors (Table 1). The histidine and CA subdomain mutations were added to AgrC-II, and as with AgrC-I, the AgrC-II_{His} and AgrC-II_{Kin} mutants were completely inactive individually (Table 5). In this case, the asymmetric, linear model of activation predicts that only the AIP specific for the sensor domain attached to a functional kinase would activate an AgrC-I/II heterodimer. For example, only AIP-I would be expected to activate AgrC-I_{His}/AgrC-II_{Kin} since only AgrC-I has a functional kinase (Figure 29A). Conversely, the symmetric model predicts that both AIP-I & II would activate an AgrC-I/-II heterodimer equally well, regardless of which protomer harbors the functional kinase domain. In fact, AgrC-I_{His}/AgrC-II_{Kin} was activated to approximately the same extent by AIP-I & II, as represented by EC_{50} values of 21 and 17 nM, respectively (Figure 29C and Table 5). The same result was obtained upon treatment of the reciprocal AgrC-I_{Kin}/AgrC-II_{His} heterodimer with AIP-I or AIP-II (Figure 29B, D and Table 5). Thus, receptors of two divergent *agr* groups formed functional heterodimers activated by both cognate AIPs, lending additional evidence to the conclusion that input from one sensor domain leads to activation of either kinase domain.

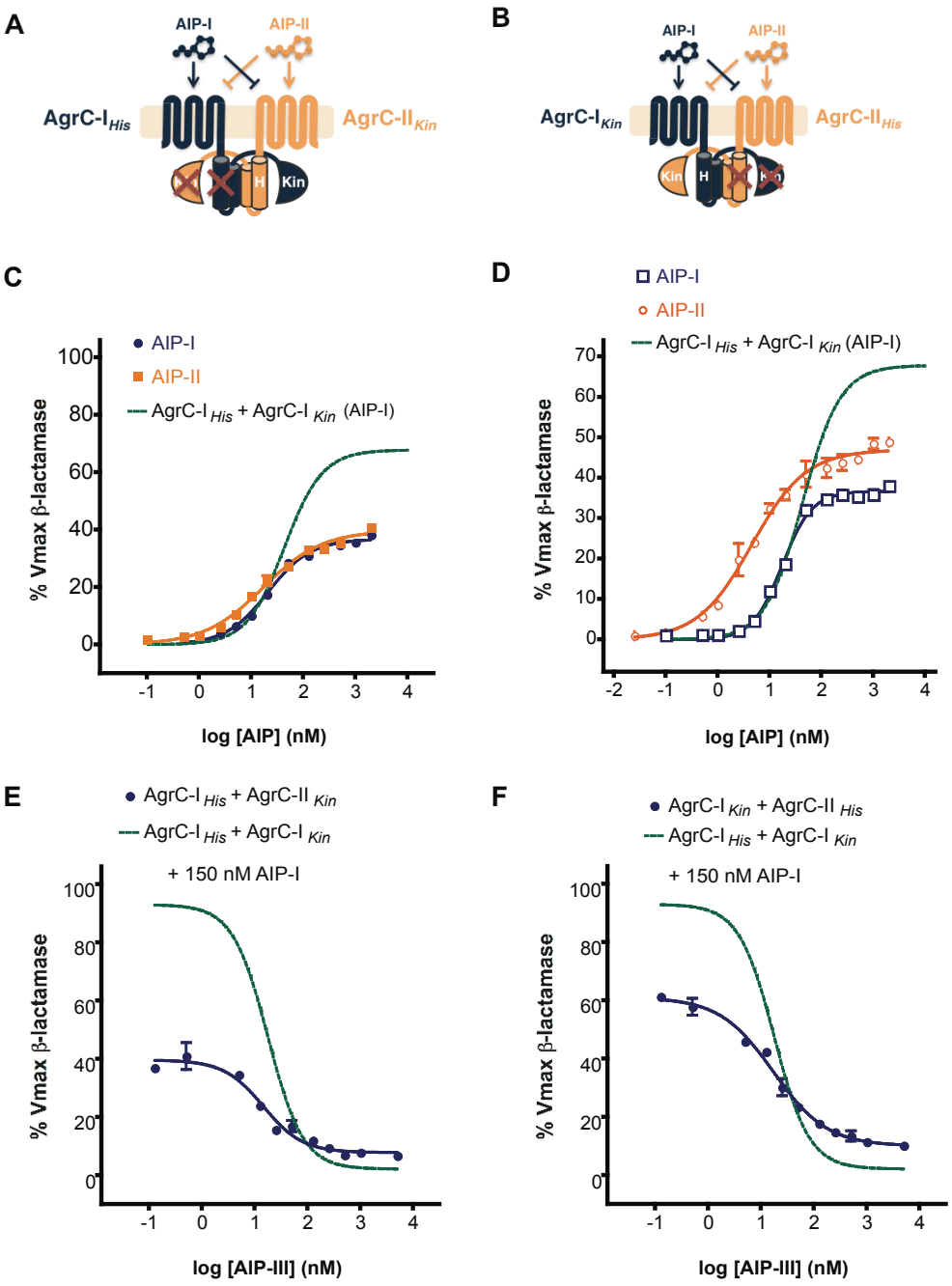

Figure 29. Analysis of Mutant Heterodimers Containing AgrC Receptors of Two Different *agr* Groups. (A, B) Schematics of AgrC-I/II mutant heterodimers. **(C, D)** Activities of the constructs shown above (A, B) treated with AIP-I or AIP-II as indicated. **(E, F)** Activities of (A) and (B) treated with 150 nM AIP-I and increasing AIP-III. Percent activity is relative to maximal activation of WT AgrC-I or AgrC-II (C, D) or of AgrC-I_{His}/AgrC-I_{Kin} (E, F) ± SEM.

To ensure that the ligand recognition by the unnatural AgrC-I/II sensor domain pairings was not fundamentally changed, inhibition by AIP-III, an antagonist of both AgrC-I & II, was tested. Indeed, the two complementary AgrC-I/II mutant heterodimers were potently inhibited by AIP-III (Figure 29E, F and Table 5).

The model taken from the above results involves propagation of activating conformational changes across the dimer interface within the intracellular HK domain, downstream of the ligand-receptor interaction. To test this model, a recently isolated constitutive DHp subdomain mutant, AgrC-I_{R238H} (42), was incorporated into complementary mutant heterodimers. R238 is adjacent to the phosphorylation site histidine (H239) in the predicted dimerization domain. In the absence of ligand, AgrC-I_{R238H} exhibits full activity, equivalent to that observed upon treatment of WT AgrC-I with a saturating concentration of AIP-I (Figure 30C). Like WT AgrC-I, the constitutive mutant exists as a pre-formed dimer (Figure 26B, C); however, the level of homodimerization was less than that of the WT receptor, a finding that may be relevant to the mechanism of the constitutively active receptor.

Provided that AgrC-I_{R238H} assumes the conformational state associated with normal ligand-dependent receptor activation, the symmetric signaling mechanism predicts that this conformation can be transduced to a WT AgrC protomer in a heterodimer configuration, resulting in constitutive *trans*-autophosphorylation. To test this prediction, the histidine and G2-box mutations were introduced to AgrC-I_{R238H}. Individually, the AgrC-$I_{R238H, His}$ and AgrC-$I_{R238H, Kin}$ mutants were inactive (Figure 30C), confirming that ligand-independent activity depends on these critical residues. When co-expressed, complementation

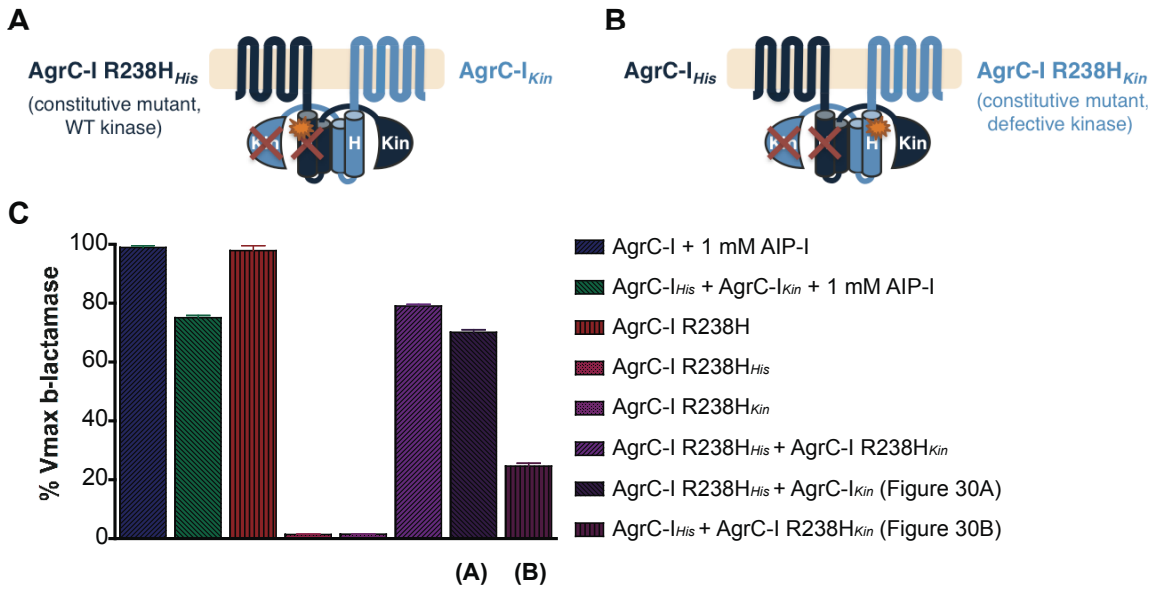

Figure 30. Ligand-independent Signaling by AgrC Mutant Heterodimers Containing One Constitutive R238H Mutant. (A) Schematic of AgrC-I$_{R238H, His}$/AgrC-I$_{Kin}$ in which the protomer with the constitutive mutation also has a WT kinase domain. **(B)** Schematic of AgrC-I$_{His}$/AgrC-I$_{R238H, Kin}$ in which the protomer with the constitutive mutation has a dysfunctional kinase domain. **(C)** Activities of reporter cells expressing the indicated AgrC-I constructs following treatment with or without AIP-I, as indicated. Data are presented as percent maximal activation of WT AgrC-I ± SEM.

between the mutants was observed, with constitutive activity reaching a level similar to that seen with AIP-I-induced activation of the AgrC-I_{His}/AgrC-I_{Kin} complementary pair (Figure 30C). Next, mutant heterodimers composed of one constitutive and one non-constitutive receptor were analyzed. The combination of AgrC-$I_{R238H,\ His}$ and AgrC-I_{Kin}, as illustrated in Figure 30A, resulted in ligand-independent activation at a magnitude nearly as high as that observed with the homologous AgrC-$I_{R238H,\ His}$/AgrC-$I_{R238H,\ Kin}$ pairing (Figure 30C). The key reciprocal combination of AgrC-I_{His} and AgrC-$I_{R238H,\ Kin}$ (Figure 30B), in which the receptor with a functional kinase is missing the constitutive mutation, also exhibited activity in the absence of AIP-I (Figure 30C), In this case, the magnitude of activation was about one third of that seen with AgrC-$I_{R238H,\ His}$/AgrC-I_{Kin}, indicating that the symmetry was imperfect. Nonetheless, an activating conformational change imparted by one point mutation was transferred between protomers of an AgrC dimer.

3.4 Model of AgrC Signaling

On the basis of these results, a working model of AgrC signal transduction has been developed in which cognate ligand binding to one or both transmembrane sensor domains of an AgrC homodimer stabilizes or induces an active conformational state, in turn stabilizing or inducing a conformational change in the corresponding cytoplasmic DHp subdomain(s). Intermolecular interactions across the coiled-coil dimer interface result in functionally parallel conformational changes in both protomers whether or not they are ligand-bound. The concerted adoption of the activated conformational state in both protomers leads to concurrent phosphorylation of both histidines by the contralateral kinase subdomains. While the nature of the conformational changes

responsible for symmetric signaling by AgrC is yet to be determined, they are likely mediated by coiled-coils in the predicted dimerization (DHp) domain. There is one published study demonstrating symmetric signaling in an HPK, in which various chimeras of the aspartate receptor, Tar, and the *E. coli* osmosensor, EnvZ, were analyzed (60). The HAMP domain, a small coiled-coil linking the sensor and HK domains in many HPKs, was determined to be the site of symmetric signaling within the chimeras, based on the observation that homologous HAMP domain pairings enabled symmetric signal transduction through the receptors, whereas heterologous HAMP pairings resulted only in linear, asymmetric receptor signaling. AgrC and other HPK_{10} members do not contain HAMP domains, but their DHp subdomains contain putative coiled-coils. One feasible way a conformational shift could be transmitted between dimeric receptors is via concerted rotation of the coiled-coils. Structural analysis of an archaeal HAMP domain by NMR implied that signaling involves a concerted, gear-like rotational transition between distinct helical packing mode (61). A rotational activation mechanism has also been suggested for the *A. tumefaciens* VirA and yeast Sln1 HPKs, in which the effects of altering the coiled-coil domain helical register were analyzed using N-terminally fused leucine-zipper insertions (94, 95).

Stimulus modulation by cross-talk within dimeric receptors may be adaptive for particular biological functions. Regarding AgrC dimers in staphylococci, symmetric activation may act as a mechanism for signal amplification that is important for the physiological process of quorum sensing, in which a swift, exponential response to a particular concentration of ligand is desired.

Chapter 4: Discussion

4.1 Summary and Implications of this Work

In this work, the tools of chemistry and biology were used to extend the understanding of signal transduction in the *agr* system of *S. aureus*. First, a new, convenient method for the synthesis of AIPs and α-thioester peptides was developed and used to facilitate an analysis of the inhibitory AIP pharmacophore. While previous AIP structure–activity relationships (SAR) had revealed that many substantial perturbations do not prevent AgrC inhibition even though minor changes often result in loss of AgrC activation, the limit of plasticity of the inhibitory AIP structure was not known. In fact, only two bulky, hydrophobic amino acids at the C-terminus and an acylated N-terminus must be present within the thiolactone macrocyclic scaffold to block activation by cognate AIPs (Figure 20). Second, genetic and biochemical approaches led to the discovery that AgrC is a pre-formed dimer that transduces activating conformational change(s) upon AIP binding both linearly within one protomer and laterally across the dimer interface to the sister protomer, resulting in symmetric *trans*-autophosphorylation. This study was the first direct investigation of the activation mechanism of AgrC, the *S. aureus* receptor histidine kinase of the *agr* quorum sensing system that controls virulence.

The new synthetic route to AIPs via Fmoc-SPPS described in Section 2.2 is based on the handle design of Botti et al. (74) but extends this latent thioester linker concept to any resin type. The thiolactone-containing AIP structure can be obtained by simply incubating the corresponding protected peptide α-oxyester precursor in aqueous buffer in the presence of a non-nucleophilic reducing agent

such as TCEP (Figure 12D). Collectively, the data support the cascade-type mechanism shown, in which the reducing agent first triggers the O-to-S acyl transfer at the C-terminus, thereby setting up a transthioesterification reaction between the nascent α-thioester and the cysteine sulfhydryl, yielding the thiolactone with concomitant expulsion of the linker.

In addition to AIP synthesis, the α-hydroxy cysteine linker (**5)** is generally useful for the preparation of peptide α-thioesters for use in native chemical ligation (76) and expressed protein ligation (96) studies. Most of the AIPs and AIP derivatives used in this work were synthesized via the α-hydroxy cysteine linker, and in some cases, an automated microwave-assisted peptide synthesizer was used, highlighting the stability of the linker (Materials and Methods). The linker was also successfully used in the Fmoc-SPPS synthesis of phosphopeptide α-thioesters for use in protein semisynthesis (Mette Jensen, unpublished). However, one important limitation is that the stability of the linker is somewhat sequence dependent. An *N*-methylated residue (Section 2.3.1) or Gly-Gly sequence (Kyle Chiang and Maya Bar-Dagan) at the C-terminus of the peptide prevented attainment of the desired sequences, presumably via diketopiperazine formation during deprotection of the second amino acid coupled to the resin (80, 81). Nonetheless, this method appears amenable to most peptide sequences and offers an improved route to Fmoc-based α-thioester peptides and AIPs. In comparison to the method of Botti et al. (74) upon which the linker was based, this method circumvents the need to repeat the linker installation on every batch of resin used and avoids the exclusive use of resins that swell in water, which are difficult to handle and have low loading capacities, resulting in low yields.

The ability to prepare AIPs via the new Fmoc-SPPS route enabled a systematic SAR analysis of truncated AIP-II (**6**), which was previously found to inhibit *S. aureus* virulence of all four *agr* groups (40). The inhibitory activities of ten trAIP-II analogues were tested against AgrC-II and AgrC-I to evaluate cognate and non-cognate inhibition, respectively. The rank order of the peptides according to potency was roughly the same for both receptors, but as potency decreased, selectivity of the molecules for AgrC-I over AgrC-II increased (Table 4 and Figure 17). Although the main mode of inhibition is still hypothesized to be competitive antagonism at the orthosteric agonist binding site (41), recent work demonstrated that some non-cognate AIPs are inverse agonists of some constitutively active AgrC mutants (42). Of the four *S. aureus agr* groups, group II is the most divergent from the others, and inverse agonism was only observed in AIP–AgrC pairings that included either AIP-II or AgrC-II. Thus, the behavior of inhibitory AIPs may be more complex than that of neutral antagonists, and the mode(s) of inhibition may differ depending on the *agr* groups involved. One or both of these possibilities may explain why the weakest trAIP-II derivative antagonists inhibited AgrC-I much more strongly than AgrC-II.

Cross-group antagonism of the *agr* response by non-cognate AIPs has been used to attenuate the spread of an infection in an animal model (19). Thus, understanding the minimal determinants of inhibition by AIP analogues may be directly applicable to development of an antimicrobial if AgrC proves to be a viable therapeutic target. The Meth Link analogue (**14**) of trAIP-II (Figure 15) encompasses only the elements determined to be required for inhibition in this study (Figure 20) and may represent a good starting point for further medicinal chemistry efforts. Although Meth Link is a very poor inhibitor of AgrC-II, it is a

modest inhibitor of AgrC-I, with an IC_{50} of approximately 1 μM (Table 4). The peptidic character of this molecule has already been reduced compared to the trAIP-II parent peptide via the removal of one amide bond, and its molecular weight of 504 Da is comparable to small molecule therapeutics. The stability of the molecule may be significantly improved if a substitute can be found for the thioester that does not greatly sacrifice inhibitory potency. Notably, such an analogue could provide important clues to solve the longstanding mystery of the basis for the importance of the thioester. The results obtained with the Lactam analogue (**15**) (Table 4) suggest that an amide is not a good choice. Construction of a trAIP-II lactone derivative was attempted via a route analogous to that used to construct full-length AIP-II lactone (19), but the NMR spectra were not consistent with the expected structure although the product had the expected mass. The discrepancy was unfortunately not resolved, leaving open the question of whether an ester is a viable substitution for the thioester in this context. Nonetheless, the lactone variant may not be worth pursuing considering that the full-length AIP-II lactone structure differs dramatically from that of native AIP-II (79), as seen with the lactam derivatives (52, 77, 79). A thioether linkage, which has been proposed as a stabilizing substitute for the thioester (79), may be a better option. Another alternative to the thioester may be an *N*-methylated amide, as such a substitution in the non-ribosomal peptide thiocoraline was recently shown to have no effect on the molecule's antitumor activity, while the oxyester substitution greatly reduced it (97). Finally, work to further reduce the peptidic character of the scaffold and explore SAR of the region lacking important inhibition determinants may prove to increase the drug-like properties and potencies of these AIP-derived antagonists.

As noted above, the reasons for the presence of the thioester linkage in staphylococcal AIPs and the specific requirement of the thiolactone for significant AgrC activation are unknown. These questions are particularly intriguing given the fact that thioesters are rarely found in bioactive natural products. With few known exceptions, such as thiocoraline (98), most thioesters in biology are used as reactive handles to transfer molecules from one protein to another protein. Thus, thioester-containing molecules and protein adducts are typically transient intermediates in biosynthesis or conjugation pathways. In the cases of at least two thioester-containing natural products, largazole (99) and lactacystin (100), the parent molecules are inactive and undergo spontaneous or enzyme-catalyzed modifications to yield active molecules that do not contain thioesters. Overall, these observations are consistent with the intuitive hypothesis that thioester linkages are better suited for biological intermediates than for end products, as thioesters are relatively unstable compared to amides and esters. In contrast to amides and esters, thioesters lack resonance stabilization due to the poor overlap between the non-bonding electrons of the sulfur spd hybrid orbitals and the electrons of the p orbitals of the carbonyl carbon. Additionally, thiols have lower pKa values then the corresponding hydroxyls and are therefore better leaving groups. Given this backdrop of information, a very appealing hypothesis is that the thiolactone AIPs represent transient intermediates. Indeed, Lyon et al. proposed that the AIPs may acylate AgrC (40); however, the results of order-of-addition and wash-out experiments were not consistent with covalent binding to the receptor (41). As AIPs appear to be a rare example of bioactive, thioester-containing final products, perhaps the inherent instability of the thiolactone is advantageous from the perspective of

staphylococci *in vivo*. Spontaneous AIP hydrolysis may contribute to the temporal control of AIP concentration by preventing excessive accumulation of AIP at low bacterial population density and/or persistent AgrC activation. Additionally, RNAIII expression and toxin production decrease in alkaline pH (> 8.0) (101, 102), and AIP hydrolysis may be the mechanism for the observed pH dependence of *agr* output.

The role of the AIP thiolactone in AgrC activation *in vitro* may be related to structural differences among thioesters, esters, and amides that are subtler than the pronounced differences in stability. The resonance stabilization of amides and esters imparts rigidity, whereas thioesters are more flexible. The differences in NMR chemical shifts observed among AIP-II lactam and AIP-II lactone derivatives and native AIP-II suggest that the rigid amide and ester substitutions may change the overall structure of the AIP macrocycle such that it can no longer activate AgrC (52, 77, 79). If so, a thioether linkage may be the ideal thioester substitute to test this possibility and to improve the therapeutic potential of AIP antagonists by imparting stability without sacrificing flexibility.

The mechanistic analysis of AgrC in Chapter 3 yielded the first definitive insights into the activation mechanism of a polytopic, peptide-sensing receptor histidine kinase. Intermolecular complementation of histidine phosphorylation site and kinase domain mutants and co-immunoprecipitation of differentially tagged AgrC variants demonstrated that AgrC is a pre-formed dimer that undergoes *trans*-autophosphorylation. The mechanistic link between AIP binding to an AgrC dimer and the consequential signal transduction to the kinase domains was investigated by further elaborating the robust complementation scheme. Several sensor domain variants were combined with

the complementary mutants to construct AgrC heterodimers in which signaling by individual protomers could be tracked. The observation of ligand-induced activation by a pairing between a truncated receptor and an intact one suggested that one AIP binding event per dimer is sufficient for activation and that the AIP:AgrC stoichiometry is 1:1. Activation in this configuration was rather weak, possibly due to poor expression and incomplete membrane localization of the truncated mutant. To circumvent these limitations, full-length AgrC-I_{Sensor} mutants were used in which only three sensor domain residues are changed, resulting in a 50-fold reduction in the response to AIP-I (58). Accordingly, activation levels of pairings between one AgrC-I_{Sensor} mutant and one WT sensor domain were restored to the magnitude observed with the initial complementary heterodimers containing two WT sensor domains. Remarkably, receptor activation was unaffected by whether or not the sensor domain directly linked to the functional kinase was mutated. Thus, a signal received by one sensor led to activation of either kinase domain, indicating that the mechanism of signal transduction is symmetric within AgrC dimers. Further support for this concept was provided by constructing heterodimers of receptors belonging to the two most divergent *agr* specificity groups, I & II. Although AIP-I is an antagonist of AgrC-II and vice versa, both AIP-I & II activated mutant AgrC-I/II heterodimers equally well. Finally, using a constitutive mutant with a single amino acid change in the DHp domain, activation of a non-constitutive receptor in the heterodimeric configuration was observed, demonstrating that ligand-independent activity is also symmetrically transduced within a dimer.

One key to these results was the ability to directly detect AgrC expression and localization, which had previously been elusive (55). A few important technical considerations enabled the use of fluorescence microscopy and western blot of epitope-tagged variants of AgrC to characterize the mutants used in the study and analysis of AgrC dimers by co-immunoprecipitation. Despite the hypothesis that low abundance of AgrC prevented its visualization (55), past difficulties in detecting AgrC by western blot are most likely attributable to incompatibility of standard denaturation procedures with AgrC, a polytopic membrane protein. Boiling samples prior to gel loading reproducibly resulted in a lack of bands in the western blot, possibly due to aggregation of AgrC (data not shown). Similarly, certain lysis procedures could result in a failure to recover an adequate amount of AgrC for detection. In this study, osmotic shock and detergents were both successfully used to lyse *S. aureus* cells and subsequently detect AgrC in samples that were either treated with dilute acid or that did not undergo any denaturation step at all (Materials and Methods). There are innumerable potential applications for techniques that enable monitoring of AgrC protein levels and localization, and these new tools are expected to greatly aid in future investigations of AgrC (see Section 4.2).

The efficacy and potency of AIP-I toward the initial AgrC-I_{His}/AgrC-I_{Kin} complementary pair was moderately reduced compared to WT AgrC (Figure 25 and Table 5). The drop in efficacy is consistent with the possibility of a statistical mixture of dimers that includes inactive mutant homodimers and the loss of one out of two potential phosphorylation sites per heterodimer. The explanation for the modest change in potency indicated by the change in EC_{50} from 10 to 40 nM is less readily apparent. The EC_{50} values depend on three unknown quantities, as

described in the following equation from Black and Leff's operational model of agonism (103):

$$EC_{50} = K_A/(1 + ([R_T]/K_E)).$$

K_A is the agonist (AIP) affinity for the receptor (AgrC), $[R_T]$ is the total receptor concentration, and K_E is the concentration of agonist-bound receptor that elicits a half-maximal response. This equation is used for standard sigmoidal curves with Hill Slopes equal to one, as is the case for the AgrC reporter assay results. Presumably, the K_A of AIP-I for WT AgrC is the same as that for the complementary AgrC mutants, as the sensor domains are identical in WT AgrC, $AgrC_{His}$, and $AgrC_{Kin}$. According to the analysis of AgrC expression levels by fluorescence microscopy and western blot (Figures 23 and 24), there is little to no difference in expression between WT AgrC and the complementary mutants, suggesting that $[R_T]$ also remains relatively constant in these experiments. However, the total concentration of agonist-bound AgrC that elicits a half-maximal response, K_E, is predicted to increase due to AIP-I binding to the inactive mutant homodimers and the availability of only one out of two phosphorylation sites per active heterodimer. The K_E would change further if the complementary mutations alter events downstream of AgrC activation, such as a change in the affinity between AgrC and AgrA. Thus, both the observed decrease in efficacy and increase in EC_{50} are most likely due to an increase in K_E caused by formation of inactive AgrC homodimers and the loss of one phosphorylation site per active mutant heterodimer.

In the mutant heterodimers formed by AgrC-I & II, the maximal activation levels were further decreased, reaching maximum levels of approximately 40-60% of that observed for AgrC-I_{His}/AgrC-I_{Kin} (Figure 29C, D). This result could

reflect a decreased propensity for the divergent receptors to form dimers, especially if the sensor domains interact at the dimer interface. Co-immunoprecipitation analysis of complementary AgrC-I/II mutant heterodimers could be used to test this possibility. The differential effects of the ligand on each protomer could also result in submaximal signaling by the receptor complex. For example, if AIP-I, an inverse agonist of a constitutive AgrC-II mutant (42), stabilizes or induces an inactive state of AgrC-II, this effect could interfere with an activating conformational change transduced by AgrC-I. Nonetheless, the agonist-induced activation outweighs any interfering effects as evidenced by the robust activation of AgrC-I/II mutant heterodimers by AIP-I and AIP-II.

Inhibition tests of the heterodimers using AIP-III confirmed that the artificial pairings maintained native ligand recognition. However, there was an unexpected subtlety to some of the dose-response curves in which AIP-III appeared to act as a partial agonist at low concentrations. For example, concentrations of AIP-III between 0.5 and 50 nM increased activation of AgrC-I_{His}/AgrC-II_{Kin} by AIP-II (Figure 31A) but not by AIP-I (Figure 31B). To a lesser extent, the same effect was observed for AIP-III inhibition of AgrC-I_{Kin}/AgrC-$I_{Sensor,\ His}$ (Figure 31C). In both cases, AIP-III slightly increased activation at low concentrations only when the mutated kinase was linked to the sensor domain that could perceive the AIP agonist, although AgrC-II_{His}/AgrC-I_{Kin} did not follow this trend when AIP-I was used as the agonist (Figure 31B). The biphasic dose-response curves may be indicative of an allosteric binding site for AIP-III that remained undetected until now since this effect is only observed when the linear pathway for receptor signaling is blocked. An analogous effect called functional selectivity, in which the same ligand acts as a partial agonist or antagonist of the

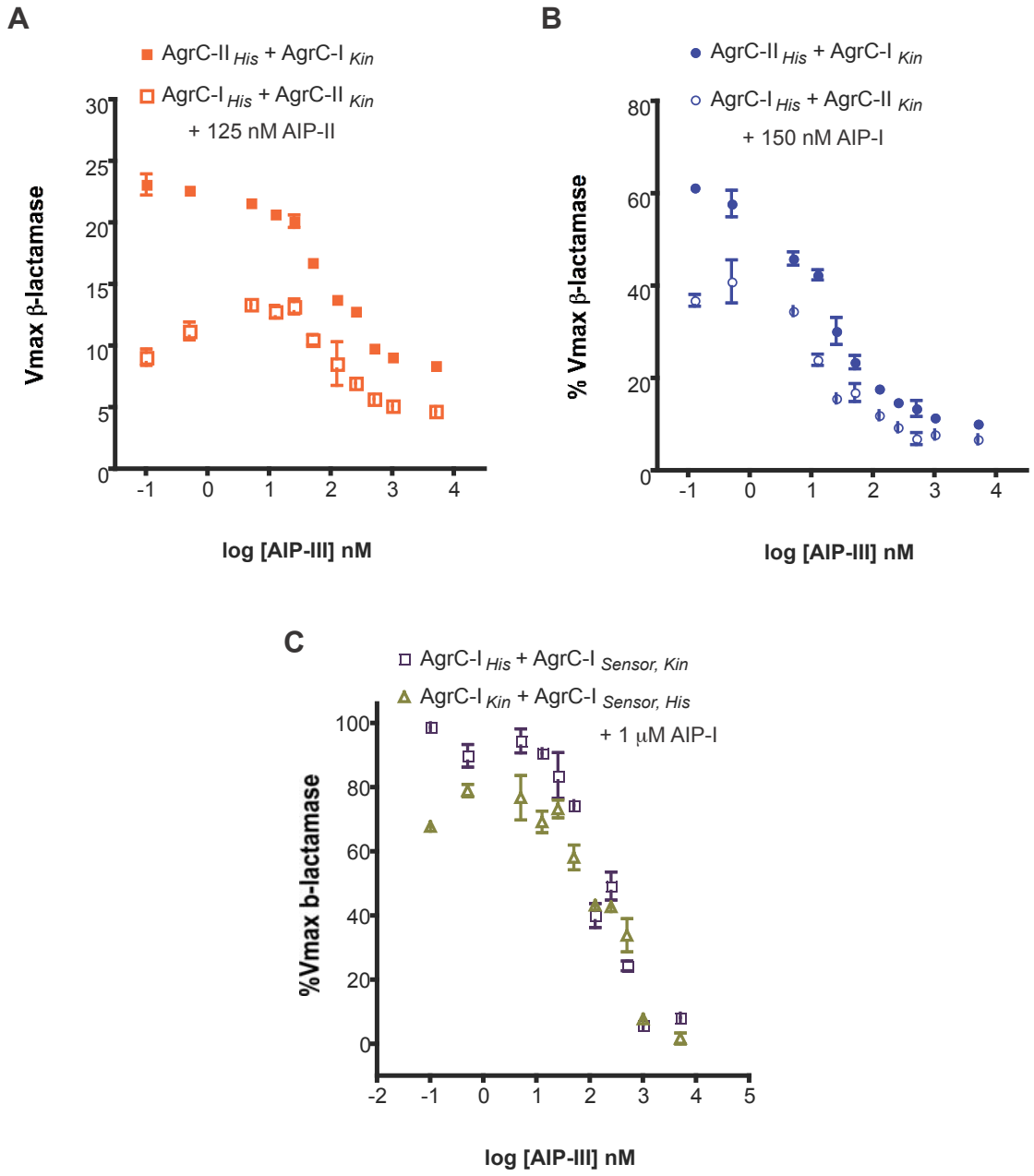

Figure 31. Inhibition of AgrC Mutant Heterodimers by AIP-III. (A, B) AIP-III inhibition of AgrC-I-II heterodimers activated with AIP-II (A) or AIP-I (B). **(C)** Inhibition of AgrC-I_{Sensor} heterodimers activated by AIP-I as in Figure 28D. Error bars represent SEM.

same receptor depending on the context, is attributed to allosteric binding sites in G-protein coupled receptors (GPCRs) (104). Moreover, in some cases, particular effects of the allosteric agonists are only observed in the presence of an orthosteric agonist (104, 105). Alternatively, the apparent partial agonism of AIP-III could be an artifact of the heterodimeric pairings. The development of a direct AgrC binding assay would be an invaluable tool to test for allostery and to better understand the mechanisms of inhibition and inverse agonism.

The ligand-independent activation level of the heterodimer in which the receptor with the R238H mutation had a mutated kinase domain (Figure 30B) was approximately one third that of the heterodimer in which the receptor with the R238H mutation had a WT kinase domain and mutated phosphorylation site (Figure 30A). This imperfect symmetry of signaling by the AgrC R238H mutant may be a clue to the mechanism of this mutant's constitutive activity. Since the AgrC activity was weaker when the R238H mutation was directly adjacent to the H239 phosphorylation site of the same protomer, the constitutive effect of the R238H mutation is neither to recruit the kinase domain to the H239 phosphorylation site nor to cause a conformational change that exposes the adjacent H239 for phosphorylation. Instead, the R238H mutation appears to confer constitutive activity mainly via a direct, *cis* effect on the C-terminal kinase domain of its own protomer and secondarily via an indirect, *trans* effect on the kinase domain of the sister protomer mediated by intermolecular interactions between the two coiled-coils. A second, less favorable possibility is that the R238H mutation mainly promotes an activating conformational change in the sister protomer, which is indirectly transduced to its own coiled-coil and kinase domain via intermolecular interactions at the dimer interface. Although the

former is simpler and ostensibly more likely than the latter, both hypothetical mechanisms could contribute to the low ligand-independent activity observed when the receptor harboring the constitutive mutant lacks a functional kinase domain.

Based on all of the results presented in Chapter 3, the working model of AgrC signaling is that AIP binding to a pre-formed dimer triggers symmetric conformational changes in both protomers directly and/or by intermolecular interactions at the dimer interface (Figure 32). Thus, whether one or both protomer(s) is ligand-bound, they are both activated, resulting in *trans*-autophosphorylation by both kinase domains. This activation mechanism is predicted to be mediated by the putative coiled-coil in the DHp subdomain, the probable site of dimerization. Most of the point mutations within the cytoplasmic HK domains of AgrC and other HPK_{10} receptors found to confer constitutive activity were localized at or very near the putative coiled-coils of the receptors (42, 84, 85). Together, these results suggest that symmetric signaling via concerted conformational changes at the coiled-coil dimer interface may be a general mechanism of activation by quorum sensing HPK_{10} receptors. Beyond the HPK_{10} family, evidence for symmetric signaling via the coiled-coil HAMP linkers of distantly related HPKs was obtained using chimeric mutants of aspartate receptor, Tar, and the osmosensor, EnvZ (60). However, in the case of HPKs such as EnvZ, which sense a general property of the extracellular environment as opposed to discrete chemical ligands, the role of symmetric signaling would necessarily be something other than activating an unliganded sister protomer within a dimer. Perhaps, symmetric signaling could serve to reinforce activating conformational changes and stabilize the activated state. Further study will be

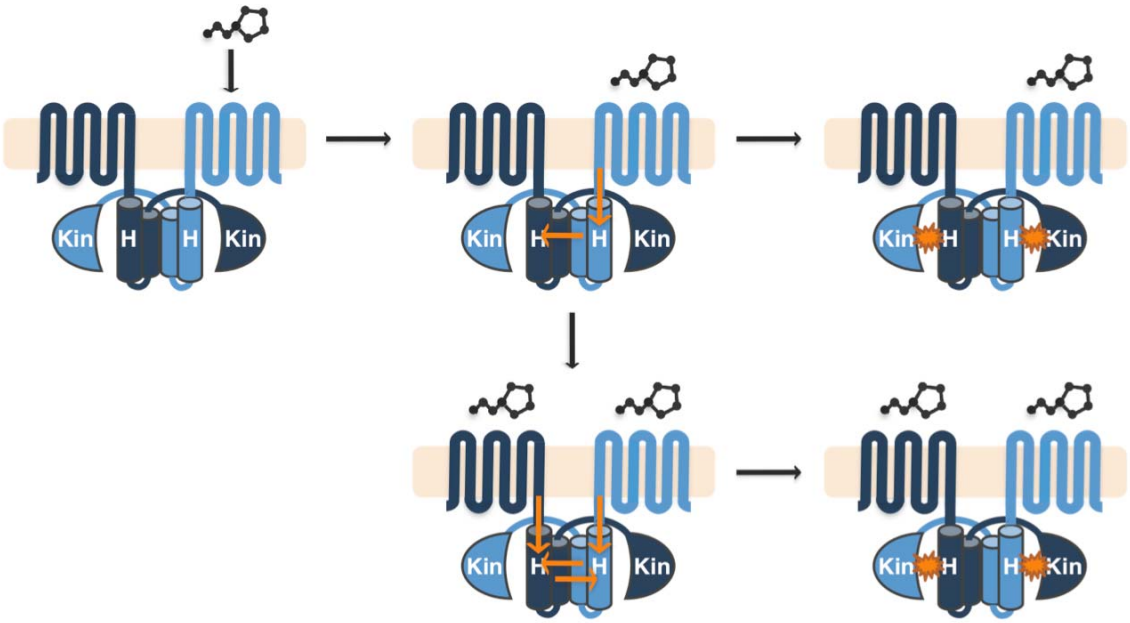

Figure 32. Model of AgrC Signal Transduction. Upon binding of one AIP molecule to an AgrC dimer, a conformational change (orange arrow) is transferred both linearly, to the kinase domain of the liganded protomer, and laterally, across the dimer interface (top). As a result, both kinase domains are activated and *trans*-autophosphorylate. Additionally, a second AIP binding event may occur (bottom), reinforcing the conformational changes in both protomers and thereby further stabilizing the active state.

required to probe the extent to which symmetric signaling is a general mechanism of HPK activation.

In the eukaryotic GPCRs, another class of polytopic receptors in which dimerization is important (106), conformational changes transduced across the dimer interface have been recently observed. In analyses of purified leukotriene B4 GPCR dimers labeled with spectroscopic probes, intermolecular conformational changes were shown to be transmitted between a ligand-bound protomer and an unbound one (107). However, these conformational changes were asymmetric (107) and not sufficient to activate the G-protein associated with the unliganded protomer (108). In another study, FRET experiments used to track specific ligand-induced conformational changes within μ-opioid and α_{2A}-adrenergic receptor heterodimers revealed that interprotomer cross-talk resulted in inhibition of G-protein activation (109). Finally, co-expression of two inactive somastatin-5 (SSTR5) receptor mutants, one that hampered ligand binding and one that disabled signaling, restored activity (110), indicative of symmetric signaling analogous to that observed by AgrC.

The various concerted conformational changes observed in different GPCRs and AgrC may be indicative of an adaptive value of fine-tuned, concerted conformational changes within dimeric receptors for particular biological functions. The ability to modulate stimuli by this type of mechanism may be a major reason why some receptors dimerize or oligomerize instead of simply functioning as monomers. In bacteria, amplification of the autoinducing signal by this mechanism may be particularly beneficial for cell density-dependent processes regulated by quorum sensing receptors, such as virulence, competence, and bacteriocin production (31).

4.2 Future Directions

4.2.1 AIP–AgrC Cross-linking

Previous investigations of the AIP binding determinants within the AgrC sensor domain relied on powerful and readily available genetic methods: site-directed mutagenesis (58, 62); construction of chimeric receptors between different *agr* groups (55); and error-prone PCR followed by activity screening (42). Individual residues responsible for inhibition of AgrC-I (42) and group-specific interactions of *agr* groups I & IV (58, 62) were identified, as well as a putative hydrophobic pocket essential for AIP binding (55) (see Section 1.2.3). In order to build on these findings, work is underway to precisely locate the AIP binding site(s) via covalent AIP–AgrC cross-linking. To this end, AIP-I & II derivatives containing photo-activatable cross-linkers at the N-terminus or in place of a natural amino acid were designed and constructed (Figure 33). First, benzophenone was chosen as the cross-linking moiety, and the amino acid *p*-benzoylphenylalanine (Bpa) was added to AIP-II. Two opposing considerations guided the placement of Bpa within the AIP-II amino acid sequence. Installment of the cross-linker in place of or adjacent to residues known to be critical for AgrC activation may maximize the probability that it will contact the receptor and form a productive cross-link at the binding site. However, this benefit is lost if the cross-linker reduces the AIP affinity for the receptor, suggesting that the cross-linker should be positioned away from critical activation determinants. Thus, Bpa was installed at various positions in the AIP-II sequence, namely Ala4, Ser6, Ser7, and the N-terminus. Although Phe9 is both a key residue for activation and the amino acid that most closely resembles Bpa, AIP-II F9Bpa was

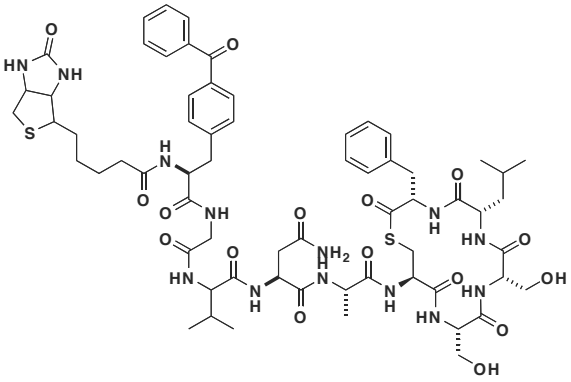

AIP-II Bpa-Biotin (**17**)

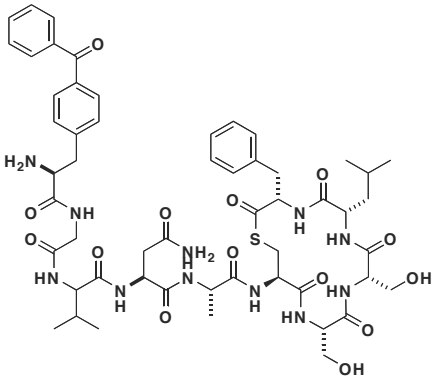

AIP-II Bpa (**18**)

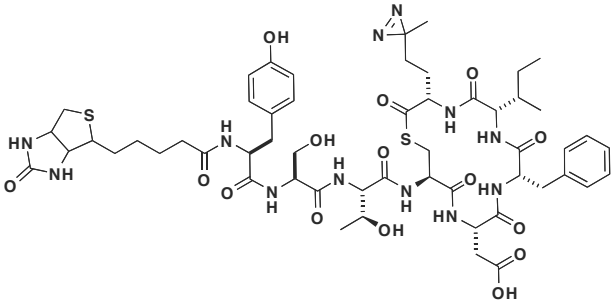

AIP-I M8pMet-Biotin (**19**)

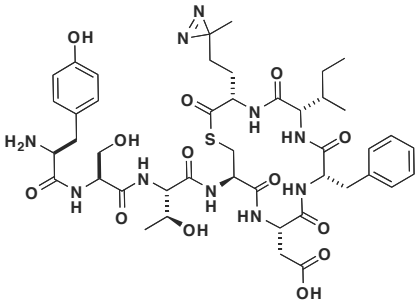

AIP-I M8pMet (**20**)

Figure 33. Structures of AIP Derivatives Containing Cross-linkers.

not made since a similarly bulky naphthylalanine substitution at that position rendered the peptide inactive (55). A biotin handle was added to the N-terminus of each peptide for detection, and control peptides lacking the biotin modification were also prepared to assess its effect on activity. The linear versions of the cross-linker AIP-II analogues were obtained, but the cyclization reactions of AIP-II Ala4Bpa, Ser6Bpa, and Ser7Bpa were low yielding, likely due to interference by the bulky benzophenone side chain (data not shown). Only AIP-II with Bpa coupled to the N-terminus (AIP-II-Bpa-Biotin (**17**), Figure 33) was successfully cyclized and subsequently tested for its ability to activate AgrC-II. Although the control peptide AIP-II-Bpa (**18**) exhibited moderate activation of AgrC-II as compared to that of AIP-II, AIP-II-Bpa-Biotin (**17**) was completely inactive (Table 6) and therefore could not be used in cross-linking experiments.

Subsequent AIP cross-linkers were designed using a photo-reactive analogue of methionine, photo-Met (pMet) (111). The photo-reactive moiety is a diazirine that replaces the thioether sulfur of methionine (Figure 33) and decomposes to a carbene upon irradiation with 330–370 nm light. pMet is sterically similar to methionine; thus, replacement of methionine by pMet in an AIP was anticipated to be a minor perturbation that would not impede AIP cyclization and permit genuine interactions with AgrC. In AIP-I, methionine is the C-terminal amino acid, one of the two hydrophobic residues hypothesized to interact with a hydrophobic pocket in the receptor (55). Thus, AIP-I M8pMet was constructed with and without biotin (**19**, **20**) and tested for activity against AgrC-I (Figure 33 and Table 6). Unlike Bpa, pMet was not commercially available, and Fmoc-pMet was synthesized by Frej Tulin and Matthew Pratt of the Muir Lab (112). Cyclization reactions of AIP-I M8pMet and AIP-I M8pMet-Biotin

Table 6. Activities of AIP Derivatives Containing Cross-linkers

AIP Derivative	AgrC Activation EC_{50} (nM), (95% CI)
AIP-II	12, (4.9-27)
AIP-II-Bpa-Biotin (**17**)	–
AIP-II Bpa (**18**)	59, (23-150)
AIP-I	15, (13-18)
AIP-I M8pMet-Biotin (**19**)	144, (37-565)
AIP-I M8pMet (**20**)	2.5, (1.4-4.3)

– = no activity up to the highest concentration of AIP tested, >10 μM.

proceeded without difficulty, and the substitution of pMet for methionine actually improved potency against AgrC-I (Table 6). The additional biotin handle caused a reduction in activity, but with an EC_{50} value of 140 nM, AIP-I M8pMet-Biotin (**19**) was determined to be suitable for further use in cross-linking studies. Work is currently underway to cross-link **19** to AgrC-I.

Methionines are only present in AIP-I & IV (Figure 3), but cross-linkers that resemble other natural amino acids are also available. For example, photo-leucine and photo-isoleucine, two additional diazirine containing analogues (111), could be used in place of leucine in AIP-II & III and isoleucine in AIP-I, III, & IV; and azido and nitro-phenylalanine analogues (113) could be used in place of phenylalanine or tyrosine in all four AIPs. Use of these additional cross-linking AIP analogues, in which positions of the cross-linking amino acids are varied, may facilitate more complete mapping of the AIP binding site(s) on AgrC as well as enable comparison of cognate and non-cognate binding sites in the four *S. aureus* AgrC receptors.

4.2.2 Inhibition of AgrB (This work was performed in collaboration with Matthew Pratt.)

In addition to inhibition of cognate AIP–AgrC interactions, another possible mode of *agr* interference is targeting of AgrB processing of its propeptide substrate. Based on evidence that AgrB is a cysteine protease (43), the enzyme may be inhibited by epoxysuccinyl derivatives known to target this class of enzymes (114). A bona fide AgrB inhibitor of this type would provide strong support for the proposal that AgrB is in fact a cysteine protease, and perhaps the identity of the catalytic cysteine could be confirmed (43). Furthermore, AgrB is a potential therapeutic target, perhaps more promising than AgrC since prevention

of AIP biosynthesis may be a more effective way to block *agr* activation than administering competitive AgrC antagonists. Thus, an epoxysuccinyl peptide (**26**) designed to inhibit AgrB was constructed (Figure 34).

Like many other cysteine protease inhibitors (114), the AgrB inhibitor design was based on the natural product E-64 (Figure 34), the first reported epoxysuccinyl peptide cysteine protease inhibitor (115). In order to be recognized by AgrB, the conserved Asp-Glu dipeptide at the P1′ and P2′ positions (Figure 4) was incorporated in the molecule, and the electrophilic epoxysuccinyl moiety was appended at the P1 position (Figure 34). The carboxylic acid functionalities were protected as esters to promote passage across the cell membrane where they would presumably be removed by non-specific esterases. In order to synthesize desired product **26**, each *N*-Boc-protected amino acid was activated as a pentafluorophenyl ester (**21** and **22**). An azide handle was appended to the resulting glutamate (**22**) by acylation with *N*,3-dibromopropan-1-ammonium (**23**), followed by displacement of the bromide with sodium azide to form intermediate **24**. Following deprotection of the glutamate Boc group with TFA, the aspartate ester (**22**) and glutamate **24** were coupled to form dipeptide **25**. Finally, the epoxysuccinyl pentafluorophenyl ester, which was synthesized by Matt Pratt, was coupled to the dipeptide to form the final product (**26**).

AgrB inhibition by epoxysuccinyl peptide **26** was assessed by testing its ability to block AIP biosynthesis. *S. aureus* cultures of *agr* group I strains were grown in the presence of various concentrations of **26**, and the supernatants were collected and added to β-lactamase reporter cells. Unfortunately, the addition of the peptide inhibitor had no effect on the supernatants' ability to activate AgrC (data not shown), indicating that it did not block AIP biosynthesis and secretion

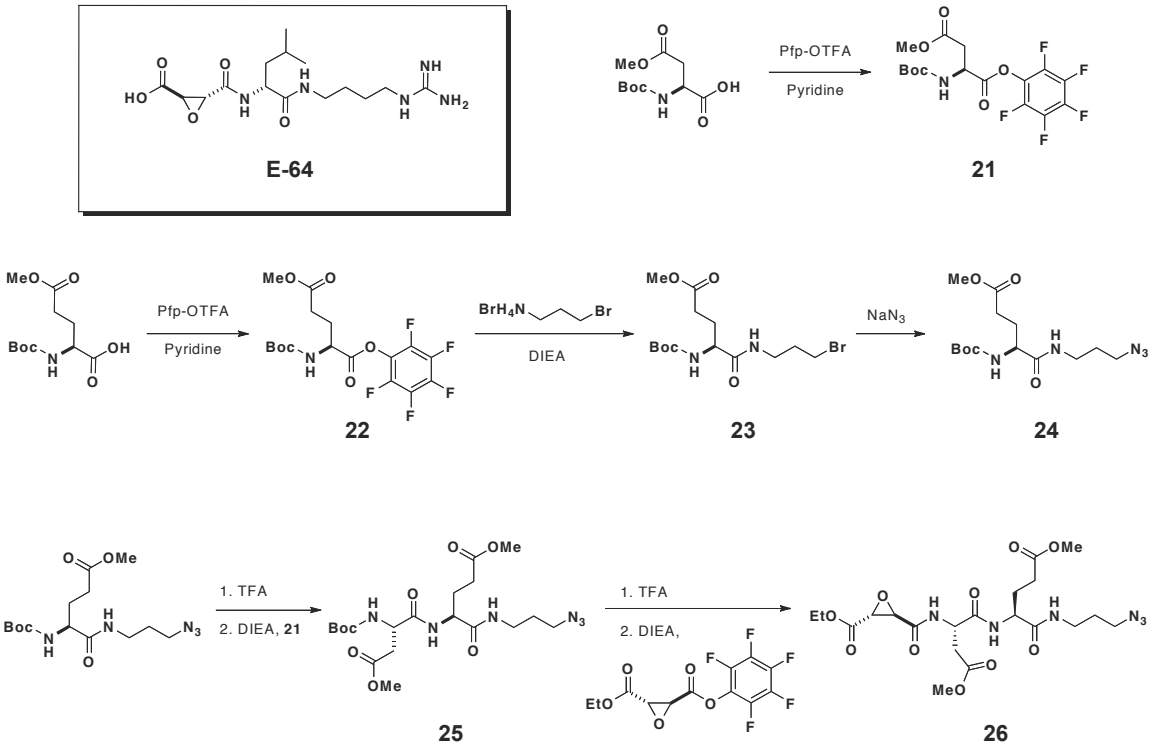

Figure 34. Synthesis of Cysteine Protease Inhibitor Designed for AgrB. The natural product E-64, the first reported epoxysuccinyl peptide cysteine protease inhibitor is shown.

into the medium. In order to rule out the possibility that AIP production occurs before the peptide passes through the membrane, is deprotected by esterases, and reacts with AgrB, the experiment was repeated with cells that received two treatments of peptide **26**. After the first treatment, the supernatants were removed, and the cells were re-suspended in medium containing the inhibitor a second time. However, the same result was obtained. In future efforts, direct labeling of an epitope-tagged version of AgrB in cells or *in vitro* could be probed by western blot with an azide-reactive detection agent such as phosphine-biotin. The most definitive experiment would be to purify AgrB and add the inhibitor without the ester protecting groups *in vitro*. Alternatively, if AgrB purification proved prohibitive, labeling of AgrB could be attempted in *S. aureus* lysates.

4.2.3 Quantitative AIP–AgrC Binding Assay

While the *agr* β-lactamase reporter assay (52) has been an incredibly powerful and useful tool in the study of *agr*, it has limitations nonetheless. Specifically, direct investigation of the receptor–ligand interactions are not possible since the output is a transcriptional read-out downstream of AgrC activation. The development of a direct AIP–AgrC binding assay would immediately help resolve several outstanding questions in the field. First, the binding constants of cognate and non-cognate AIPs could be determined with WT and mutant variants of AgrC missing important determinants for group-specific activation (58, 62). Accordingly, any cooperative effects exerted upon AIP binding to AgrC dimers may be delineated. A direct binding assay would also facilitate definitive determination of the mode(s) of inhibition by non-cognate AIPs (competitive, non-competitive, or uncompetitive) using classical techniques. Finally, the ability to detect AIP–AgrC cross-links (Section 4.2.1) may

be a useful tool to ensure that AgrC is properly folded following isolation for a binding assay; and conversely, a binding assay system could be a useful tool to increase the yield of AIP–AgrC cross-linking. These advances would be a tremendous complement to previous investigations and significantly increase understanding of the *agr* system.

Thus far, a major obstacle to developing a direct AIP–AgrC binding assay has been the isolation of AgrC. Attempts in the lab to over-express and purify AgrC from *E. coli* have been unsuccessful. However, AgrC dimers were successfully isolated by co-immunoprecipitation (Section 3.2.2). These experimental conditions, in which AgrC intermolecular interactions are maintained, are a key step toward the development of conditions to isolate AgrC for a binding assay. Future efforts are aimed at inducing expression of AgrC in *S. aureus* and incorporating the receptor into nanoscale apolipoprotein bound bilayer (NABB) particles, as done previously with GPCRs (116, 117).

4.2.4 AgrC Structure and Further Mechanistic Insights

Although AgrC was shown to be activated via symmetric signaling (see Section 3.3), the structural consequences accompanying this mechanism remain unknown. Thus, the successful application of NMR or crystallographic methods to determine the structure of AgrC in different activation states would be extremely informative. As AgrC is a polytopic membrane protein, determination of the structure of the full-length protein is expected to be very challenging. Even elucidation of the entire cytoplasmic HK domain structure could be equally difficult, as the first complete HK domain crystal structure of a sensor histidine kinase was only recently determined (118). Nonetheless, a structure of only one subdomain may provide great insight into remaining mechanistic questions

regarding AgrC. For example, dimerization plays a key role in the function of AgrC (see Section 3.2), and a crystal structure of the putative coiled-coil dimerization (DHp) subdomain could reveal the location and intermolecular contacts of the dimerization interface. Computational programs that predict the presence of coiled-coils in proteins are available (119) and could be used to design constructs for crystallization. In addition to the WT DHp subdomain, structural studies of a construct containing the R238H constitutive mutant may provide insight into the mechanism of ligand-independent activity and reduced propensity for homodimerization (Figure 26) imparted by the mutation.

As proposed above, symmetric signaling by AgrC may be important for efficient kinase activation at the appropriate AIP concentration. This possibility could be tested by comparing WT AgrC activity in the β-lactamase reporter assay with that of an AgrC mutant that can undergo only asymmetric signaling. In this way, the effect of symmetric signaling on activation efficacy and EC_{50} may be determined. The biggest challenge in this experiment would be to find an AgrC mutant containing change(s) in the coiled-coil sequence that disrupt intermolecular interactions required for symmetric signaling but not dimerization or asymmetric signaling. One good starting point for finding such mutants would be an AgrC coiled-coil structure, if available. Alternatively, the library of AgrC-I mutants already generated via error-prone PCR by Geisinger et al. (42) could be used. In this experiment, AgrC mutants that signal asymmetrically would be isolated by a process of elimination. First, the mutants would be screened for activity in the presence of AIP-I, and any mutants previously identified as constitutively active (42) would be eliminated. Next, variants that signal symmetrically would be eliminated by testing for

complementation between the remaining AgrC-I mutants and AgrC-II_{Kin} in the β-lactamase reporter assay. Those that can signal symmetrically would be activated by AIP-II and eliminated, while AgrC-I mutants that can signal only asymmetrically would not form functional heterodimers with AgrC-II_{Kin} and fail to be activated by AIP-II. In the final elimination step, co-immunoprecipitation analysis would be performed to remove mutants that are not pre-formed dimers. Notably, the discovery of any mutants that fail to exhibit dimerization would not be useful in this experiment, but they would be extremely interesting for further study, as they may undergo *cis*-autophosphorylation. Finally, the contribution of symmetric signaling to overall AgrC activity may be determined by comparing the AIP-I-induced activities of the selected mutants to that of WT AgrC. One caveat to this experiment is that symmetric signaling may contribute only to the kinetics of activation, and this effect would not be observed in the reporter assay. Thus, the potential result of no change between the activities of WT AgrC and asymmetric signaling mutants would be uninterpretable. Secondly, the asymmetric signaling mutants may alter signaling in unpredictable ways independent of blockage of symmetric signaling. In this case, the activities of different asymmetric signaling mutants would vary and prevent determination of the specific contribution of symmetric signaling to AgrC activity. Nonetheless, such an outcome may lead to new insights into the AgrC signaling mechanism.

A second hypothesis generated from the results described in Chapter 3 is that symmetric signaling may be a general phenomenon among quorum sensing receptors, especially those of the HPK_{10} family of AgrC. In order to test this possibility, the predicte coiled-coil region of AgrC could be replaced with that of other HPK_{10} family members in the context of the complementary mutant

schemes and tested for symmetric signaling as described in Chapter 3. Furthermore, mixed combinations could be used to determine whether a heterodimer containing two different coiled-coils still signals symmetrically.

A major outstanding question regarding the mechanism of AgrC activation is whether, in the ground state, the phosphorylation site histidine is occluded from the catalytic (CA) kinase domain or the CA domain is held an inactive conformation, apart from the phosphorylation site. In other words, does AIP binding trigger solvent exposure of the phosphorylation site histidine or release of the CA domain, or both? One experiment that may delineate between these possibilities is co-expression of a construct containing the sensor and DHp domains with a construct containing the CA subdomain in *trans* in the β-lactamase reporter assay (Figure 35). If, in WT AgrC, the phosphorylation site histidine is occluded from the kinase prior to ligand binding, activation would only occur upon addition of AIP. Alternatively, if the kinase is held in an inactive conformation or apart from the phosphorylation site prior to activation, co-expression of the constructs would be predicted to result in constitutive activity. In a similar experiment involving EnvZ of *E. coli*, kinase activity was successfully reconstituted via *trans* expression of the DHp and CA subdomains (120), although the sensor domain was absent. A critical assumption in this experiment is that native conformational changes triggered by AIP binding will be transduced from the sensor domain to the DHp subdomain regardless of whether a CA subdomain is present in *cis* or *trans*. Nonetheless, if this assumption is incorrect, the outcome would likely be lack of activity, and an alternative approach could be to co-express the full-length AgrC-I_{Kin} mutant and the WT CA subdomain.

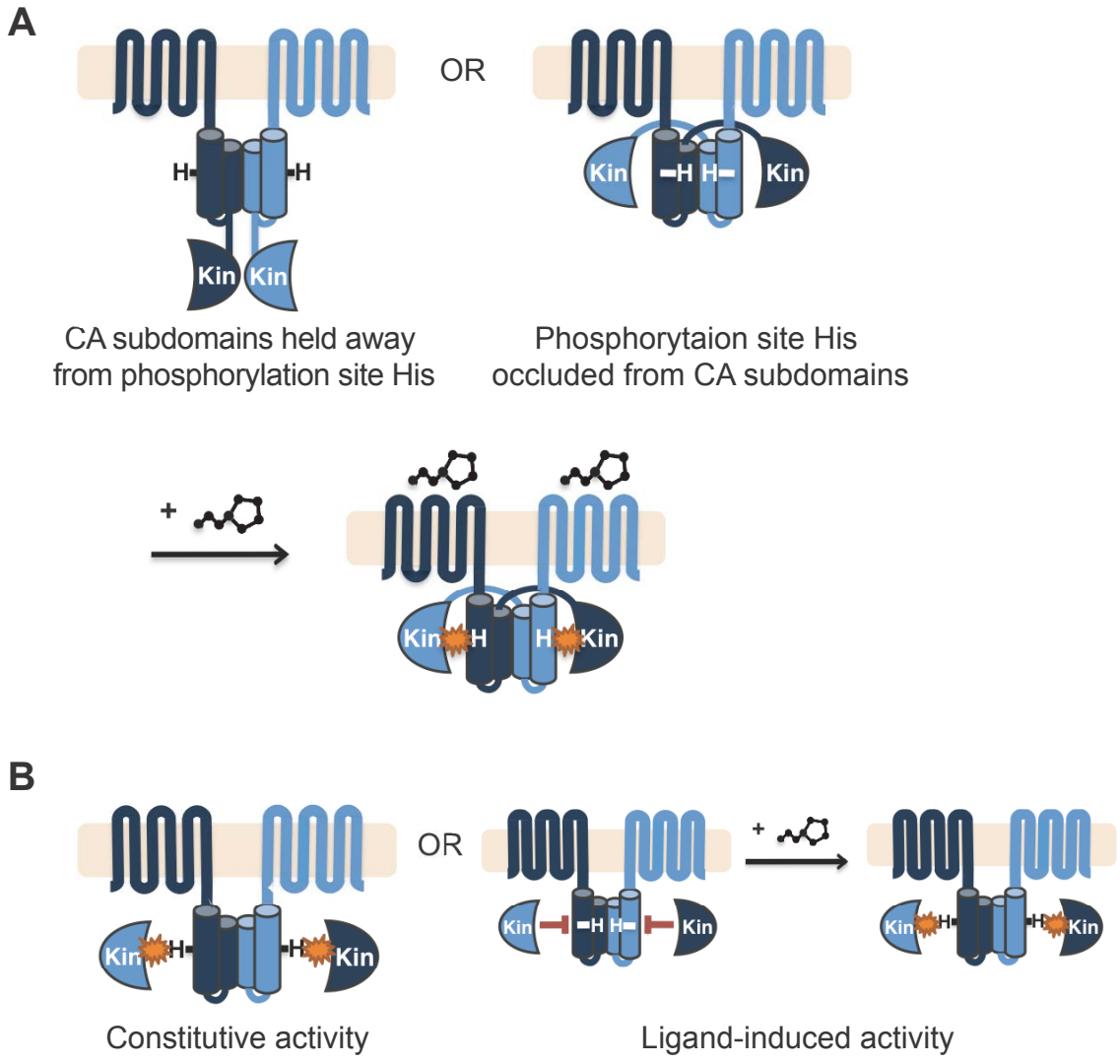

Figure 35. Experimental Scheme for *trans* Expression of AgrC Domains. (A) Two possible mechanisms of AgrC activation. Either the CA subdomains are held away from the target phosphorylation sites or the phosphorylation site histidines are occluded from CA subdomains. Upon addition of AIP, the restraint is removed. **(B)** If AgrC is split between the DHp and CA subdomains and expressed in *trans*, activity is predicted to be constitutive or ligand-dependent, based on the two hypothetical mechanisms.

4.2.5 The *in vivo* Role of *agr* in Virulence

The role of *agr* activation and cross-group interference in establishment and maintenance of *S. aureus* infection is a critical, unresolved problem in the field (121). Certain diseases such as toxic shock syndrome are correlated with a certain *agr* group (122), while others such as cystic fibrosis are associated with all four *agr* groups (123), and indeed some patients are colonized with two or three different groups. There are also varying results regarding the influence of *agr* group identity on host colonization. In one study of patients infected with *S. aureus*, a significant number of individuals were colonized with multiple *agr* groups (124). In contrast, a separate analysis of the nasal flora of healthy volunteers yielded no incidences of multiple *agr* group colonization of *S. aureus*, although many participants harbored multiple *agr* groups of *S. epidermidis* (125). Since cross-group interference has no direct effect on growth, it is unlikely to impact commensal colonization. Instead, certain *agr* groups may have a survival advantage in certain niches. In an insect model of virulence, a correlation was found between relative fitness and specific *agr* groups by monitoring their population densities before and after infection within a mixed culture (126). Thus, there is a plausible role for interference in infection, but it is also conceivable that certain *agr* groups have an enhanced ability to carry out a particular disease process unrelated to cross-group inhibition.

The temporal regulation of *agr in vivo* has been examined by Wright et al. (127) who used an *agr* P3::lux reporter system to monitor *agr* activation in real time in a mouse abscess model of *S. aureus* infection. As expected, *agr* was activated a few hours after injection of the bacteria, and this initial burst of activity lasted only a few hours. Remarkably, a second burst of *agr* activity was

observed approximately 72 hours after the initial infection. This behavior does not represent a temporary diminishment of the bacterial population based on consistent cell density; although it may be indicative of low metabolic activity or phagocytosis by neutrophils. Co-injection of a non-cognate AIP with the bacteria led to a reduction in *agr* activation at the early time points and, importantly, no abscess formed over five days. Interestingly, the second burst of *agr* activity did not occur in this case, suggesting that the initial burst of *agr* activity is required for the resurgence. This result was especially surprising considering that the AIP half-life is a few hours in serum (127). Analogous experiments in which mice were injected with agr^- strains confirmed that *agr* activation is required to establish an infection in this experimental model.

Despite considerable evidence that virulence of *S. aureus* strains lacking a functional *agr* locus is attenuated and are not competent to establish infection (18-21, 127), many drug-resistant strains and clinical isolates are paradoxically missing a functional *agr* locus (16, 128-130). At least some of these dysfunctional *agr* mutations arise following the initial establishment of infection (131), and mixed populations of agr^+ and agr^- strains have been isolated from the same individual (131, 132), raising the possibility that *agr* activation by part but not all of the bacterial population is required for infection. Perhaps a subsequent loss of *agr* function confers an advantage for long-term survival in the host due to the metabolic demand of *agr* activation. In any case, the fundamental question of whether *S. aureus* can cause an infection without *agr* activation has yet to be definitively answered. Thus, the viability of *agr* as a prophylactic or therapeutic target is promising but unknown pending future work in this area.

4.3 Conclusion

The work presented here elucidated several mechanistic features of the *agr* system and produced methods expected to aid greatly in future studies. The identification of the minimal determinants for AIP inhibition of AgrC lays a foundation for future medicinal chemistry efforts to increase the physiological stability and efficacy of potential AIP-based therapeutics. The finding that AgrC activation occurs via symmetric signaling by pre-formed dimers represents a significant advance in the mechanistic understanding of AgrC, and the development of fluorescence imaging and western blot analysis of AgrC provides the long awaited ability to monitor receptor expression. Intriguing future directions for investigation of *agr* include analysis of AIP–AgrC interactions by cross-linking and direct binding assays, elucidation of the structural basis for AgrC symmetric signaling, and clarification of the significance of *agr* in infection.

Whether or not *agr* proves to be therapeutically relevant, a deeper understanding of the mechanisms that contribute to virulence will increase knowledge of *S. aureus* infections and provide the foundation for new discoveries and eventual advances in treatment. The insights described in this work will hopefully be applicable to other quorum sensing receptors and serve to build connections between the molecular mechanisms of AgrC activation and inhibition and *S. aureus* virulence *in vivo*.

Chapter 5: Materials and Methods

Materials. Amino acids, HBTU, HATU, PyBop, and Rink and MBHA resins were purchased from Novabiochem (San Diego, CA) with the exceptions of Boc-*N*-methylphenylalanine (Fluka, Buchs, Switzerland) and Fmoc-DAPA(Boc)-OH (Neosystem Laboratoire, Strasbourg, France). All solvents were obtained from Fisher (Pittsburgh, PA), and trifluoroacetic acid was obtained from Halocarbon (River Edge, NJ). All other chemical reagents, including DNase and poly-lysine solution, were purchased from Sigma Aldrich (Milwaukee, WI). Oligonucleotide primers were synthesized by Integrated DNA Technologies (Coralville, Iowa). QuikChange kits for site-directed mutagenesis were obtained from Stratagene/Agilent (Cedar Creek, TX). Lysostaphin was purchased from AMBI Products LLC (Lawrence, NY), and Criterion Tris-HCl gels were purchased from Bio-Rad (Hercules, CA). Immuno Elution Buffer and BCA assay kit were obtained from Pierce (Rockford, IL). Protease inhibitors and mouse anti-GFP antibodies were obtained from Roche (Indianapolis, IN). Mouse anti-HA antibodies and anti-HA affinity matrix were purchased from Covance (Emeryville, CA), rabbit anti-Sortase antibodies from Abcam (Cambridge, MA) and anti-mouse horse radish peroxidase (HRP) and anti-rabbit HRP antibodies from Bio-Rad (Hercules, CA). ECL and ECL Plus were obtained from Amersham (Buckinghamshire, UK), and glass slides and coverslips were obtained from Fisher (Pittsburgh, PA).

Reversed-Phase HPLC and Mass Spectrometry. Analytical and semipreparative HPLC was performed using a Hewlett-Packard 1100 series instrument with diode array detection. A Vydac C-18 column (5 μm, 4.6 x 150 mm) with a 1 mL/min flow rate was used for analytical scale HPLC, a Vydac C-18 column (10

μm, 10 x 250 mm) with a 4 mL/min flow rate was used for semipreparative HPLC, and a Vydac C-18 column (10 μm, 22 x 250 mm) with an 18 mL/min flow rate was used for preparative HPLC. A Waters 2795 Separations Module plus 996 photodiode array detector with a Vydac C18 column (3μm, 2.1 x 150 mm) and a 0.2 mL/min flow rate was used for LC-MS. In all cases, linear gradients of 0.1% aqueous TFA (solvent A) versus 90% acetonitrile, 10% water, and 0.1% TFA (solvent B) were utilized. ESI-MS was performed on a PE Sciex API-100 single quadrupole electrospray mass spectrometer. ESI-HRMS was performed on a Q–TOF Ultima hybrid quadrupole time-of-flight electrospray mass spectrometer (University of Illinois at Urbana-Champaign Mass Spectrometry Laboratory).

NMR Spectroscopy. Compounds **12**-**16** were dissolved in CD_3-OD or $CDCl_3$, and ^1H and ^{13}C NMR spectra were recorded with a Bruker 400 MHz spectrometer. Measurements were taken at 298 K, and chemical shift values are relative to methanol (^1H 3.31 ppm, ^{13}C 49.00 ppm) or chloroform (^1H 7.26 ppm, ^{13}C 77.16 ppm). Peptides **6**-**16** were dissolved in DMSO-d_6, and 1-D ^1H, homonuclear ^1H TOCSY, and ROESY experiments were performed on a Bruker 400 MHz spectrometer, Bruker 600 MHz spectrometer with cryoprobe, or Bruker Avance 700 MHz spectrometer with cryoprobe, respectively. The mixing times were 77 and 200 ms for TOCSY and ROESY experiments, respectively. In all cases, the sample temperature was 298 K, and the reported chemical shift values are relative to DMSO at 2.50 ppm. The chemical shift index (CSI) of each peptide was calculated using the formula

$$\mathrm{CSI} = \sum (|\mathbf{a}\delta_i - \mathbf{6}\delta_i|)/n$$

where **a** is the peptide of interest, **6** is peptide **6**, i is the proton type (e.g., Cys1

NH), and n is the total number of protons included in the calculation. Protons directly bonded to the macrocyclic scaffold plus the exocyclic N-terminal amide proton were included in each CSI (Cys1 NH, αH, βH; Ser2 NH, αH; Ser3 NH, αH; Leu NH, αH; and Phe NH, αH). The protons of the modified residue(s) were excluded.

Synthesis. 3-*t*-Butyldisulfanyl-propane-1,2-diol (1). A solution containing 1-mercapto-ethane-1,2-diol (3.0 g, 27.7 mmol, 1.0 equiv), 2-methyl-propane-2-thiol (25 g, 277 mmol, 10.0 equiv), and triethylamine (7.0 g, 69.3 mmol, 2.5 equiv) dissolved in methanol (55 mL) was stirred at room temperature with bubbling O_2 overnight (>10 h). Methanol and excess 2-methyl-propane-2-thiol were removed in vacuo, and the crude product was purified by flash chromatography using 3:2 hexanes/ethyl acetate to give 5.4 g of **1** (99%) as a clear oil. ^{1}H NMR (400 MHz, CD_3OD) δ 3.83 (m, 1H), δ 3.58 (dd, 1H, J = 11.3, 4.8 Hz), δ 3.52 (dd, 1H, J = 11.3, 5.8 Hz), δ 2.90 (dd, 1H, J = 13.3, 5.3 Hz), δ 2.78 (dd, 1H, J = 13.3, 7.3 Hz), δ 1.34 (s, 9H); ^{13}C NMR (100 MHz, CD_3OD) δ 72.33, δ 65.90, δ 48.45, δ 45.64, δ 30.25, ESI-MS m/z calcd for $C_7H_{16}O_2S_2$ 196.3, found 393.0 ([2M + H^+]).

In an updated route to **1** in two steps, a solution containing 2-methyl-propane-2-thiol (4.5 g, 49.9 mmol, 1.1 equiv), 2,2′-dithiodipyridine (10.0 g, 45.4 mmol, 1.0 equiv), and triethylamine (4.6 g, 45.4 mmol, 1.0 equiv), dissolved in methanol (230 mL) was stirred at room temperature overnight (>10 h). Methanol and excess 2-methyl-propane-2-thiol were removed in vacuo, and the crude product was purified by flash chromatography using 1:1 dichlorometane /methanol to give 9.1 g of 2-(*tert*-butyldisulfanyl)pyridine (99%). ^{1}H NMR (400 MHz, $CDCl_3$) δ 8.42 (m, 1H), δ 7.79 (m, 1H), δ 7.63 (m, 1H), δ 7.05 (m, 1H), δ 1.34

(s, 9H). In the subsequent step, a solution containing 2-(*tert*-butyldisulfanyl)pyridine (9.1 g, 45.4 mmol, 1.0 equiv), 1-mercapto-ethane-1,2-diol (5.4 g, 50.2 mmol, 1.2 equiv), and triethylamine (9.3 g, 91.4 mmol, 2.0 equiv), dissolved in methanol (150 mL) was stirred at room temperature overnight (>10 h). Methanol was removed in vacuo, and the crude product was extracted with ethyl acetate, washed with 1 N HCl, 1 N NaOH, brine, and dried over Na_2SO_4, filtered, and further dried in vacuo. Purification by flash chromatography using 3:2 hexanes/ethyl aectate to give 6.7 g of **1** (75%).

1,2-Bis-(*t*-butyl-dimethyl-silanyloxy)-3-*t*-butyldisulfanylbutyldisulfanyl-propane (2). *t*-Butyl-chloro-dimethyl-silane (11 g, 72 mmol, 3.0 equiv), imidazole (9.8 g, 144 mmol, 6.0 equiv), and 4-dimethylaminopyridine (170 mg, 1.4 mmol, 0.06 equiv) were added on ice to a solution of **1** (4.7 g, 24 mmol, 1.0 equiv) dissolved in 240 mL of anhydrous DMF. The reaction was stirred under N_2 at room temperature overnight at which point 0.5 N NaOH was added to quench the reaction, and the product was extracted with ethyl acetate, washed with 1 N HCl, dried over Na_2SO_4, filtered, and dried in vacuo. Excess DMF was removed by an azeotrope with hexanes to yield 10 g (99%) of **2**, which was taken on to the next step without further purification. ^{1}H NMR (400 MHz, $CDCl_3$) δ 3.89 (m, 1H), δ 3.61 (dd, 1H, J = 10.1, 5.0 Hz), δ 3.53 (dd, 1H, J = 10.1, 6.3 Hz), δ 2.99 (dd, 1H, J = 13.1, 4.9 Hz), δ 2.73 (dd, 1H, J = 13.1, 6.7 Hz), δ 1.33 (s, 9H), δ 0.90 (s, 18H), δ 0.08 (m, 12H); ^{13}C NMR (100 MHz, $CDCl_3$) δ 72.70, 66.40, 47.81, 46.00, 30.06, 26.10, 26.04, 25.86, 25.82, 18.50, 18.30, -2.79, -3.41, -4.39, -4.20, -5.20, -5.18, ESI-MS m/z calcd for $C_{19}H_{44}O_2S_2Si_2$ 424.2, found 423.0 ([M$^-$]).

2-(*t*-Butyl-dimethyl-silanyloxy)-3-*t*-butyldisulfanyl-propan-1-ol (3). A cold 1:1 mixture of TFA and water (18 mL) was added dropwise to a solution of **2** (4.4 g, 10 mmol, 1.0 equiv) in 45 mL of THF. The reaction was stirred at 0 °C for 4.5 h, and then it was slowly poured into a separation funnel containing an ice cold solution of $NaHCO_3$ to bring the pH above 7. The product was extracted with ethyl acetate, washed with water and brine, dried over Na_2SO_4, and filtered, and the solvents were removed in vacuo. Purification by flash chromatography with 15:1 hexanes/ethyl acetate yielded 2.0 g (65%) of **3**. ^{1}H NMR (400 MHz, CD_3Cl) δ 3.97 (m, 1H), δ 3.70 (dd, 1H, J = 11.3, 3.5 Hz), δ 3.62 (dd, 1H, J = 11.3, 4.0 Hz), δ 2.87 (dd, 1H, J = 13.4, 7.2 Hz), δ 2.79 (dd, 1H, J = 13.4, 5.4 Hz), δ 1.34 (s, 9H), δ 0.91 (s, 9H), δ 0.13 (s, 3H), δ 0.10 (s, 3H); ^{13}C NMR (100 MHz, $CDCl_3$) δ 72.14, 65.01, 48.06, 44.05, 29.98, 25.93, 18.19, -4.29, -4.48, -4.62, ESIMS m/z calcd for $C_{13}H_{30}O_2S_2Si_2$ 310.2, found 309.0 ([M^-]).

2-(*t*-Butyl-dimethyl-silanyloxy)-3-*t*-butyldisulfanyl-propionaldehyde (4). Dess-Martin periodinane (1.3 g, 3.1 mmol, 1.2 equiv) was added to a solution of **3** (800 mg, 2.6 mmol, 1.0 equiv) in 26 mL of CH_2Cl_2 under N_2. The reaction was stirred at room temperature for 2 h, then diluted with CH_2Cl_2 and ethyl acetate. The product was washed with 0.1 N HCl, 1 N NaOH, and brine, dried over Na_2SO_4, and filtered, and the solvents were removed in vacuo. Purification by flash chromatography using 19:1 hexanes/ethyl acetate yielded 590 mg (73%) of **4**. ^{1}H NMR (400 MHz, $CDCl_3$) δ 9.64 (s, 1H), δ 4.22 (m, 1H), δ 2.99 (dd, 1H, J = 13.4, 4.2 Hz), δ 2.80 (dd, 1H, J = 13.4, 7.9 Hz), δ 1.31 (s, 9H), δ 0.91 (s, 9H), δ 0.12 (s, 3H), δ 0.10 (s, 3H); ^{13}C NMR (100 MHz, CDCl3) δ 202.17, 76.57, 48.22, 43.66, 29.97, 25.84, 18.30, -4.55, -4.63, ESI-MS m/z calcd for $C_{13}H_{28}O_2S_2Si$ 308.1, found 309.0 ([M+H^+]).

2-(*t*-Butyl-dimethyl-silanyloxy)-3-*t*-butyldisulfanyl-propionic Acid (5).

Compound **4** (227 mg, 0.74 mmol, 1.0 equiv) was dissolved in 4 mL of *t*-butyl alcohol. 2-Methyl-2-butene (3.02 g, 42.9 mmol, 58 equiv) was added to the solution on ice, followed by a pre-dissolved solution of monobasic sodium phosphate (225 mg, 1.63 mmol, 2.2 equiv) and 80% sodium chlorite (251 mg, 2.22 mmol, 3.0 equiv) in water (4 mL). The reaction was stirred vigorously to ensure mixing of the two phases at room temperature for 2 h. The reaction mixture was diluted with ethyl acetate, washed with 0.1 N HCl and brine, dried over Na_2SO_4, and filtered, and the solvents were removed in vacuo. Purification by flash chromatography using 19:1 CH_2Cl_2/methanol yielded 160 mg (66%) of **5** as a clear oil. ^{1}H NMR (400 MHz, $CDCl_3$) δ 4.47 (m, 1H), δ 3.12 (dd, 1H, J = 13.4, 3.6 Hz), δ 2.93 (dd, 1H, J = 13.4, 7.9 Hz), δ 1.33 (s, 9H), δ 0.92 (s, 9H), δ 0.15 (s, 3H), δ 0.13 (s, 3H); ^{13}C NMR (100 MHz, $CDCl_3$) δ 176.60, 71.27, 48.23, 45.77, 30.00, 25.82, 18.29, -4.80, -4.86, ESI-HRMS m/z calcd for $C_{13}H_{28}O_3S2Si$ [M + H^+] 325.1327, found 325.1329.

Fmoc-SPPS of AIPs. Native AIPs and peptides **6**-**12**, **14**, **16**, **19**, and **20** were synthesized manually or with a Liberty microwave-assisted automated peptide synthesizer (CEM). Linker **5** (188 mg, 0.61 mmol, 1.1 equiv relative to resin substitution) was added to a solution of HBTU (207 mg, 0.55 mmol, 1.0 equiv relative to resin loading) in DMF (1.2 mL), followed by DIEA (diisopropylethylamine) (0.25 mL, 1.44 mmol, 2.6 equiv relative to resin) to pre-activate the acid. After 3 min, the solution was added to Rink amide resin and stirred by bubbling N_2 through the vessel at room temperature for 4 h. Remaining free amines were acetylated by two treatments with a 1:1:8 solution of

acetic anhydride/DIEA/DMF for 10 min. Deprotection of the TBS group was accomplished by the addition of tetrabutyl ammonium fluoride (10 mL of a 1.0 M solution in THF) overnight at room temperature. 4-Dimethylaminopyridine (0.1 equiv relative to the C-terminal amino acid) was used in addition to HBTU and DIEA to double couple the C-terminal amino acid to the hydroxyl group of the linker. For automated syntheses, the resin was loaded onto the peptide synthesizer at this point. Subsequent steps were completed with standard HBTU/DIEA activation and piperidine deprotection protocols for Fmoc solid-phase peptide chemistry with a few exceptions. *N*-Methylated amino acids were double coupled, once with HBTU and once with HATU. Other unnatural monomers were coupled with standard methods. Finally, peptides **6–12**, **14**, and **16** were acetylated at the N-terminus with a 1:1:8 solution of acetic anhydride/DIEA/DMF for 10 min. Each peptide was cleaved from the solid support by treatment with 95:2.5:2.5 TFA/TIS/water for 3-4 h at room temperature, followed by filtration and washing of the beads with the TFA cleavage cocktail. The peptides were either purified by semipreparative or preparative HPLC or taken on to the cyclization step without purification.

The cyclization buffer contained 20% acetonitrile and 80% 6 M guanidinium chloride in 0.1 M sodium phosphate buffer pH 6.5. TCEP (tris-(2-carboxy)ethyl phosphine) (70 mM) was added to this solution, and the pH was brought back up to 6.6-6.8 with 4 M NaOH. Each linear peptide was dissolved in this solution to a final concentration of 100 μM and rocked at room temperature for 2-24 h, and the reaction was monitored by analytical HPLC. The desired AIP product was then purified by semipreparative or preparative HPLC.

Data for trAIP-II (6). ^{1}H NMR (400 MHz, DMSO-d_6) δ 8.68 (d, ^{1}H, J = 8.8 Hz), δ 8.46 (d, 1H, J = 8.2 Hz), δ 8.12 (m, 2H), δ 7.60 (d, 1H, J = 8.7 Hz), δ 7.25 (m, 2H), δ 7.21 (m, 3H), δ 5.12 (t, 1H, J = 5.4 Hz), δ 5.03 (t, 1H, J = 5.4 Hz), δ 4.56 (m, 1H), δ 4.39 (m, 1H), δ 4.28 (m, 1H), δ 4.22 (m, 1H), δ 3.92 (m, 1H), δ 3.64 (m, 1H), δ 3.58 (m, 2H), δ 3.52 (m, 1H), δ 3.31 (obsc 1H), δ 3.16 (m, 1H), δ 2.84 (m, 2H), δ 1.86 (s, 3H), δ 1.38 (m, 1H), δ 1.30 (m, 1H), δ 1.22 (m, 1H), δ 0.74 (d, 3H, J = 6.3 Hz), δ 0.71 (d, 3H, J = 6.3 Hz), ESI-MS m/z calcd for $C_{26}H_{37}N_5O_8S$ 579.2, found 580.0 ([M + H^+]). See appendix for chemical shift assignments of peptides **6–16**.

Data for S2G (7). ^{1}H NMR (400 MHz, DMSO-d_6) δ 8.67 (d, 1H, J = 9.0 Hz) δ 8.44 (d, 1H, J = 7.9 Hz), δ 8.21 (m, 1H), δ 7.99 (d, 1H, J = 7.7 Hz), δ 7.59 (d, 1H, J = 8.3 Hz), δ 7.26 (m, 2H), δ 7.20 (m, 3H), δ 5.21 (t, 1H, J = 5.5 Hz), δ 4.59 (m, 1H), δ 4.32 (m, 1H), δ 4.21 (m, 1H), δ 3.98 (m, 1H), δ 3.89 (m, 1H), δ 3.62 (m, 1H), δ 3.52 (m, 1H), δ 3.32 (obsc, 1H), δ 3.31 (obsc, 1H), δ 3.16 (m, 1H), δ 2.84 (m, 2H), δ 1.86 (s, 3H), δ 1.31 (m, 2H), δ 1.18 (m, 1H), δ 0.74 (d, 3H, J = 6.2 Hz), δ 0.69 (d, 3H, J = 6.2 Hz), ESI-MS m/z calcd for $C_{25}H_{35}N_5O_7S$ 549.2, found 550.0 ([M+H^+]).

Data for S3G (8). ^{1}H NMR (400 MHz, DMSO-d_6) δ 8.46 (m, 1H), δ 8.36 (d, 1H, J = 7.4 Hz), δ 8.30 (d, 1H, J = 8.0 Hz), δ 8.02 (m, 2H), δ 7.24 (m, 5H), δ 4.64 (m, 1H), δ 4.41 (m, 2H), δ 3.99 (m, 1H), δ 3.79 (dd, 1H, J = 14.0, 3.6 Hz), δ 3.57 (m, 3H), δ 3.35 (obsc, 1H), δ 3.13 (m, 1H), δ 2.91 (m, 1H), δ 2.62 (m, 1H), δ 1.86 (s, 3H), δ 1.49 (m, 1H), δ 1.12 (m, 2H), δ 0.78 (d, 3H, J = 6.5 Hz), δ 0.71 (d, 3H, J = 6.5 Hz); ESI-MS m/z calcd for $C_{25}H_{35}N_5O_7S$ 549.2, found 550.0 ([M+H^+]).

Data for GG (9). ^{1}H NMR (400 MHz, DMSO-d_6) δ 8.39 (m, 1H) δ 8.29 (m, 2H), δ 8.15 (d, 1H, J = 9.4 Hz), δ 8.08 (m, 1H), δ 7.23 (m, 5H), δ 4.67 (m, 1H), δ 4.42 (m, 1H), δ 4.10 (m, 1H), δ 3.98 (m, 1H), δ 3.79 (m, 1H), δ 3.58 (dd, 1H, J = 14.2, 6.4 Hz),

δ 3.28 (obsc, 1H), δ 3.18 (m, 1H), δ 2.87 (m, 1H), δ 2.72 (m, 1H), δ 1.86 (s, 3H), δ 1.43 (m, 2H), δ 1.10 (m, 1H), δ 0.78 (d, 3H, J = 6.5 Hz), δ 0.71 (d, 3H, J = 6.5 Hz); ESI-MS m/z calcd for $C_{24}H_{33}N_5O_6S$ 519.2, found 520.3 ([M+H$^+$]).

Data for *N*-MeS2 (10). ^{1}H NMR (400 MHz, DMSO-d_6) δ 8.73 (d, 1H, J = 8.3 Hz), δ 8.56 (d, 1H J = 9.0 Hz), δ 7.98 (d, 1H J = 7.4 Hz), δ 7.49 (d, 1H, J = 8.1 Hz), δ 7.25 (m, 2H), δ 7.18 (m, 3H), δ 5.25 (m, 1H), δ 4.95 (m, 3H), δ 4.38 (m, 1H), δ 4.16 (m, 1H), δ 4.08 (m, 1H), δ 3.80 (m, 1H), δ 3.73 (m, 2H), δ 3.33 (obsc, 1H), δ 3.12 (m, 1H), δ 3.00 (s, 3H), δ 2.90 (m, 1H), δ 2.83 (m, 1H), δ 1.87 (s, 3H), δ 1.26 (m, 3H), δ 0.73 (m, 6H); ESI-MS m/z calcd for $C_{27}H_{39}N_5O_8S$ 593.3, found 595.0 ([M+H$^+$]).

Data for *N*-MeS3 (11a and 11b). (*cis* and *trans* amide isomers ~50% each)**:** ^{1}H NMR (400 MHz, DMSO-d_6) δ 8.66 (d, 1H, J = 7.4 Hz), δ 8.47 (d, 1H, J = 7.6 Hz), δ 8.24 (d, 1H, J = 8.6 Hz), δ 8.10 (m, 3H), δ 7.48 (m, 2H), δ 7.25 (m, 5H), δ 7.14 (m, 5H), δ 4.90 (m, 1H), δ 4.83 (m, 1H), δ 4.59 (m, 1H), δ 4.51 (m, 1H), δ 4.45 (m, 1H), δ 4.35 (m, 1H), δ 4.26 (m, 1H), δ 4.12 (m, 2H), δ 3.99 (m, 1H), δ 3.88 (m, 1H), δ 3.77 (m, 1H), δ 3.63 (m, 1H), δ 3.56 (m, 3H), δ 3.34 (obsc, 1H), δ 3.29 (obsc, 1H), δ 3.26 (obsc, 1H), δ 3.24 (obsc, 1H), δ 3.14 (m, 2H), δ 3.02 (m, 1H), δ 2.97 (m, 2H), δ 2.66 (s, 6H), δ 2.49 (obsc, 1H), δ 1.86 (s, 6H), δ 1.39 (m, 5H), δ 1.29 (m, 1H), δ 0.77 (m, 6H), δ 0.73 (m, 6H); ESI-MS m/z calcd for $C_{27}H_{39}N_5O_8S$ 593.3, found 595.0 ([M+H$^+$]).

Data for *N*-MeL (12). ^{1}H NMR (400 MHz, DMSO-d_6) δ 8.45 (d, 1H, J = 8.2 Hz), δ 8.25 (d, 1H, J = 9.9 Hz), δ 8.05 (d, 1H, J = 8.5 Hz), δ 7.76 (d, 1H, J = 9.1 Hz), δ 7.25 (m, 3H), δ 7.21 (m, 2H), δ 5.15 (m, 1H), δ 4.82 (m, 1H), δ 4.75 (m, 1H), δ 4.67 (m, 1H), δ 4.44 (m, 1H), δ 4.22 (m, 1H), δ 3.63 (m, 2H), δ 3.50 (m, 1H), δ 3.45 (m, 1H), δ 3.37 (obsc, 1H), δ 3.36 (obsc, 1H), δ 3.11 (m, 1H), δ 3.01 (s, 3H), δ 2.89 (m, 1H), δ

2.70 (m, 1H), δ 1.90 (m, 1H), δ 1.85 (s, 3H), δ 1.37 (m, 1H), δ 1.25 (m, 1H), δ 0.75 (d, 3H, J = 6.5 Hz), δ 0.69 (d, 3H, J = 6.4 Hz); ESI-MS m/z calcd for $C_{27}H_{39}N_5O_8S$ 593.3, found 595.0 ([M+H$^+$]).

Data for Meth Link (14). ^{1}H NMR (400 MHz, DMSO-d_6) δ 8.24 (d, 1H, J = 7.8 Hz), δ 8.09 (m, 1H), δ 7.94 (d, 1H, J = 8.9 Hz), δ 7.74 (d, 1H, J = 9.2 Hz), δ 7.26 (m, 3H), δ 7.20 (m, 2H), δ 4.67 (m, 1H), δ 4.34 (m, 1H), δ 4.20 (m, 1H), δ 3.43 (m, 1H), δ 3.28 (obsc, 1H), δ 3.21 (obsc, 1H), δ 2.90 (m, 1H), δ 2.76 (m, 2H), δ 2.11 (m, 1H), δ 2.01 (m, 1H), δ 1.84 (s, 3H), δ 1.50 (m, 3H), δ 1.32 (m, 1H), δ 1.20 (m, 2H), δ 0.97 (m, 1H), δ 0.75 (d, 3H, J = 6.5 Hz), δ 0.68 (d, 3H, J = 6.5 Hz); ESI-MS m/z calcd for $C_{25}H_{36}N_4O_5S$ 504.2, found 505.0 ([M+H$^+$]).

Data for Δ N-term (16). ^{1}H NMR (400 MHz, DMSO-d_6) δ 8.76 (d, 1H, J = 8.4 Hz), δ 8.18 (d, 1H, J = 7.5 Hz), δ 8.06 (d, 1H, J = 7.8 Hz), δ 7.34 (d, 1H, J = 8.7 Hz), δ 7.26 (m, 3H), δ 7.20 (m, 2H), δ 5.09 (t, 1H, J = 5.0 Hz), δ 4.98 (t, 1H, J = 5.3 Hz), δ 4.54 (m, 1H), δ 4.26 (m, 1H), δ 4.18 (m, 1H), δ 3.88 (m, 1H), δ 3.64 (m, 4H), δ 3.33 (obsc, 1H), δ 3.21 (m, 1H), δ 2.85 (m, 2H), δ 2.62 (obsc, 1H), δ 2.34 (m, 1H), δ 1.42 (m, 1H), δ 1.24 (m, 2H), δ 0.74 (d, 3H, J = 6.3 Hz), δ 0.70 (d, 3H, J = 6.3 Hz); ESI-MS m/z calcd for $C_{24}H_{34}N_4O_7S$ 522.2, found 523.0 ([M+H$^+$]).

Data for AIP-I M8pMet-Biotin (19). ESI-MS m/z calcd for $C_{54}H_{74}N_{12}O_{15}S_2$ 1195.4, found 1195.9 ([M+H$^+$]).

Data for AIP-I M8pMet (20). ESI-MS m/z calcd for $C_{44}H_{60}N_{10}O_{13}S$ 969.1, found 969.9 ([M+H$^+$]).

trAIP-II Lactam (15) Synthesis. The peptide was synthesized similarly to the full-length AIP-II lactam (19). Chain elongation was completed using Fmoc-SPPS protocols. Fmoc-Serine(benzyl)-OH was used in residue positions two and three.

Fmoc-DAPA(Boc)-OH was used in place of cysteine in position one. Once cleaved from the resin with TFA, the partially protected linear peptide was cyclized with PyBop and DIEA, purified by semipreparative HPLC, and treated with 25:1 HF:4-methyl-phenol (*p*-cresol) for 1 h at 0 °C to remove the benzyl groups. The final product was purified with semipreparative HPLC. ^{1}H NMR (400 MHz, DMSO-d_6) δ 8.67 (m, 1H), δ 8.11 (m, 1H), δ 8.04 (m, 1H), δ 7.72 (m, 1H), δ 7.59 (m, 1H), δ 7.49 (m, 1H), δ 7.20 (m, 5H), δ 4.38 (m, 2H), δ 4.31 (m, 1H), δ 3.94 (m, 1H), δ 3.84 (m, 1H), δ 3.79 (m, 1H), δ 3.71 (m, 1H), δ 3.62 (m, 3H), δ 3.21 (obsc, 1H), δ 3.00 (m, 1H), δ 2.85 (m, 1H), δ 1.84 (s, 3H), δ 1.37 (m, 1H), δ 1.25 (m, 1H), δ 1.10 (m, 1H), δ 0.76 (d, 3H, J = 6.5 Hz), δ 0.69 (d, 3H, J = 6.2 Hz); ESI-MS m/z calcd for $C_{26}H_{38}N_6O_8S$ 562.3, found 563.5 ([M+H$^+$]).

Boc-SPPS of AIPs. AIP-II N3A, L8A, F9A, F9Nal, native AIPs, and peptides **13**, **17**, and **18** were manually synthesized. Manual solid phase peptide synthesis with standard *in situ* neutralization/HBTU activation protocol for Boc chemistry (82) was used for chain elongation on a mercaptopropionamide MBHA resin. Leucine was double-coupled to *N*-methylated phenylalanine with HBTU, then HATU. Peptides were cleaved from the resin by treatment with 25:1 HF:*p*-cresol for 1 h at 0 °C, precipitated and washed with diethyl ether, and purified by semipreparative or preparative HPLC. After lyophilization, the linear peptides were dissolved again in MeCN, water, and 0.1% TFA and cyclized in solution by the addition of 4x volume of 0.1 M sodium phosphate buffer, pH 7, for 2 h at room temperature. The final products were purified by semipreparative or preparative HPLC.

Data for AIP-II N3A. ESI-MS *m*/*z* calcd for $C_{37}H_{57}N_9O_{11}S$ 836.0, found 836.9 ([M+H$^+$]).

Data for AIP-II L8A. ESI-MS *m*/*z* calcd for $C_{35}H_{52}N_{10}O_{12}S$ 836.9, found 837.9 ([M+H$^+$]).

Data for AIP-II F9A. ESI-MS *m*/*z* calcd for $C_{32}H_{54}N_{10}O_{12}S$ 802.9, found 803.9 ([M+H$^+$]).

Data for AIP-II F9Nal. ESI-MS *m*/*z* calcd for $C_{42}H_{60}N_{10}O_{12}S$ 929.1, found 929.9 ([M+H$^+$]).

Data for *N*-MeF (13). ^{1}H NMR (400 MHz, DMSO-d_6) δ 8.50 (d, 1H, J = 8.3 Hz), δ 8.25 (d, 1H, J = 8.6 Hz), δ 7.86 (d, 1H, J = 9.2 Hz), δ 7.80 (d, 1H, J = 9.1 Hz), δ 7.25 (m, 3H), δ 7.14 (m, 2H), δ 5.16 (m, 1H), δ 5.00 (m, 1H), δ 4.63 (m, 1H), δ 4.39 (m, 1H), δ 4.28 (m, 1H), δ 4.25 (m, 1H), δ 4.20 (m, 1H), δ 3.63 (m, 1H), δ 3.53 (m, 3H), δ 3.21 (obsc, 2H), δ 3.19 (obsc, 1H), δ 2.89 (m, 1H), δ 2.64 (s, 3H), δ 1.88 (s, 3H), δ 1.52 (m, 2H), δ 1.32 (m, 1H), δ 0.86 (d, 3H, J = 6.0 Hz), δ 0.81 (d, 1H, J = 6.1 Hz); ESI-MS *m*/*z* calcd for $C_{27}H_{39}N_5O_8S$ 593.3, found 595.0 ([M+H$^+$]).

Data for AIP-II Bpa-Biotin (17). ESI-MS *m*/*z* calcd for $C_{64}H_{85}N_{13}O_{16}S_2$ 1356.6, found 1357.9 ([M+H$^+$]).

Data for AIP-II Bpa (18). ESI-MS *m*/*z* calcd for $C_{54}H_{71}N_{11}O_{14}S$ 1130.3, found 1131.6 ([M+H$^+$]).

(*S*)-4-methyl 1-perfluorophenyl 2-(*tert*-butoxycarbonylamino)succinate (21). Boc-Glu(OMe)-OH·DCHA (5.0 g, 11.3 mmol, 1.0 equiv) was added to 1.5 M H_2SO_4 (9 mL), extracted with ethyl acetate (35 mL), washed with H_2O, dried over Na_2SO_4, filtered, and solvent was removed in vacuo to give 3.0 g Boc-Glu(OMe)-OH (99%) as a yellow oil. Boc-Glu(OMe)-OH (3.0 g, 11.3 mmol, 1.0 equiv) was

next dissolved in DMF (76 mL) and pyridine (1.10 mL, 13.7 mmol, 1.2 equiv) under Ar. Pentafluorophenyl trifluoroacetate (2.46 mL, 14.3 mmol, 1.25 equiv) was added slowly, the reaction was stirred at room temperature 1 h, then diluted with ethyl acetate. The product was washed with 1 N HCl, $NaHCO_3$, H_2O, and brine, dried over Na_2SO_4, filtered, and the solvent was removed in vacuo to give 4.6 g of **21** as a yellow oil (94%). The product was taken onto the next step without further purification.

(*S*)-5-methyl 1-perfluorophenyl 2-(*tert*-butoxycarbonylamino)pentanedioate (22). Boc-Asp(OMe)-OH (3.7 g, 14.9 mmol, 1.0 equiv) was next dissolved in DMF (65 mL) and pyridine (1.44 mL, 17.8 mmol, 1.2 equiv) under Ar. Pentafluorophenyl trifluoroacetate (3.2 mL, 18.6 mmol, 1.25 equiv) was added slowly, the reaction was stirred at room temperature 1 h, then diluted with ethyl acetate. The product was washed with 1 N HCl, $NaHCO_3$, H_2O, and brine, dried over $MgSO_4$, filtered, and the solvent was removed in vacuo to give 4.9 g of **22** as a yellow oil (79%). The product was taken onto the next step without further purification.

(*S*)-methyl 5-(3-bromopropylamino)-4-(*tert*-butoxycarbonylamino)-5-oxopentanoate (23). A solution of **21** (4.6 g, 10.7 mmol, 1.2 equiv) dissolved in DIEA (1.86 mL, 10.7 mmol, 1.2 equiv) and DMF (24 mL) was stirred at room temperature 30 min under Ar. A solution of 3-bromopropyl ammonium bromide (1.95 g, 8.9 mmol, 1.0 equiv) in DIEA (1.55 mL, 8.9 mmol, 1.0 equiv) and DMF (8 mL) was added to the reaction mixture, which was stirred at room temperature 5 h, diluted with ethyl acetate, washed with H_2O, dried over Na_2SO_4, filtered, and the solvent was removed in vacuo. The product was purified by flash chromatography using 2:5 ethyl acetate/hexanes to give 1.8 g of **23** (52%).

(*S*)-methyl 5-(3-azidopropylamino)-4-(*tert*-butoxycarbonylamino)-5-oxopentanoate (24). (This step was completed by Matthew Pratt.) Bromide **23** (1 g, 2.6 mmol, 1.0 equiv) was dissolved in DMF (20 mL) and the mixture was heated to 45 °C. NaN_3 (660 mg, 13.1 mmol, 5.0 equiv) was added, and the reaction was stirred for 16 h. At this time, the reaction was cooled to room temperature, diluted with ethyl acetate (100 mL) and washed with H_2O (50 mL) two times. The organic layer was dried over Na_2SO_4, filtered, and concentrated. Silica gel chromatography (50% ethyl acetate in hexanes) yielded 620 mg of **24** (70%) as a clear oil. The reaction was repeated to give 1.3 g of **24** for the next step.

(*S*)-methyl 5-(3-azidopropylamino)-4-((*S*)-2-(*tert*-butoxycarbonylamino)-4-methoxy-4-oxobutanamido)-5-oxopentanoate (25). A solution of **24** (1.3 g, 3.82 mmol, 1.0 equiv) in 95:5 TFA/H_2O (21 mL) was stirred at room temperature 1 h. The solvent was removed by azeotrope with toluene, and the product ((*S*)-methyl 4-amino-5-(3-azidopropylamino)-5-oxopentanoate, 928 mg, 3.82 mmol, 1.0 equiv), was then added to a solution of **22** (1.9 g, 4.43 mmol, 1.2 equiv) in DIEA (664 μL, 3.82 mmol, 1.0 equiv) and DMF (13 mL). The reaction was stirred at room temperature 21 h, diluted with ethyl acetate, washed with 1 N HCl, $NaHCO_3$, H_2O, and brine, dried over $MgSO_4$, filtered, and the solvent was removed in vacuo. The product was purified by flash chromatography using 4:1 ethyl acetate/hexanes to give 406 mg of **25** (23%) as a clear oil.

(2*S*,3*S*)-2-ethyl 3-perfluorophenyl oxirane-2,3-dicarboxylate. (This step was completed by Matthew Pratt.) First, the epoxide, (2*S*,3*S*)-3-(ethoxycarbonyl)oxirane-2-carboxylic acid, was synthesized by the route reported by Meara et al. (126). This expoxide (1 g, 6.25 mmol) was dissolved in DMF (20 mL) and pyridine (560 uL, 6.88 mmol) under an inert atmosphere.

Pentafluorophenyl trifluoroacetate (1.24 mL, 7.19 mmol) was then added slowly, and the reaction was stirred for 16 h. Dilution with ethyl acetate (50 mL) was followed by washes with 1 N HCl, H_2O, and brine. The organic layer was dried over Na_2SO_4, filtered, and concentrated. The resulting pink solid was used in the next reaction without further purification.

(2*R*,3*R*)-ethyl 3-((*S*)-1-((*S*)-1-(3-azidopropylamino)-5-methoxy-1,5-dioxopentan-2-ylamino)-4-methoxy-1,4-dioxobutan-2-ylcarbamoyl)oxirane-2-carboxylate (26). A solution of **25** (100 mg, 0.212 mmol, 1.0 equiv) in 95:5 TFA/H_2O (18 mL) was stirred at room temperature 1 h. The solvent was removed by azeotrope with toluene, and the product, ((*S*)-methyl 4-((*S*)-2-amino-4-methoxy-4-oxobutanamido)-5-(3-azidopropylamino)-5-oxopentanoate, 79 mg, 0.212 mmol, 1.0 equiv), was then added to a solution of (2*S*,3*S*)-2-ethyl 3-perfluorophenyl oxirane-2,3-dicarboxylate (83 mg, 0.254 mmol, 1.2 equiv) in DIEA (37 μL, 0.212 mmol, 1.0 equiv) and DMF (4.5 mL). The reaction was stirred at room temperature 19 h, diluted with ethyl acetate, washed with 1 N HCl, $NaHCO_3$, H_2O, and brine, dried over $MgSO_4$, filtered, and the solvent was removed in vacuo. The product was purified by flash chromatography using 15% hexanes in ethyl acetate to give 52 mg of **26** (48%) as a white solid. ^{1}H-NMR (100 MHz, $CDCl_3$) δ 7.58 (d, 1H, J = 7.2 Hz), δ 7.07 (d, 1H, J = 7.9 Hz), δ 6.73-6.70 (m, 1H), δ 4.72 (q, 1H, J = 6.0 Hz), δ 4.38-4.33 (m, 1H), δ 4.32-4.23 (m, 2H), δ 3.89 (s, 1H), δ 3.73 (m, 7H), δ 3.34 (m, 4H), δ 3.05 (dd, 1H, J = 17.2, 4.3 Hz), δ 2.79 (dd, 1H, J = 17.3, 6.1 Hz), δ 2.59 (m, 1H), δ 2.46-2.39 (m, 1H), δ 2.14-2.08 (m, 2H), δ 1.81-1.78 (m, 2H), δ 1.32 (t, 3H J = 7.1 Hz); ^{13}C-NMR (101 MHz, $CDCl_3$) δ 175.30, 172.13, 171.04, 170.29, 167.06, 166.96, 62.72, 54.17, 53.80, 53.04, 52.66, 52.55, 49.84, 49.45,

37.40, 36.11, 30.70, 28.91, 26.75, 14.43; ESI-MS *m*/*z* calcd for $C_{20}H_{30}N_6O_{10}$ 514.5, found 537.0 ([M+Na^+]) and 515.0 ([M+H^+]).

AgrB Inhibition Assay. Cultures of strains RN7206 (*agr* null) and RN6734 (*agr* group I) were grown to early exponential phase, pelletted and washed with media, and the supernatants were discarded. The cultures were re-suspended in media containing 0.5 nM–100 μM compound **26** or only DMSO vehicle and grown 1 h. Cells were pelleted, and the supernatants were recovered, filtered, and tested for AIP activity in the reporter assay. The cell pellets were then re-suspended in media containing 0.5 nM–100 μM compound **26** or only DMSO vehicle a second time and grown for 40 min. The supernatants were recovered and tested for activity as in the first test.

Reporter Assays. AIP activities were analyzed using a previously described method with a β-lactamase reporter gene read-out (52). Strains RN9222, RN9372 containing plasmid-borne *agrC* and P3-*blaZ* (assays performed in Chapters 2 & 4), or derivatives of RN10829 containing plasmid-borne *agrC* and chromosomal P3-*blaZ* (assays performed in Chapter 3) were grown to mid-exponential phase and transferred to microtiter plates. In experiments involving constitutive mutants, growth proceeded without transfer to microtiter plates. 80 μL aliquots were treated in duplicate with synthetic AIPs or supernatants for 1 h with shaking at 37 °C in a THERMOmax microplate reader (Molecular Devices). Cell density was monitored by OD_{650} readings taken every 1 min. Immediately following Nitrocefin addition, hydrolysis was monitored by OD_{490} readings taken every 20 seconds over 20 min. All peptide stock solution concentrations were

determined by amino acid analysis (AAA) at the Keck AAA and Protein Sequencing Lab (Yale University, New Haven, CT).

Assay data were normalized to percent maximal activation and plotted as initial β-lactamase reaction velocity versus log peptide concentration. PRISM 4.0 (GraphPad, San Diego) was used to fit individual agonist or antagonist dose-response curves via nonlinear regression to the following four-parameter logistic equation:

$$E = \text{basal} + \frac{E_{\max} - \text{basal}}{1 + 10^{\log \text{EC}_{50} - \log[\text{A}]n_H}}$$

in which E denotes effect, [A] denotes the agonist concentration, n_{H} denotes the midpoint slope, EC_{50} denotes the midpoint location parameter, and $E_{\max}$ and basal denote the upper and lower asymptotes, respectively. For inhibition curves, the midpoint location parameter from the above equation reflects the IC_{50}. Each data point represents two or three replicates, and error bars represent standard error measurements. All curves shown in the same graph correspond to experiments performed on the same day.

Bacterial Strains and Growth Conditions. The *S. aureus* strains used in this study (Table 7) are derivatives of NCTC8325. RN7206 is a derivative of the standard *agr* group I laboratory strain, RN6734, in which the *agr* locus has been replaced by *tetM*. Cloning was performed using *E. coli* strain DH5α. All clones were first transformed into RN4220, the standard recipient for *E. coli* DNA, before transduction to other strains. *S. aureus* cells from overnight plates containing the appropriate selective antibiotics (chloramphenicol, 10 mg/ml and/or erythromycin, 10 mg/ml) were used as inocula for all experiments. Subsequent growth in CYGP or MH broth without antibiotics was performed at

Table 7. Strains and Plasmids Used in this Study.

Strain or Plasmid	Genotype or Description	Reference
S. aureus strains		
RN4220	Restriction-deficient mutant of strain 8325-4	(127)
RN6734	Standard *agr-I* laboratory strain	(13)
RN7206	*agr::tetM* replacement in RN6734	(13)
RN9222	RN6911 (*agr::tetM* replacement in *agr*-I strain) containing pRN7062 (P2-*agrCA-I*; P3-*blaZ*) (Group I β-lactamase reporter strain)	(40)
RN9372	RN9120 (*agr::tetM* replacement in *agr*-II strain) containing pRN7035 (P2-*agrCA-II*; P3-*blaZ*) (Group II β-lactamase reporter strain)	(40)
RN10828	RN7206 containing pRN9253 (P2-*agrBDA*; P3-RNAIII) integrated into the SaPI1 *att* site (hemolysis assay strain)	(58)
RN10829	RN7206 containing pRN9254 (P2-*agrA*; P3-*blaZ*) integrated into the SaPI1 *att* site (β-lactamase reporter strain)	(58)
EG61	RN7206 containing pRN9256 (P2-*agrBD*; P3-RNAIII) integrated into the SaPI1 *att* site (Δ *agrA* strain)	This work
E. coli strains		
DH5α	Standard recipient for plasmid cloning	Promega
XL1-Blue	Supercompetent cells	Stratagene
Plasmids		
pRN9256	Shuttle/suicide vector pJC1111 (58) containing SaPI1 integration cassette and Δ*agrA* construct (P2-*agrBD*; P3-RNAIII)	This work
pRN9231	Shuttle vector with promoter P2, insertion site for *agrC*, P2 terminator, pT181 replicon, and Em marker	(58)
pEG54	pRN9231 containing replacements by pC194 replicon and Cm marker	This work
pRN9232	pRN9231 with *agrC-I*	(58)
pEG55	pEG54 with *agrC-I*	This work
pEG58	pRN9231 with *agrC-I*$_{Kin}$ *(G394A,G396A) -HA*	This work
pEG59	pEG54 with *agrC-I*$_{His}$ *(H239Q) -PKA*	This work
pEG60	pRN9231 with *agrC-I G394A*	This work
pEG61	pRN9231 with *agrC-I G396A*	This work
pEG62	pRN9231 with *agrC-I N339D*	This work
pEG63	pRN9231 with *agrC-I-gfp*	This work
pEG64	pRN9231 with *agrC-I*$_{Kin}$*-gfp*	This work
pEG65	pEG54 with *agrC-I*$_{His}$*-gfp*	This work
pEG66	pRN9231 with *agrC-I* Δ*1-204*	This work
pEG67	pRN9231 with *agrC-I* Δ*1-175*	This work
pEG68	pRN9231 with *agrC-I* Δ*35-175*	This work
pEG69	pRN9231 with *agrC-I* Δ*1-135*	This work
pEG70	pRN9231 with *agrC-I* Δ*1-72*	This work
pEG71	pRN9231 with *agrC-I*$_{Kin}$ Δ*1-204*	This work
pEG72	pRN9231 with *agrC-I*$_{Kin}$ Δ*1-175*	This work

Table 7. (continued)

pEG73	pRN9231 with *agrC-I_{Kin} Δ35-175*	This work
pEG74	pRN9231 with *agrC-I_{Kin} Δ1-135*	This work
pEG75	pRN9231 with *agrC-I_{Kin} Δ1-72*	This work
pEG78	pRN9231 with *agrC-I Δ1-204-gfp*	This work
pEG79	pRN9231 with *agrC-I Δ1-175-gfp*	This work
pEG80	pRN9231 with *agrC-I Δ35-175-gfp*	This work
pEG81	pRN9231 with *agrC-I Δ1-135-gfp*	This work
pEG82	pRN9231 with *agrC-I Δ1-72-gfp*	This work
pRN9248	pRN9231 with *agrC-I_{Sensor} (T104V, S107V, S116I)*	(58)
pEG83	pRN9231 with *agrC-$I_{Sensor,}$* Kin	This work
pEG84	pEG54 with *agrC-$I_{Sensor,}$* His	This work
pEG85	pRN9231 with *agrC-I_{Sensor}-gfp*	This work
pEG86	pRN9231 with *agrC-I R238H* (42)	This work
pEG87	pRN9231 with *agrC-I_{Kin} R238H*	This work
pEG88	pEG54 with *agrC-I_{His} R238H*	This work
pEG89	pRN9231 with *agrC-I R238H-gfp*	This work
pEG90	pEG54 with *agrC-I R238H-HA*	This work
pEG97	pRN9231 with *agrC-II*	This work
pEG99	pEG54 with *agrC-II_{His}*	This work
pEG100	pRN9231 with *agrC-II_{Kin}*	This work

37 °C with shaking. Cell density was determined using a THERMOMax microplate reader (Molecular Devices) to measure the OD_{650} of 100 μL culture samples.

Plasmid and Reporter Construction. The plasmids used in this study (Table 7) were prepared by cloning PCR products obtained from oligonucleotide primers (Table 8). Clones were sequenced by the Skirball DNA Sequencing Core Facility or Genewiz. Plasmid pRN9231 was used as the backbone vector for WT *agrC* and G-box mutant constructs and contains the *agr*P2 promoter, an erythromycin resistance cassette, and the pT181 replicon (58). Compatible plasmid pEG54, which served as the backbone vector for H-box mutant *agrC* constructs, was created by replacing the resistance cassette and replicon of pRN9231 with a chloramphenicol resistance cassette and the pC194 replicon, cloned with ApaI and NarI sites. These plasmids contain an insertion site for *agrC,* formed by PstI and KpnI restriction sites, such that *agrC* expression is driven by *agr*P2. Point mutations in *agrC* were introduced via QuikChange (Stratagene) or by two-step PCR. *agrC* truncation and deletion mutants were constructed by inverse PCR on pUC18 subclones, closing on silent AflII or BglII sites. A C-terminal AgrC translational fusion to GFP was constructed using an in-frame XbaI site, and subsequent GFP-tagged mutants were created either by site-directed mutagenesis as above or using a ClaI site endogenous to *agrC* to swap in the mutant sequences. A chromosomal *agr* locus derivative lacking *agrC*, *B*, and *D* was constructed by deleting *agrB* and *D* from pRN9254.

Fluorescence Microscopy. Cultures were grown to high optical density (OD_{650} >0.5), pelleted, and re-suspended in PBS, concentrating the cells up to 50-fold relative to the liquid culture density. 5 mL aliquots of cells were added to # 1.5

Table 8. Oligonucleotide Primers Used in this Study.

Primer	Sequence (5′ – 3′)*	RE site used
AgrC-I-F	CCAGCTGCAGGAAGTACCAAAAGAATTAACACAA	PstI
KpnI-R	GAGCTCGGTACCTTCATACATTCACATCCTTATGGCTAGTTG	KpnI
H239Q-F	GCGCAAGTTCCGTCAGGATTATGTCAATATC	
H239Q-R	GATATTGACATAATCCTGACGGAACTTGCGC	
G394A-F	GGTGAAGGTCGTGCTTTAGGTCTATCAAC	
G394A-R	GTTGATAGACCTAAAGCACGACCTTCACC	
G396A-F	GGTGAAGGTCGTGGTTTAGCTCTATCAAC	
G396A-R	GTTGATAGAGCTAAACCACGACCTTCACC	
G394, 6A-F	GGTGAAGGTCGTGCTTTAGCTCTATCAAC	
G394, 6A-R	GTTGATAGAGCTAAAGCACGACCTTCACC	
N339D-F	GGTATTATTCTTGATGATGCAATTGAGGCATC	
N339D-R	GATGCCTCAATTGCATCATCAAGAATAATACC	
Δ 1-175-F	ACTCGCTTAAGGCTAAAGTAATAAGGCAGTATTC	Afl-II
Δ 35-175-F	ACTCGCTCGAGGCTAAAGTAATAAGGCAGTATTC	XhoI
Δ 35-175-R	AATACTCGAGTTTACTGTACTTAATACCACTAATTATAGCTG	XhoI
Δ 1-135-F	GAGTTCTTAAGAAAATTAGCACACCATATCTAATAC	AflII
Δ 1-72-F	ATTTTCTTAAGATCAAATGGTATTCTATTTTGTTG	AflII
aflII-R	TAACTATTTAACTTAAGCACCTACTATCACACTCTC	AflII
AgrCI-I H239Q-R	GACATAATCCTGACGGAACTTGCGCATTTCATTATTAATTG	
AgrC-II-H239Q-F	GCGCAAGTTCCGTCAGGATTATGTCAATATCTTAACGACAC	
AgrC-I-GFP-Xba-R	CTTATCTAGAATTGTTAATAATTTCAACTTTTTGAATAAAGAAAC C	XbaI
AgrC-I-GFP-Kpn-F	TAAGGGTACC*TGCAG*AAGTACCAAAAGAATTAACACAATTACA CG	PstI, KpnI
R238H, H239Q-R	GTAGCCCGGGCATGTCATCTTCTCGAATGTATTCTGAAAGTGTC GTTAAGATATTGACATAATCCTGATGGAACTTGCGCATTTCGTTG TTG	XmaI
XmaI-F	GACATGCCCGGGCTACGTGATTATTTCAATAAAAATATTGTACC	XmaI
R238H-HA-F	GCGCAAGTTCCATCATGATTATGTCAATATC	
R238H-HA-R	GATATTGACATAATCATGATGGAACTTGCGC	
R238H-GFP-F	GCGCAAGTTCCATCATGATTATGTC	
R238H-GFP-R	GACATAATCATGATGGAACTTGCGC	

Restriction sites are underlined. Overlapping restriction sites in AgrC-I-GFP-Kpn-F are underlined (KpnI) and italicized (Pst1).

coverslips that were previously coated with poly-lysine solution and placed on glass slides. Imaging was immediately carried out on a DeltaVision image restoration microscope (Applied Precision/Olympus). Images were deconvolved with SoftWoRx (Applied Precision).

Western Blotting. Cultures were grown to high optical density (OD_{650} >0.5), pelleted, and washed with buffer containing 10mM Tris-HCl, pH 7.4, 1.5 mM $MgCl_2$, 10 mM KCl, 0.5 mM dithiothreitol, and 1.1 M sucrose (wash buffer). Cells were lysed by treatment with 100 μg/mL lysostaphin in wash buffer containing protease inhibitors, followed by rocking for 10 min at 37 °C, high speed spin (30 min, 8,000g), removal of supernatant, and resuspension in lysis buffer (50 mM Tris-HCl, pH 7.4, 0.5% NP-40, 5 mM $MgCl_2$; or 50 mM Tris-HCl, pH 7.4, 1.0% NP-40, 0.25% DOC, 150 mM NaCl, and 1 mM EGTA) containing 10 μg/mL DNase and protease inhibitors. Lysates were incubated on ice 10 min, and the soluble fractions were removed following 30 min spin at 10,000g. Total protein concentrations of the soluble fractions were determined by BCA assay. SDS loading buffer (50 mM Tris-HCl, pH 6.8, 2% SDS, 1 mg/mL bromophenol blue, 10% glycerol) was added to samples, which were then untreated or acidified with Immuno Elution buffer (Pierce) prior to loading on 10-20% Criterion Tris-HCl gel. Protein transfer to nitrocellulose membrane was followed by immunoblotting with mouse anti-GFP, mouse anti-HA, or rabbit anti-Sortase primary antibodies and anti-mouse HRP or anti-rabbit HRP secondary antibodies. Visualization was carried out with ECL or ECL Plus.

Immunoprecipitation. Cultures of derivatives of RN10306 containing GFP and/or HA-tagged AgrC were grown to high optical density (OD_{650} >0.5). Each

culture was split into two subcultures, one treated with 1 uM AIP-I and one with buffer. All subcultures were grown for an additional 15 minutes. Cells were then pelleted, washed, and lysed, as for western blotting. 250 μg aliquots of total protein, diluted with lysis buffer to uniform final volumes, were added to 25 μL aliquots of anti-HA affinity matrix washed with lysis buffer. Samples were incubated 1 h at 4 ^{a}C, with mixing by slow rotation. Unbound material was removed following centrifugation. Beads were washed gently three times with lysis buffer, and bound proteins were eluted with Immuno Elution buffer (Pierce) by gentle mixing for three minutes. Analysis of samples was completed by western blot, as above.

Appendix: NMR Chemical Shift Assignments of trAIP-II and Derivatives.

AIP Derivative	NH	αH	βH	γH	Other
6 trAIP-II					
Cys	8.46	4.39	3.16, 2.85		
Ser	8.11	4.22	3.64, 3.52		5.03
Ser	7.60	4.28	3.58		5.12
Leu	8.13	3.92	1.38, 1.30	1.22	0.74, 0.71
Phe	8.68	4.56	3.31, 2.83		7.25, 7.21
Ac					1.86
7 S2G					
Cys	8.44	4.32	3.16, 2.87		
Gly	8.21	3.89, 3.52			
Ser	7.59	4.21	3.62, 3.32		5.21
Leu	7.99	3.98	1.31	1.18	0.74, 0.69
Phe	8.67	4.59	3.31, 2.81		7.26, 7.20
Ac					1.86
8 S3G					
Cys	8.30	4.44	3.13, 2.62		
Ser	7.99	4.39	3.57		4.94
Gly	8.46	3.79, 3.58			
Leu	8.36	3.99	1.12	1.49	0.78, 0.71
Phe	8.02	4.64	3.35, 2.91		7.24, 7.20
Ac					1.86
9 GG					
Cys	8.30	4.42	3.18, 2.72		
Gly	8.39	4.10, 3.29			
Gly	8.08	3.79, 3.58			
Leu	8.28	3.98	1.43	1.10	0.78, 0.71
Phe	8.15	4.67	3.28, 2.87		7.26, 7.22
Ac					1.86
10 *N*-MeS2					
Cys	8.56	5.00	3.12, 2.83		
N-MeSer		4.14	3.79		OH 4.92, Me 3.01
Ser	7.49	4.95	3.73		5.25
Leu	7.98	4.08	1.26	1.15	0.73
Phe	8.73	4.38	3.33, 2.90		7.25, 7.19
Ac					1.87

NMR Chemical Shift Assignments (continued).

	NH	αH	βH	γH	Other
11a *N*-MeS3 (*trans*)					
Cys	8.47	4.12	3.13, 2.96		
Ser	8.11	4.90	3.57, 3.26		
N-MeSer		4.11	3.77, 3.63		Me 2.66
Leu	7.48	4.35	1.41, 1.34	1.29	0.77, 0.76
Phe	8.66	4.26	3.24, 2.97		7.14
Ac					1.86
11b *N*-MeS3 (*cis*)					
Cys	8.24	4.45	3.15, 2.49		
Ser	8.09	4.83	3.56, 3.34		
N-MeSer		4.51	3.88, 3.55		Me 2.66
Leu	7.48	3.99	1.35	1.46	0.74, 0.72
Phe	8.08	4.59	3.29, 3.02		7.25
Ac					1.86
12 *N*-MeL					
Cys	8.45	4.44	3.11, 2.89		
Ser	8.05	4.22	3.63, 3.50		4.82
Ser	7.76	4.67	3.63, 3.36		5.15
N-MeLeu		3.45	1.90, 1.37	1.25	0.75, 0.69, Me 3.01
Phe	8.25	4.75	3.37, 2.70		7.25, 7.21
Ac					1.85
13 *N*-MeF					
Cys	8.50	4.39	3.19, 2.89		
Ser	8.25	4.20	3.55		5.16
Ser	7.80	4.28	3.63, 3.51		5.00
Leu	7.86	4.63	1.52	1.32	0.86, 0.81
N-MePhe		4.25	3.21		Ar 7.25, 7.14, Me 2.64
Ac					1.86
14 Meth Link					
Cys	8.24	4.34	3.21, 2.90		
Pent	8.09	3.43, 2.73	2.11, 2.01	1.55, 1.32	1.50
Leu	7.74	4.20	1.25, 1.14	0.97	0.75, 0.68
Phe	7.94	4.67	3.28, 2.79		7.26, 7.20
Ac					1.84

NMR Chemical Shift Assignments (continued).

	NH	αH	βH	γH	Other
15 Lactam					
Dapa	8.11	4.38	3.62, 2.85		7.59
Ser	8.04	4.31	3.79, 3.71		5.32
Ser	8.67	3.84	3.62		
Leu	7.72	3.94	1.10, 1.25	1.37	0.69, 0.76
Phe	7.49	4.36	3.21, 3.00		7.20
Ac					1.84
16 Δ N-term					
Mercap		2.62, 2.34	2.87, 3.21		
Ser	8.06	4.18	3.64		4.98
Ser	7.34	4.26	3.64		5.09
Leu	8.18	3.88	1.24	1.42	0.74, 0.70
Phe	8.76	4.54	3.33, 2.83		7.26, 7.20

Ac = N-terminal acetyl group. Pent = 5-aminopentanoic acid.

Dapa = 2,3-diaminopropanoic acid. Mercap = 3-mercaptopropanoic acid.

References

1. Gordon RJ & Lowy FD (2008) Pathogenesis of methicillin-resistant Staphylococcus aureus infection. *Clin Infect Dis* 46 Suppl 5:S350-359.

2. Wisplinghoff H, *et al.* (2004) Nosocomial bloodstream infections in US hospitals: analysis of 24,179 cases from a prospective nationwide surveillance study. *Clin Infect Dis* 39(3):309-317.

3. Klevens RM, *et al.* (2007) Invasive methicillin-resistant Staphylococcus aureus infections in the United States. *Jama* 298(15):1763-1771.

4. Diep BA & Otto M (2008) The role of virulence determinants in community-associated MRSA pathogenesis. *Trends Microbiol* 16(8):361-369.

5. Smith TL, *et al.* (1999) Emergence of vancomycin resistance in Staphylococcus aureus. Glycopeptide-Intermediate Staphylococcus aureus Working Group. *N Engl J Med* 340(7):493-501.

6. Sieradzki K, Roberts RB, Haber SW, & Tomasz A (1999) The development of vancomycin resistance in a patient with methicillin-resistant Staphylococcus aureus infection. *N Engl J Med* 340(7):517-523.

7. Farr BM (2004) Prevention and control of methicillin-resistant Staphylococcus aureus infections. *Curr Opin Infect Dis* 17(4):317-322.

8. Varkey JB, Anderson DJ, & Kaye KS (2008) Preventing Surgical Site Infections in the Era of Methicillin-Resistant Staphylococcus aureus. *Curr Infect Dis Rep* 10(5):341-342.

9. Wright TI, *et al.* (2008) Antibiotic prophylaxis in dermatologic surgery: advisory statement 2008. *J Am Acad Dermatol* 59(3):464-473.

10. Massey RC, Horsburgh MJ, Lina G, Hook M, & Recker M (2006) The evolution and maintenance of virulence in Staphylococcus aureus: a role for host-to-host transmission? *Nat Rev Microbiol* 4(12):953-958.

11. Honeyman A, Friedman H, & Bendinelli M (2001) *Staphylococcus aureus infection and disease* (Kluwer Academic/Plenum Publishers, New York) 330 p.

12. Recsei P, *et al.* (1986) Regulation of exoprotein gene expression in Staphylococcus aureus by agar. *Mol Gen Genet* 202(1):58-61.

13. Novick RP, *et al.* (1993) Synthesis of staphylococcal virulence factors is controlled by a regulatory RNA molecule. *Embo J* 12(10):3967-3975.

14. Bronner S, Monteil H, & Prevost G (2004) Regulation of virulence determinants in Staphylococcus aureus: complexity and applications. *FEMS Microbiol Rev* 28(2):183-200.

15. Novick RP (2003) Autoinduction and signal transduction in the regulation of staphylococcal virulence. *Molec Microbiol* 48(6):1429-1449.

16. Pragman AA & Schlievert PM (2004) Virulence regulation in Staphylococcus aureus: the need for in vivo analysis of virulence factor regulation. *Fems Immunol Med Mic* 42(2):147-154.

17. Cheung AL, Bayer AS, Zhang G, Gresham H, & Xiong YQ (2004) Regulation of virulence determinants in vitro and in vivo in Staphylococcus aureus. *FEMS Immunol Med Microbiol* 40(1):1-9.

18. Cheung AL, *et al.* (1994) Diminished virulence of a sar-/agr- mutant of Staphylococcus aureus in the rabbit model of endocarditis. *J Clin Invest* 94(5):1815-1822.

19. Mayville P, *et al.* (1999) Structure-activity analysis of synthetic autoinducing thiolactone peptides from Staphylococcus aureus responsible for virulence. *Proc Natl Acad Sci U S A* 96(4):1218-1223.

20. Blevins JS, *et al.* (2003) Role of sarA in the pathogenesis of Staphylococcus aureus musculoskeletal infection. *Infect Immun* 71(1):516-523.

21. Giese MJ, Berliner JA, Riesner A, Wagar EA, & Mondino BJ (1999) A comparison of the early inflammatory effects of an agr-/sar- versus a wild type strain of Staphylococcus aureus in a rat model of endophthalmitis. *Curr Eye Res* 18(3):177-185.

22. Giraudo AT, Raspanti CG, Calzolari A, & Nagel R (1994) Characterization of a Tn551-mutant of Staphylococcus aureus defective in the production of several exoproteins. *Can J Microbiol* 40(8):677-681.

23. Novick RP & Jiang D (2003) The staphylococcal saeRS system coordinates environmental signals with agr quorum sensing. *Microbiology* 149(Pt 10):2709-2717.

24. Pragman aa, Yarwood JM, Tripp TJ, & Schlievert PM (2004) Characterization of virulence factor regulation by SrrAB, a two-component system in Staphylococcus aureus. *Journal of Bacteriology* 186(8):2430-2438.

25. Said-Salim B, *et al.* (2003) Global regulation of Staphylococcus aureus genes by Rot. *J Bacteriol* 185(2):610-619.

26. Geisinger E, Adhikari RP, Jin R, Ross HF, & Novick RP (2006) Inhibition of rot translation by RNAIII, a key feature of agr function. *Mol Microbiol* 61(4):1038-1048.

27. McNamara PJ, Milligan-Monroe KC, Khalili S, & Proctor RA (2000) Identification, cloning, and initial characterization of rot, a locus encoding a regulator of virulence factor expression in Staphylococcus aureus. *J Bacteriol* 182(11):3197-3203.

28. Bassler BL & Losick R (2006) Bacterially speaking. *Cell* 125(2):237-246.

29. Ji G, Beavis RC, & Novick RP (1995) Cell density control of staphylococcal virulence mediated by an octapeptide pheromone. *Proc Natl Acad Sci U S A* 92(26):12055-12059.

30. Novick RP, *et al.* (1995) The agr P2 operon: an autocatalytic sensory transduction system in Staphylococcus aureus. *Mol Gen Genet* 248(4):446-458.

31. Mascher T, Helmann JD, & Unden G (2006) Stimulus Perception in Bacterial Signal-Transducing Histidine Kinases. *Microbiol. Molec. Biol. Rev.* 70(4):910-938.

32. Dutta R, Qin L, & Inouye M (1999) Histidine kinases: diversity of domain organization. *Molec Microbiol* 34(4):633-640.

33. Koenig RL, Ray JL, Maleki SJ, Smeltzer MS, & Hurlburt BK (2004) Staphylococcus aureus AgrA binding to the RNAIII-agr regulatory region. *J Bacteriol* 186(22):7549-7555.

34. Janzon L & Arvidson S (1990) The role of the delta-lysin gene (hld) in the regulation of virulence genes by the accessory gene regulator (agr) in Staphylococcus aureus. *Embo J* 9(5):1391-1399.

35. Queck SY, *et al.* (2008) RNAIII-independent target gene control by the agr quorum-sensing system: insight into the evolution of virulence regulation in Staphylococcus aureus. *Mol Cell* 32(1):150-158.

36. Wang R, *et al.* (2007) Identification of novel cytolytic peptides as key virulence determinants for community-associated MRSA. *Nat Med* 13(12):1510-1514.

37. Ji G, Beavis R, & Novick RP (1997) Bacterial interference caused by autoinducing peptide variants. *Science* 276(5321):2027-2030.

38. Jarraud S, *et al.* (2000) Exfoliatin-producing strains define a fourth agr specificity group in Staphylococcus aureus. *J Bacteriol* 182(22):6517-6522.

39. Dufour P, *et al.* (2002) High genetic variability of the agr locus in Staphylococcus species. *J Bacteriol* 184(4):1180-1186.

40. Lyon GJ, Mayville P, Muir TW, & Novick RP (2000) Rational design of a global inhibitor of the virulence response in Staphylococcus aureus, based in part on localization of the site of inhibition to the receptor-histidine kinase, AgrC. *Proc Natl Acad Sci U S A* 97(24):13330-13335.

41. Lyon GJ, Wright JS, Christopoulos A, Novick RP, & Muir TW (2002) Reversible and specific extracellular antagonism of receptor-histidine kinase signaling. *J Biol Chem* 277(8):6247-6253.

42. Geisinger E, Muir TW, & Novick RP (2009) agr receptor mutants reveal distinct modes of inhibition by staphylococcal autoinducing peptides. *Proc Natl Acad Sci U S A* 106(4):1216-1221.

43. Qiu R, Pei W, Zhang L, Lin J, & Ji G (2005) Identification of the putative staphylococcal AgrB catalytic residues involving the proteolytic cleavage of AgrD to generate autoinducing peptide. *J Biol Chem* 280(17):16695-16704.

44. Zhang L, Gray L, Novick RP, & Ji G (2002) Transmembrane Topology of AgrB, the Protein Involved in the Post- translational Modification of AgrD in Staphylococcus aureus. *J Biol Chem* 277(38):34736-34742.

45. Saenz HL, *et al.* (2000) Inducible expression and cellular location of AgrB, a protein involved in the maturation of the staphylococcal quorum-sensing pheromone. *Arch Microbiol* 174(6):452-455.

46. Kavanaugh JS, Thoendel M, & Horswill AR (2007) A role for type I signal peptidase in Staphylococcus aureus quorum sensing. *Mol Microbiol* 65(3):780-798.

47. Paetzel M, Dalbey RE, & Strynadka NC (2000) The structure and mechanism of bacterial type I signal peptidases. A novel antibiotic target. *Pharmacol Ther* 87(1):27-49.

48. Zhang L, Lin J, & Ji G (2004) Membrane anchoring of the AgrD N-terminal amphipathic region is required for its processing to produce a quorum-sensing pheromone in Staphylococcus aureus. *J Biol Chem* 279(19):19448-19456.

49. Bruton G, *et al.* (2003) Lipopeptide substrates for SpsB, the Staphylococcus aureus type I signal peptidase: design, conformation and conversion to alpha-ketoamide inhibitors. *Eur J Med Chem* 38(4):351-356.

50. Sharkov NA & Cai D (2002) Discovery of substrate for type I signal peptidase SpsB from Staphylococcus aureus. *J Biol Chem* 277(8):5796-5803.

51. Zhang L & Ji G (2004) Identification of a staphylococcal AgrB segment(s) responsible for group-specific processing of AgrD by gene swapping. *J Bacteriol* 186(20):6706-6713.

52. Lyon GJ, Wright JS, Muir TW, & Novick RP (2002) Key determinants of receptor activation in the agr autoinducing peptides of Staphylococcus aureus. *Biochemistry* 41(31):10095-10104.

53. McDowell P, *et al.* (2001) Structure, activity and evolution of the group I thiolactone peptide quorum-sensing system of Staphylococcus aureus. *Mol Microbiol* 41(2):503-512.

54. Scott RJ, Lian, L., Muharram, S.H., Cockayne, A., Wood, S.J., Bycroft, B.W., Williams, P., Chan, W.C. (2003) Side-chain-to-tail thiolcatone peptide inhibitors of the Staphylococcal quorum-sensing system. *Bioorg & Med Chem Lett* 13:2449-2453.

55. Wright JS, 3rd, Lyon GJ, George EA, Muir TW, & Novick RP (2004) Hydrophobic interactions drive ligand-receptor recognition for activation and inhibition of staphylococcal quorum sensing. *Proc Natl Acad Sci U S A* 101(46):16168-16173.

56. Grebe TW & Stock JB (1999) The histidine protein kinase superfamily. *Adv Microb Physiol* 41:139-227.

57. Lina G, *et al.* (1998) Transmembrane topology and histidine protein kinase activity of AgrC, the agr signal receptor in Staphylococcus aureus. *Mol Microbiol* 28(3):655-662.

58. Geisinger E, George EA, Muir TW, & Novick RP (2008) Identification of ligand specificity determinants in AgrC, the Staphylococcus aureus quorum-sensing receptor. *J Biol Chem* 283(14):8930-8938.

59. Aravind L & Ponting CP (1999) The cytoplasmic helical linker domain of receptor histidine kinase and methyl-accepting proteins is common to many prokaryotic signalling proteins. *FEMS Microbiol Lett* 176(1):111-116.

60. Zhu Y & Inouye M (2004) The HAMP linker in histidine kinase dimeric receptors is critical for symmetric transmembrane signal transduction. *J Biol Chem* 279(46):48152-48158.

61. Hulko M, *et al.* (2006) The HAMP domain structure implies helix rotation in transmembrane signaling. *Cell* 126(5):929-940.

62. Jensen RO, Winzer K, Clarke SR, Chan WC, & Williams P (2008) Differential recognition of Staphylococcus aureus quorum-sensing signals depends on both extracellular loops 1 and 2 of the transmembrane sensor AgrC. *J Mol Biol* 381(2):300-309.

63. Nikolskaya AN & Galperin MY (2002) A novel type of conserved DNA-binding domain in the transcriptional regulators of the AlgR/AgrA/LytR family. *Nucleic Acids Res* 30(11):2453-2459.

64. Sidote DJ, Barbieri CM, Wu T, & Stock AM (2008) Structure of the Staphylococcus aureus AgrA LytTR domain bound to DNA reveals a beta fold with an unusual mode of binding. *Structure* 16(5):727-735.

65. Traber K & Novick R (2006) A slipped-mispairing mutation in AgrA of laboratory strains and clinical isolates results in delayed activation of agr and failure to translate delta- and alpha-haemolysins. *Mol Microbiol* 59(5):1519-1530.

66. Benito Y, *et al.* (2000) Probing the structure of RNAIII, the Staphylococcus aureus agr regulatory RNA, and identification of the RNA domain involved in repression of protein A expression. *RNA* 6(5):668-679.

67. Balaban N & Novick RP (1995) Translation of RNAIII, the Staphylococcus aureus agr regulatory RNA molecule, can be activated by a 3'-end deletion. *FEMS Microbiol Lett* 133(1-2):155-161.

68. Morfeldt E, Taylor D, von Gabain A, & Arvidson S (1995) Activation of alpha-toxin translation in Staphylococcus aureus by the trans-encoded antisense RNA, RNAIII. *EMBO J* 14(18):4569-4577.

69. Boisset S, *et al.* (2007) Staphylococcus aureus RNAIII coordinately represses the synthesis of virulence factors and the transcription regulator Rot by an antisense mechanism. *Genes Dev* 21(11):1353-1366.

70. Huntzinger E, *et al.* (2005) Staphylococcus aureus RNAIII and the endoribonuclease III coordinately regulate spa gene expression. *Embo J* 24(4):824-835.

71. Stock AM, Robinson VL, & Goudreau PN (2000) Two-component signal transduction. *Annu Rev Biochem* 69:183-215.

72. Muralidharan V & Muir TW (2006) Protein ligation: an enabling technology for the biophysical analysis of proteins. *Nat Methods* 3(6):429-438.

73. Camarero JA, Cotton GJ, Adeva A, & Muir TW (1998) Chemical ligation of unprotected peptides directly from a solid support. *J Pept Res* 51(4):303-316.

74. Botti P, Villain M, Manganiello S, & Gaertner H (2004) Native chemical ligation through in situ O to S acyl shift. *Org Lett* 6(26):4861-4864.

75. Warren JD, Miller JS, Keding SJ, & Danishefsky SJ (2004) Toward fully synthetic glycoproteins by ultimately convergent routes: a solution to a long-standing problem. *J Am Chem Soc* 126(21):6576-6578.

76. Dawson PE, Muir TW, Clark-Lewis I, & Kent SB (1994) Synthesis of proteins by native chemical ligation. *Science* 266(5186):776-779.

77. George EA, Novick RP, & Muir TW (2008) Cyclic peptide inhibitors of staphylococcal virulence prepared by Fmoc-based thiolactone peptide synthesis. *J Am Chem Soc* 130(14):4914-4924.

78. Jencks WP (1969) *Catalysis in chemistry and enzymology* (McGraw-Hill, New York) pp xvi, 644 p.

79. Lyon GJ (2003) Targeting receptor-histidine kinase signaling in staphylococcus aureus. Thesis (Ph. D.) (Rockefeller University.).

80. Pedroso E, Grandas, A., de las Heras, X., Eritja, R., Giralt, E. (1986) Diketopiperazine formation in soild phase peptide synthesis using p-alkoxybenzyl ester resins and Fmoc-amino acids. *Tet Lett* 27(6):743-746.

81. Khosla MC, Smeby RR, & Bumpus FM (1972) Failure sequence in solid-phase peptide synthesis due to the presence of an N-alkylamino acid. *J Am Chem Soc* 94(13):4721-4724.

82. Schnolzer M, Alewood P, Jones A, Alewood D, & Kent SB (1992) In situ neutralization in Boc-chemistry solid phase peptide synthesis. Rapid, high yield assembly of difficult sequences. *Int J Pept Protein Res* 40(3-4):180-193.

83. LaPlanche LA, Rogers, M. T. (1964) cis and trans configurations of the peptide bond in N-monosubstituted amides by nuclear magnetic resosnance. *J Am Chem Soc* 86(3):337-341.

84. Mathiesen G, Axelsen GW, Axelsson L, & Eijsink VG (2006) Isolation of constitutive variants of a subfamily 10 histidine protein kinase (SppK) from Lactobacillus using random mutagenesis. *Arch Microbiol* 184(5):327-334.

85. Martin B, Prudhomme M, Alloing G, Granadel C, & Claverys JP (2000) Cross-regulation of competence pheromone production and export in the early control of transformation in Streptococcus pneumoniae. *Mol Microbiol* 38(4):867-878.

86. Ninfa EG, Atkinson MR, Kamberov ES, & Ninfa AJ (1993) Mechanism of autophosphorylation of Escherichia coli nitrogen regulator II (NRII or NtrB): trans-phosphorylation between subunits. *J Bacteriol* 175(21):7024-7032.

87. Swanson RV, Bourret RB, & Simon MI (1993) Intermolecular complementation of the kinase activity of CheA. *Mol Microbiol* 8(3):435-441.

88. Yang Y & Inouye M (1991) Intermolecular complementation between two defective mutant signal-transducing receptors of Escherichia coli. *Proc Natl Acad Sci U S A* 88(24):11057-11061.

89. Hirschman A, Boukhvalova M, VanBruggen R, Wolfe AJ, & Stewart RC (2001) Active site mutations in CheA, the signal-transducing protein kinase of the chemotaxis system in Escherichia coli. *Biochemistry* 40(46):13876-13887.

90. Zhu Y & Inouye M (2002) The role of the G2 box, a conserved motif in the histidine kinase superfamily, in modulating the function of EnvZ. *Mol Microbiol* 45(3):653-663.

91. Ji Y (2007) *Methicillin-resistant Staphylococcus aureus (MRSA) protocols* (Humana Press, Totowa, NJ) 264 p.

92. Pan SQ, Charles T, Jin S, Wu ZL, & Nester EW (1993) Preformed dimeric state of the sensor protein VirA is involved in plant--Agrobacterium signal transduction. *Proc Natl Acad Sci U S A* 90(21):9939-9943.

93. Milligan DL & Koshland DE, Jr. (1988) Site-directed cross-linking. Establishing the dimeric structure of the aspartate receptor of bacterial chemotaxis. *J Biol Chem* 263(13):6268-6275.

94. Gao R & Lynn DG (2007) Integration of rotation and piston motions in coiled-coil signal transduction. *J Bacteriol* 189(16):6048-6056.

95. Tao W, Malone CL, Ault AD, Deschenes RJ, & Fassler JS (2002) A cytoplasmic coiled-coil domain is required for histidine kinase activity of the yeast osmosensor, SLN1. *Mol Microbiol* 43(2):459-473.

96. Muir TW, Sondhi D, & Cole PA (1998) Expressed protein ligation: a general method for protein engineering. *Proc Natl Acad Sci U S A* 95(12):6705-6710.

97. Tulla-Puche J, Marcucci E, Prats-Alfonso E, Bayo-Puxan N, & Albericio F (2009) NMe amide as a synthetic surrogate for the thioester moiety in thiocoraline. *J Med Chem* 52(3):834-839.

98. Romero F, *et al.* (1997) Thiocoraline, a new depsipeptide with antitumor activity produced by a marine Micromonospora. I. Taxonomy, fermentation, isolation, and biological activities. *J Antibiot (Tokyo)* 50(9):734-737.

99. Bowers A, *et al.* (2008) Total synthesis and biological mode of action of largazole: a potent class I histone deacetylase inhibitor. *J Am Chem Soc* 130(33):11219-11222.

100. Dick LR, *et al.* (1997) Mechanistic studies on the inactivation of the proteasome by lactacystin in cultured cells. *J Biol Chem* 272(1):182-188.

101. Regassa LB & Betley MJ (1992) Alkaline pH decreases expression of the accessory gene regulator (agr) in Staphylococcus aureus. *J Bacteriol* 174(15):5095-5100.

102. Dinges MM, Orwin PM, & Schlievert PM (2000) Exotoxins of Staphylococcus aureus. *Clin Microbiol Rev* 13(1):16-34, table of contents.

103. Black JW & Leff P (1983) Operational models of pharmacological agonism. *Proc R Soc Lond B Biol Sci* 220(1219):141-162.

104. Kenakin T (2007) Functional selectivity through protean and biased agonism: who steers the ship? *Mol Pharmacol* 72(6):1393-1401.

105. Valant C, *et al.* (2008) A novel mechanism of G protein-coupled receptor functional selectivity. Muscarinic partial agonist McN-A-343 as a bitopic orthosteric/allosteric ligand. *J Biol Chem* 283(43):29312-29321.

106. Hendrickson WA (2005) Transduction of biochemical signals across cell membranes. *Q Rev Biophys* 38(4):321-330.

107. Damian M, Martin A, Mesnier D, Pin JP, & Baneres JL (2006) Asymmetric conformational changes in a GPCR dimer controlled by G-proteins. *Embo J* 25(24):5693-5702.

108. Damian M, Mary S, Martin A, Pin JP, & Baneres JL (2008) G protein activation by the leukotriene B4 receptor dimer: Evidence for an absence of trans-activation. *J Biol Chem*.

109. Vilardaga JP, *et al.* (2008) Conformational cross-talk between alpha2A-adrenergic and mu-opioid receptors controls cell signaling. *Nat Chem Biol* 4(2):126-131.

110. Rocheville M, *et al.* (2000) Subtypes of the somatostatin receptor assemble as functional homo- and heterodimers. *J Biol Chem* 275(11):7862-7869.

111. Suchanek M, Radzikowska A, & Thiele C (2005) Photo-leucine and photo-methionine allow identification of protein-protein interactions in living cells. *Nat Methods* 2(4):261-267.

112. Vila-Perello M, Pratt MR, Tulin F, & Muir TW (2007) Covalent capture of phospho-dependent protein oligomerization by site-specific incorporation of a diazirine photo-cross-linker. *J Am Chem Soc* 129(26):8068-8069.

113. Hatanaka Y & Sadakane Y (2002) Photoaffinity labeling in drug discovery and developments: chemical gateway for entering proteomic frontier. *Curr Top Med Chem* 2(3):271-288.

114. Schirmeister T & Klockow A (2003) Cysteine protease inhibitors containing small rings. *Mini Rev Med Chem* 3(6):585-596.

115. Hanada K, *et al.* (1978) Isolation and Characterization of E-64, a new thiol protease inhibitor. *Agric Biol Chem* 42(3):523-528.

116. Bayburt TH, Grinkova YV, & Sligar SG (2002) Self-assembly of discoidal phospholipid bilayer nanoparticles with membrane scaffold proteins. *Nano Lett* 2:853-856.

117. Banerjee S, Huber T, & Sakmar TP (2008) Rapid incorporation of functional rhodopsin into nanoscale apolipoprotein bound bilayer (NABB) particles. *J Mol Biol* 377(4):1067-1081.

118. Marina A, Waldburger CD, & Hendrickson WA (2005) Structure of the entire cytoplasmic portion of a sensor histidine-kinase protein. *Embo J* 24(24):4247-4259.

119. Lupas A (1997) Predicting coiled-coil regions in proteins. *Curr Opin Struct Biol* 7(3):388-393.

120. Park H, Saha SK, & Inouye M (1998) Two-domain reconstitution of a functional protein histidine kinase. *Proc Natl Acad Sci U S A* 95(12):6728-6732.

121. Fowler VG, Jr., *et al.* (2004) Persistent bacteremia due to methicillin-resistant Staphylococcus aureus infection is associated with agr dysfunction and low-level in vitro resistance to thrombin-induced platelet microbicidal protein. *J Infect Dis* 190(6):1140-1149.

122. Musser JM, *et al.* (1990) A single clone of Staphylococcus aureus causes the majority of cases of toxic shock syndrome. *Proc Natl Acad Sci U S A* 87(1):225-229.

123. Kahl BC, *et al.* (2003) agr-dependent bacterial interference has no impact on long-term colonization of Staphylococcus aureus during persistent airway infection of cystic fibrosis patients. *J Clin Microbiol* 41(11):5199-5201.

124. van Leeuwen W, van Nieuwenhuizen W, Gijzen C, Verbrugh H, & van Belkum A (2000) Population studies of methicillin-resistant and -sensitive Staphylococcus aureus strains reveal a lack of variability in the agrD gene, encoding a staphylococcal autoinducer peptide. *J Bacteriol* 182(20):5721-5729.

125. Lina G, *et al.* (2003) Bacterial competition for human nasal cavity colonization: role of Staphylococcal agr alleles. *Appl Environ Microbiol* 69(1):18-23.

126. Fleming V, *et al.* (2006) Agr interference between clinical Staphylococcus aureus strains in an insect model of virulence. *J Bacteriol* 188(21):7686-7688.

127. Wright JS, 3rd, Jin R, & Novick RP (2005) Transient interference with staphylococcal quorum sensing blocks abscess formation. *Proc Natl Acad Sci U S A* 102(5):1691-1696.

128. George EA & Muir TW (2007) Molecular mechanisms of agr quorum sensing in virulent staphylococci. *Chembiochem* 8(8):847-855.

129. Goerke C, *et al.* (2000) Direct quantitative transcript analysis of the agr regulon of Staphylococcus aureus during human infection in comparison to the expression profile in vitro. *Infect Immun* 68(3):1304-1311.

130. Yarwood JM, McCormick JK, Paustian ML, Kapur V, & Schlievert PM (2002) Repression of the Staphylococcus aureus accessory gene regulator in serum and in vivo. *J Bacteriol* 184(4):1095-1101.

131. Traber KE, *et al.* (2008) agr function in clinical Staphylococcus aureus isolates. *Microbiology* 154(Pt 8):2265-2274.

132. Shopsin B, *et al.* (2008) Prevalence of agr dysfunction among colonizing Staphylococcus aureus strains. *J Infect Dis* 198(8):1171-1174.